

Squark Production in the R -Symmetric Supersymmetric Standardmodel

Masterarbeit
zur Erlangung des Hochschulgrades
Master of Science
im Master-Studiengang Physik

vorgelegt von

Sebastian Liebschner
geboren am 08.05.1990 in Meerane

Institut für Kern- und Teilchenphysik
Fachrichtung Physik
Fakultät Mathematik und Naturwissenschaften
Technische Universität Dresden
2016

Eingereicht am 15. Juli 2016

Abgeänderte Fassung vom 18. November 2016

1. Gutachter: Prof. Dr. Dominik Stöckinger

2. Gutachter: Prof. Dr. Arno Straessner

Kurzdarstellung

Im Streben der Physik, die fundamentalen Bausteine der Natur zu beschreiben, stellt die Entwicklung des Standardmodells der Teilchenphysik einen Meilenstein dar. Dieses beschreibt alle bekannten Elementarteilchen sowie deren nicht-gravitativ Wechselwirkungen. Neben diesen Erfolgen ist aber auch bekannt, dass es unvollständig ist, da es keine Gravitation oder dunkle Materie beinhaltet. Supersymmetrie ist eine attraktive Erweiterung des Standardmodells, weil sie viele Probleme desselben auf eine elegante Weise löst.

Diese Arbeit untersucht eine supersymmetrische Erweiterung des Standardmodells welche zusätzlich R -symmetrisch ist. Neben der Berechnung von Wirkungsquerschnitten von stark wechselwirkenden supersymmetrischen Teilchen in der führenden Ordnung werden Einschleifenkorrekturen zum Produktionswirkungsquerschnitt von Squarks in diesem Modell berechnet und phänomenologisch ausgewertet.

Abstract

In the ambition of understanding the fundamental mechanisms of nature, the Standard Model of particle physics constitutes a cornerstone in physics. It describes all known elementary particles and their non-gravitational interactions. Besides these successes it is known to be incomplete since it does not include gravity or dark matter. Supersymmetry is an attractive extension of the Standard Model as it solves many problems of it elegantly.

Within this thesis, a supersymmetric model which also exhibits R -symmetry is considered. Besides the calculation of tree-level cross sections for the production of strongly interacting supersymmetric particles, also one-loop corrections to the production cross section of squarks are calculated and phenomenologically analyzed.

Contents

1	Introduction	1
2	The Standard Model	3
2.1	Symmetries and Transformations	3
2.2	The Particles of the Standard Model	5
2.3	Electroweak Symmetry Breaking	8
2.4	Quantization	10
2.5	Lagrangian of the Standard Model	11
3	The Minimal Supersymmetric Standard Model	12
3.1	Supersymmetry as an Extension of the Poincaré Symmetry	12
3.2	A Generic Supersymmetric Model in Superspace Formulation	13
3.3	The Minimal Supersymmetric Standard Model	15
3.3.1	Supersymmetry Breaking and Mass Eigenstates	17
3.3.2	R -Parity	19
4	R-Symmetry	20
4.1	R -Symmetry Transformations	20
4.2	The Minimal R -Symmetric Supersymmetric Standard Model	21
4.3	The R -Symmetric Supersymmetric Quantum Chromodynamics	22
5	Squark and Gluino Production at Tree Level	25
5.1	Partonic Processes and their Cross Section	25
5.2	Hadronic Cross Section	32
5.3	Results for Squark and Gluino Production at Tree-Level	35
6	Virtual and Real Corrections	44
6.1	Virtual Corrections	44
6.2	Real Corrections	46
6.2.1	Real Gluon Radiation	48
6.2.2	Real Quark Radiation	48
7	Renormalization of the MRSSM	50
7.1	Regularization Schemes	50
7.2	Regularization Scheme Dependences	51
7.3	On-Shell Renormalization	53
7.4	Renormalization of the Gauge Coupling	59
7.5	The Beta Function	63

7.6	Supersymmetry Restoring Counterterm	64
7.7	$\overline{\text{MS}}$ - Renormalization	66
7.8	The Renormalization of the Matrix Element	67
7.8.1	Implementation into the Model File	67
7.8.2	The Renormalized Matrix Element	69
8	Squark Production at One-Loop	73
8.1	The LSZ Theorem	73
8.2	The Squark Production Cross Section at Next-to-Leading Order	75
8.2.1	The Setup of the Calculation	76
8.2.2	Remark on Prefactors in the Calculation	77
8.2.3	K -factors for Squark Production in the MRSSM	78
8.2.4	K -factors for Squark Production in the MSSM	82
8.3	The Cross Section in the Limit of Large Sgluon Masses	86
9	Summary	88
10	Appendix	91
10.1	System of Units and Metric	91
10.2	Constants of the Color Algebra $SU(N)$	91
10.3	Weyl Basis and Two-Spinor Notation	92
10.4	Anticommuting Numbers	93
10.5	Feynman Rules for the RSQCD	94
10.6	Passarino-Veltman Integrals	98
10.7	Cross Section and Phase Space Integration	100
11	References	103

1 Introduction

The Standard Model of particle physics is a quantum field theory which relies on the principle of gauge invariance. It describes all known fundamental particles and the non-gravitational interactions among them and predicts the most accurately measured observables in physics. Besides these successes, it is known to be incomplete for example for not including dark matter or a description of gravity. Because of these and other flaws, one studies extensions of the Standard Model. One mathematically very appealing extension is the concept of supersymmetry. Within this framework one often studies the Minimal Supersymmetric Standard Model (MSSM). This theory may provide a candidate for dark matter and elegant solutions of e.g. the hierarchy problem. However, the MSSM does not come without problems. One of these is that supersymmetric particles have not been discovered so far. This is actually reasoned by introducing supersymmetry breaking. However, in order to still solve the hierarchy problem, supersymmetry breaking should not be too large. According to searches for supersymmetry at the Large Hadron Collider (LHC), supersymmetric particles are at the moment on the verge of being too heavy for the MSSM to solve the hierarchy problem without losing its attractiveness. A non-trivial extension of supersymmetry – R -symmetry – may explain this and other issues. R -symmetry is, according to the Haag-Łopuszański-Sohnius theorem, the only conceivable extension of the symmetry group of the MSSM. This is, the combination of Poincaré symmetry, supersymmetry and R -symmetry is the maximal symmetry a reasonable quantum field theory can have.

Motivated by these facts, the Minimal R -Symmetric Supersymmetric Standard Model (MRSSM) is the subject of investigations within this thesis. More specifically, the production cross section of strongly interacting supersymmetric particles in the MRSSM is studied. This is because within supersymmetry strongly interacting particles are the ones which are most likely to be produced at the LHC should supersymmetry at all be realized in nature. It will turn out that there are significant changes in the production of squarks and gluinos when turning from the MSSM to the MRSSM.

This thesis starts with summarizing the main aspects of the Standard Model before the concepts of supersymmetry and R -symmetry are introduced. This includes the introduction of the models which incorporate the minimal form of the symmetry in question. Section 5 compares the production cross sections of squarks and gluinos in both models at tree-level. After identifying an attractive region of parameter space in the MRSSM, it will turn out that the most interesting difference manifests in the channel of squark production. As there are no computer programs available with whom next-to-leading order cross sections within the MRSSM can be calculated, the rest of the thesis focuses on the next-to-leading order calculation of the squark production cross section. Section 6 outlines the structure of the calculation of a next-to-leading order cross section including massless external particles before section 7 gives detailed information about the renormalization of the MRSSM. This includes the explicit form

of required renormalization constants, reaching from the on-shell scheme over a mixture of $\overline{\text{MS}}$ - and zero-momentum subtraction scheme to supersymmetry restoring counterterms. This section also discusses how renormalized one-loop matrix elements are generated as an input for a program which calculates the squark production cross section in the MRSSM. The thesis closes with an explanation of how this very program is constructed and the representation of the next-to-leading order cross section for squark production in the form of K -factors.

2 The Standard Model

The Standard Model of particle physics is the commonly accepted theory describing all known fundamental particles and their non-gravitational interactions. It is a gauge quantum field theory and therefore characterized by its invariance under symmetry groups. The Standard Model contains different fields, whose quantized excitations are interpreted as particles. This chapter summarizes the most important aspects of the Standard Model.

2.1 Symmetries and Transformations

Space-Time Symmetries

The Standard Model is defined on Minkowski space, whose coordinates are labeled with x^μ $\mu \in \{0, 1, 2, 3\}$. As a relativistic theory it is invariant under Poincaré transformations, i.e. it is invariant under Lorentz-transformations (with generators $J^{\mu\nu}$) and translations (with generators P^μ) in space-time. The set of all Poincaré transformations form the Poincaré group, which is a Lie group. Its generators obey the Poincaré algebra

$$\begin{aligned} [P^\mu, P^\nu] &= 0, \\ [P^\mu, J^{\nu\rho}] &= i(g^{\mu\nu} P^\rho - g^{\mu\rho} P^\nu), \\ [J^{\mu\nu}, J^{\rho\sigma}] &= i(g^{\nu\rho} J^{\mu\sigma} + g^{\mu\sigma} J^{\nu\rho} - g^{\mu\rho} J^{\nu\sigma} - g^{\nu\sigma} J^{\mu\rho}). \end{aligned} \quad (2.1)$$

The fields of the Standard Model transform in different representations of the Poincaré group [1].

Gauge Symmetries

In order to describe interactions of matter particles with spin-1 force mediators, gauge theories are used. In the Standard Model matter fields are described by Dirac spinors. The Lagrangian of a free Dirac field reads

$$\mathcal{L}_{\text{Dirac}} = \bar{\Psi}(i\not{\partial} - m)\Psi, \quad (2.2)$$

where m denotes the particle's mass. To include interactions, one imposes a local group symmetry (gauge symmetry) upon this Lagrangian. A spinor transforms under a generic gauge transformation like

$$\Psi(x) \rightarrow U(x)\Psi(x), \quad (2.3)$$

where $U(x)$ is an element of the gauge group in question. Because the gauge group is an unitary matrix Lie group, it can be written like $U(x) = \exp(-igT^a\theta^a(x))$. Here, T^a are the

self-adjoint generators of the associated Lie algebra which obey

$$[T^a, T^b] = if_{abc}T^c, \quad (2.4)$$

with f_{abc} being the structure constants of a Lie algebra, g is the coupling constant of the gauge group and $\theta^a(x)$ are local parameters.

As the parameters of the gauge group are local, the derivative in eq. (2.2) spoils gauge invariance. In order to rectify the gauge invariance of the Lagrangian, one introduces a further field for each index a of the generators, the gauge vector $G^{a\mu}$. Defining the transformation of the matrix valued gauge vector $G^\mu := G^{a\mu}T^a$ as

$$G^\mu(x) \rightarrow U^{-1}(x) \left(G^\mu(x) + \frac{i}{g} \partial^\mu \right) U(x) \quad (2.5)$$

and introducing the gauge covariant derivative

$$D^\mu = \partial^\mu + igT^a G^{a\mu}, \quad (2.6)$$

one finds that the expression $D_\mu \Psi(x)$ transforms as

$$D_\mu \Psi(x) \rightarrow U(x) D_\mu \Psi(x). \quad (2.7)$$

Therefore, gauge invariance is restored in eq. (2.2) by replacing ∂_μ with D_μ . But if the gauge vector is interpreted as a physical field, there must also be a kinetic term associated with it. Using eq. (2.7) one defines the field strength tensor¹ $F^{a\mu\nu}$, whose matrix valued form

$$F^{\mu\nu} = F^{a\mu\nu}T^a := \frac{1}{ig}[D^\mu, D^\nu] = \partial^\mu G^\nu - \partial^\nu G^\mu - gf_{abc}T^c G^{a\mu}G^{b\nu} \quad (2.8)$$

transforms as $F^{\mu\nu} \rightarrow U(x)F^{\mu\nu}U^{-1}(x)$. Using the cyclic property of the trace and the Dynkin index $T(F)$ defined in eq. (10.6) in the Appendix, one can write down a gauge invariant kinetic term for the gauge vector:

$$\mathcal{L}_{\text{gauge}} = -\frac{1}{2}\text{Tr}(F^{\mu\nu}F_{\mu\nu}) = -\frac{T(F)}{2}F^{a\mu\nu}F_{\mu\nu}^a. \quad (2.9)$$

This completes the construction of a Lagrangian which is invariant under non-abelian gauge group transformations. The result is the famous Yang and Mills Lagrangian [3]

$$\mathcal{L}_{\text{Yang-Mills}} = \bar{\Psi}(i\not{D} - m)\Psi - \frac{1}{4}F^{a\mu\nu}F_{\mu\nu}^a \quad (2.10)$$

¹An alternative construction of the field strength tensor makes use of the gauge invariant Wilson loop. This gives some insights into the geometry of gauge transformations [2].

This Lagrangian gives rise to spin- $\frac{1}{2}$ (matter) particles which interact with spin-1 (force mediator) particles. Furthermore if the gauge group is non-abelian, i.e. $f_{abc} \neq 0$, there are self interactions among the spin-1 particles.

The gauge group of the Standard Model is a direct product of the three gauge groups²: $U(1)_Y$, $SU(2)_L$ and $SU(3)_C$. The elements $U(x)$ of those are given in table 2.1.

These gauge groups give rise to three forces: the strong force, the weak force and the electromagnetic force.

Gauge Group	Group Element
$U(1)_Y$	$U(x) = \exp\left(-ig_Y \frac{\hat{Y}}{2} \theta_Y(x)\right)$
$SU(2)_L$	$U(x) = \exp\left(-ig_w \vec{\tau} \cdot \vec{\theta}_w(x)\right)$
$SU(3)_C$	$U(x) = \exp\left(-ig_s T^a \cdot \theta_s^a(x)\right)$

Table 2.1: The table lists the explicit element $U(x)$ of the gauge groups $U(1)_Y$, $SU(2)_L$ and $SU(3)_C$ of the Standard Model. The hypercharge operator \hat{Y} gives the eigenvalue of the hypercharge of the field it is applied to (see table 2.3). $\vec{\tau}$ and T^a are the generators of $SU(2)_L$ and $SU(3)_C$ respectively. In the fundamental representation $\vec{\tau} = \frac{\vec{\sigma}}{2}$ where $\vec{\sigma}$ has the 3 Pauli matrices as components and $T^a = \frac{\lambda^a}{2}$ where λ^a are the 8 Gell-Mann matrices. ε_{abc} and f_{abc} are the structure constants of $SU(2)_L$ and $SU(3)_C$ respectively.

2.2 The Particles of the Standard Model

In the Standard Model different matter particles take part in different interactions, i.e. their corresponding spinor couples to different gauge vectors.

If a spinor couples to a certain gauge vector, it transforms non-trivially under the gauge group which is associated with this gauge vector.³ This means if a particle couples to a certain force, its charge associated with it is non-zero.

The charges of a particle related to a force are defined as the eigenvalues of the generators which correspond to the force.

The Quarks:

Quarks are strongly interacting fermions, which means their spinors transform non trivially under $SU_C(3)$. Because they transform in the fundamental representation of $SU_C(3)$ this means a quark spinor is built up by three spinors each carrying another color. This splitting of the quark spinor in colors is often suppressed for the sake of simplicity. This convention is adopted throughout this thesis.

²The subscripts stand for the associated charge of the respective groups: Y for hypercharge, L for left handedness (weak Isospin I_3) and C for color

³In the Standard Model all matter particles transform in the fundamental (or trivial) representation of gauge groups.

Furthermore, the left handed component of quarks interact weakly, which means that their spinors⁴ transform (in the fundamental representation) under $SU(2)_L$ transformations meaning that two left handed quark spinors are assembled within a doublet.

Finally, all quarks carry a hypercharge. In section 2.3 the mechanism of electroweak symmetry breaking is described. This mechanism explains how electromagnetism arises from the groups $SU(2)_L$ and $U(1)_Y$. All quarks interact electromagnetically.

All together, there are six quarks which are listed in table 2.2. They are categorized in 3 generations because their quantum numbers except for their masses reoccur in each generation. The two types of quarks within a generation which have distinct quantum numbers are referred to as up-type and down-type quarks. The up-type-quark and the down-type quark of the same generation built up a doublet.

The Leptons:

Leptons do not interact strongly. They take part in the weak and the electromagnetic interaction, i.e. their spinors transform non-trivially under the fundamental representation of $SU(2)_L$ and $U(1)_Y$. As for the quarks only the left handed components interact weakly and there are six leptons which are classified into three generations (see table 2.2). In each generation is a lepton with a negative electrical charge and an electrically neutral lepton. The latter ones are referred to as neutrinos. Right handed neutrinos have not been observed (yet) and are therefore absent in the Standard Model. The former are called electron, muon and tau. Each left handed lepton with a negative electric charge is assembled with its neutrino in a doublet.

Particle		1 st Generation		2 nd Generation		3 rd Generation	
u_i	up-type-quark	u	up-quark	c	charm-quark	t	top-quark
d_i	down-type-quark	d	down-quark	s	strange-quark	b	bottom-quark
e_i	charged lepton	e	electron	μ	muon	τ	tau
ν_i	neutrino	ν_e	electron neutrino	ν_μ	muon neutrino	ν_τ	tau neutrino

Table 2.2: The matter particles of the Standard Model. Listed are the symbol and the name of the particles. The labeling of particles has been taken from [4, 5]. The shortcut charged lepton refers to electrically charged leptons.

Quarks and leptons are the matter particles of the Standard Model. They are listed in table 2.3 including their charges for the different forces. Those are the color for strong interactions, the third component of the weak isospin I_3 for weak interactions (the eigenvalue of the third generator of the $SU(2)_L$) and the half of the hypercharge $\frac{Y}{2}$ to obtain the electric charge Q via the Gell-Mann–Nishijima formula: $Q = I_3 + \frac{Y}{2}$.

⁴The left handed part of a 4-spinor Ψ is projected out by the appropriate projector P_L . This is explained in Appendix 10.3.

Because the left- and right-handed parts of spinors transform differently under the $SU_L(2)$ they are listed separately. All quarks occur with three different colors.

In the last row, the Higgs-boson is listed. Its associated field is responsible for the mass of elementary particles. That is explained in section 2.3.

Particle	Symbol	Color	I_3	$\frac{Y}{2}$	Q
left-handed quarks	$q_{iL} = \begin{pmatrix} u_{iL} \\ d_{iL} \end{pmatrix}$	red, green, blue	$\begin{pmatrix} +\frac{1}{2} \\ -\frac{1}{2} \end{pmatrix}$	$+\frac{1}{6}$	$\begin{pmatrix} +\frac{2}{3} \\ -\frac{1}{3} \end{pmatrix}$
right-handed quarks	u_{iR}	red, green, blue	0	$+\frac{2}{3}$	$+\frac{2}{3}$
	d_{iR}	red, green, blue	0	$-\frac{1}{3}$	$-\frac{1}{3}$
left-handed leptons	$\ell_{iL} = \begin{pmatrix} \nu_{iL} \\ e_{iL} \end{pmatrix}$	-	$\begin{pmatrix} +\frac{1}{2} \\ -\frac{1}{2} \end{pmatrix}$	$-\frac{1}{2}$	$\begin{pmatrix} 0 \\ -1 \end{pmatrix}$
right-handed leptons	e_{iR}	-	0	-1	+1
Higgs	H	-	$-\frac{1}{2}$	$+\frac{1}{2}$	0

Table 2.3: This table lists all matter particles in the Standard Model and the Higgs particle with their charges for all forces. This is the color, the weak isospin I_3 , the half of their hypercharge and their electrical charge. The index $i = 1, 2, 3$ labels the generation of the matter particles and is written out in table 2.2. If there are no colors specified or charges are zero this means that the fields in question transform trivially under the pertaining gauge transformation. In fact, the Higgs particle originates from a $SU(2)_L$ -doublet. This is not given here because only the Higgs particle, is a real particle. The other degrees of freedom of the doublet can be absorbed into the longitudinally polarized degrees of freedom of the three massive gauge bosons, see section 2.3.

The Force Particles

Before EWSB			After EWSB		
Group	Coupling Constant	Gauge Field	Coupling Constant	Gauge Field	Particle
$SU(3)_C$	g_s	G_μ^a	g_s	G_μ^a	gluon
$SU(2)_L$	g_w	W_μ^b	$g_W = \sqrt{2}g_w,$ $g_Z = \sqrt{g_w^2 + g_Y^2}$	$W_\mu^\pm,$ Z_μ^0	$W^\pm,$ Z^0 boson
$U(1)_Y$	g_Y	B_μ	$e = g_Y \cdot c_w$	A_μ	photon

Table 2.4: The gauge fields and their coupling constants before and after electro weak symmetry breaking (EWSB), see section 2.3. The Gluon field is not affected by EWSB. $a = 1, \dots, 8$ and $b = 1, 2, 3$ label the number of gauge fields. c_w is the cosine of the electroweak mixing angle defined in 2.3.

The force particles are described by gauge fields. The gauge field of $SU(3)_C$ is the gluon field. Because the $SU_C(3)$ has eight generators there are eight gluons. Their coupling constant is denoted with g_s .

For the other force particles in the Standard Model - the W^\pm bosons, the Z_0 boson and the photon the situation is slightly more involved. They are obtained as a mixture of the W_μ^b ($b = 1, 2, 3$) and the B_μ field which are the gauge fields of $SU(2)_L$ and $U(1)_Y$ respectively. This mixing procedure is explained in section 2.3.

For the moment being, the coupling constants and gauge fields before and after this mixing are quoted in table 2.4.

The Lagrangian of the SM is built up by qualitatively different terms. Firstly there are the kinetic and minimal coupling terms of the matter fields

$$\mathcal{L}_{\text{matter}} = \sum_{i=1}^3 (\bar{\ell}_{iL} i \not{D} l_{iL} + \bar{e}_{iR} i \not{D} e_{iR} + \bar{q}_{iL} i \not{D} q_{iL} + \bar{u}_{iR} i \not{D} u_{iR} + \bar{d}_{iR} i \not{D} d_{iR}), \quad (2.11)$$

where $i \in \{1, 2, 3\}$ labels the generations of matter. The gauge covariant derivative is given by

$$D_\mu = \partial_\mu + ig_Y \frac{\hat{Y}}{2} + ig_w \vec{\tau} \cdot \vec{W}^\mu + ig_s T^a G_a^\mu, \quad (2.12)$$

where for each field the corresponding representation (fundamental or trivial) of the gauge group is to be inserted (see table 2.3). The hypercharge operator \hat{Y} gives the eigenvalue of the hypercharge of the field it is applied to. These can also be found in table 2.3. The kinetic terms of the gauge fields are given by

$$\mathcal{L}_{\text{gauge}} = -\frac{1}{4} F^{\mu\nu} F_{\mu\nu} - \frac{1}{4} W^{a\mu\nu} W_{\mu\nu}^a - \frac{1}{4} G^{a\mu\nu} G_{\mu\nu}^a. \quad (2.13)$$

2.3 Electroweak Symmetry Breaking

So far, no mass terms like in the Dirac Lagrangian (2.2) have been introduced. The reason for this is that they are not gauge invariant, for left- and right-handed spinors transform differently. The same argument forbids terms like $-\frac{m^2}{2} A^\mu A_\mu$ for a generic gauge boson. Electroweak symmetry breaking (EWSB) ascribes masses to those particles [6–12]. To this end one considers a complex scalar doublet

$$\Phi = \begin{pmatrix} \phi^+ \\ \phi^0 \end{pmatrix}, \quad (2.14)$$

which receives a vacuum expectation value (VEV) $\langle \Phi \rangle = \frac{1}{\sqrt{2}} \begin{pmatrix} 0 \\ v \end{pmatrix}$ by the Higgs potential

$$V(\Phi^\dagger \Phi) = -\mu^2 \Phi^\dagger \Phi + \lambda (\Phi^\dagger \Phi)^2 \quad (2.15)$$

where $\mu^2, \lambda > 0$ and v is given by $v = \sqrt{\frac{\mu^2}{\lambda}}$. The Higgs sector of the Standard Model reads

$$\mathcal{L}_{\text{Higgs}} = (D_\mu \Phi)^\dagger (D^\mu \Phi) - V(\Phi^\dagger \Phi). \quad (2.16)$$

The Higgs doublet couples to the gauge fields of $SU(2)_L$ and $U_Y(1)$ in the fundamental representation. Inserting an expansion⁵ around the VEV

$$\Phi = \begin{pmatrix} \phi^+(x) \\ \frac{1}{\sqrt{2}}(v + H(x) + i\sigma(x)) \end{pmatrix} \quad (2.17)$$

one obtains quadratic terms, i.e. mass terms, for the gauge fields in question and the Higgs field H . The mass of the Higgs boson is then given by

$$m_H = \mu. \quad (2.18)$$

In order to obtain mass eigenstates out of B_μ and W_μ^3 and charge eigenstates for Q and I_3 out of W_μ^1 and W_μ^2 one performs the transformation

$$\begin{pmatrix} A_\mu \\ Z_\mu^0 \end{pmatrix} = \begin{pmatrix} \cos \theta_w & \sin \theta_w \\ -\sin \theta_w & \cos \theta_w \end{pmatrix} \begin{pmatrix} B_\mu \\ W_\mu^3 \end{pmatrix}, \quad W_\mu^\pm = \frac{1}{\sqrt{2}}(W_\mu^1 \mp iW_\mu^2), \quad (2.19)$$

where the electroweak mixing angle is given by $\cos \theta_w = \frac{g_w}{\sqrt{g_w^2 + g_Y^2}}$. These gauge fields acquire masses:

$$m_W = \frac{g_w}{2}v, \quad m_Z = \frac{\sqrt{g_w^2 + g_Y^2}}{2}v, \quad m_A = 0. \quad (2.20)$$

Apart from the massive bosons W_μ^\pm and Z_μ^0 one obtains the massless photon A_μ . As the photon is massless it is still associated with a gauge symmetry called $U_{em}(1)$. One therefore often writes EWSB as the breaking of the gauge group $SU(2)_L \times U_Y(1)$ to $U_{em}(1)$.

Matter particles acquire mass via Yukawa couplings to the Higgs doublet. For up-type-quarks, one uses that the charge conjugate of Φ : $\Phi^C = i\sigma^2 \Phi^*$ also transforms like a $SU(2)_L$ doublet.

⁵The complex $\phi^+(x)$ and the real $\sigma(x)$ are the fields of the so-called massless Goldstone bosons. These degrees of freedom can be absorbed in the longitudinally polarized degrees of freedom of the arising gauge bosons W^\pm and Z^0 . This is referred to as unitary gauge [13]. The real $H(x)$ is the Higgs field, whose excitation is the Higgs boson.

The gauge invariant Yukawa Lagrangian is therefore given by

$$\mathcal{L}_{\text{Yukawa}} = - \sum_{i,j=1}^3 (y_{ij}^e \bar{\ell}_L \Phi e_R + y_{ij}^d \bar{q}_L \Phi d_R + y_{ij}^u \bar{q}_L \Phi^C u_R) + h.c., \quad (2.21)$$

where y^e, y^d, y^u are 3×3 matrices in generation space. The fermion mass matrices are therefore:

$$m_{ij}^e = \frac{y_{ij}^e}{\sqrt{2}} v, \quad m_{ij}^d = \frac{y_{ij}^d}{\sqrt{2}} v, \quad m_{ij}^u = \frac{y_{ij}^u}{\sqrt{2}} v. \quad (2.22)$$

The quark mass matrices are not diagonal, which is the precondition of the violation of CP invariance.⁶ One therefore has to distinguish between interaction and mass eigenstates of the quarks. The corresponding transformation matrix is the well known CKM-matrix [14, 15]. Throughout this thesis, the CKM-matrix is approximated with the unit matrix as it will have no influence upon the results.

The upshot of EWSB are masses for all matter particles except for the neutrinos and masses for the gauge bosons W^\pm and Z^0 .

2.4 Quantization

The Quantization of spin-0 and spin- $\frac{1}{2}$ fields yield no complication in the Lagrangian formalism. To quantize spin 1 fields it turns out that the usual gauge invariance needs to be replaced by the so called BRST invariance [16–18]. This results in two extra contributions in the Lagrangian. Firstly there are the gauge fixing terms:

$$\mathcal{L}_{R_\xi} = -\frac{1}{2\xi_A}(\partial^\mu A_\mu)^2 - \frac{1}{\xi_W}|\partial^\mu W_\mu^+ - im_W \xi_W \phi^+|^2 - \frac{1}{2\xi_Z}(\partial^\mu Z_\mu - m_Z \xi_Z \sigma)^2 - \frac{1}{2\xi_G}(\partial^\mu G_\mu^a)^2. \quad (2.23)$$

Here, R_ξ -gauge is chosen, where the parameters ξ_i specify the gauge further. The second and third term are modified with the Goldstone bosons from section 2.3. This is to cancel terms of the form $V_\mu \partial^\mu \phi$ up to a total derivative arising from EWSB which would lead to non-diagonal propagators, where V stands for a gauge boson W^\pm or Z^0 and ϕ for a Goldstone boson.

Secondly, there is a ghost Lagrangian

$$\mathcal{L}_{\text{ghost}} = -\bar{c}_a \partial^\mu (\partial_\mu c_a + g_s f_{abc} c_b G_{c\mu}) + \mathcal{L}_{\text{weak ghosts}}. \quad (2.24)$$

The ghost Lagrangian corresponding to the electroweak sector is not needed within this thesis and due to its lengthy form not quoted here. It can be found in [13]. In eq. (2.24) c_a and \bar{c}_a are the Faddeev-Popov ghosts and antighosts. This fields do not correspond to physical particles because they violate the spin-statistics theorem, i.e. they anticommute while being spin 0

⁶The actual CP-violating term is in the coupling term of quarks to the W -bosons.

fields. Ghost fields are an elegant way of accounting for an additional term in the Lagrangian of non-abelian gauge fields which is best seen in the path integral quantization [2].

2.5 Lagrangian of the Standard Model

The complete Lagrangian of the Standard Model reads

$$\mathcal{L}_{\text{SM}} = \mathcal{L}_{\text{matter}} + \mathcal{L}_{\text{gauge}} + \mathcal{L}_{\text{Higgs}} + \mathcal{L}_{\text{Yukawa}} + \mathcal{L}_{R_\xi} + \mathcal{L}_{\text{ghost}} \quad (2.25)$$

with the corresponding parts of the previous chapters. For further reading and the electroweak Lagrangian given completely in terms of physical fields, see [13].

3 The Minimal Supersymmetric Standard Model

Even though the Standard Model is a very well working machinery which has been tested to an impressive accuracy it is not the ultimate theory of nature. This is not only because of its incompleteness regarding gravity but also because of its missing incorporation of dark matter. This is that astrophysical observations [19] indicate that only 4.9% of the universe's mass energy consist of ordinary matter while the majority is represented by 26.8% of dark matter and 68.3% of dark energy. Another puzzle is the hierarchy problem which questions the large difference between the Higgs boson mass and its quantum correction, see [20]. Finally, the gauge groups of the Standard Model cannot be unified to a theoretically appealing single gauge group at some high energy scale for the three gauge couplings do not meet at any renormalization scale [20]. There are many other problems which are not mentioned here [5]. Supersymmetry provides a possible extension of the Standard Model. It constitutes a mathematically very aesthetic solution of the above mentioned problems⁷. This section explains briefly the mechanism of supersymmetry and the minimal supersymmetric extension of the Standard Model (MSSM).

3.1 Supersymmetry as an Extension of the Poincaré Symmetry

As already seen in the previous chapter, symmetries are of vital importance when studying particle physics. Coleman and Mandula [21] found that for any reasonable quantum field theory space-time and internal symmetries, i.e. gauge symmetries “cannot be combined in any but the trivial way” [22]. Ergo, the symmetry groups of the Standard Model are the most general ones.

This statement was corrected by the Haag-Łopuszański-Sohnius theorem [23] which weakened the condition of the quantum field theory by allowing also for anticommuting symmetry generators. This is, by introducing the generators Q_α and $\bar{Q}^{\dot{\alpha}}$ with $\alpha, \dot{\alpha} \in \{1, 2\}$, the Poincaré algebra eq. (2.1) can be nontrivially extended to the so called superalgebra (see Appendix (10.3) for the definition of the σ -matrices):

$$\begin{aligned} \{Q_\alpha, Q_\beta\} &= \{\bar{Q}_{\dot{\alpha}}, \bar{Q}_{\dot{\beta}}\} = 0, \\ \{Q_\alpha, \bar{Q}_{\dot{\alpha}}\} &= 2\sigma_{\alpha\dot{\alpha}}^\mu P_\mu, \\ [P^\mu, Q_\alpha] &= [P^\mu, \bar{Q}_{\dot{\alpha}}] = 0, \\ [Q_\alpha, J^{\mu\nu}] &= \frac{1}{2}(\sigma^{\mu\nu})_\alpha{}^\beta Q_\beta. \end{aligned} \tag{3.1}$$

As $J^{\mu\nu}$ is the generalized angular momentum operator, the last line in eq. (3.1) implies that Q_α is a spin- $\frac{1}{2}$ operator. Applying Q_α to a field will change the spin of it by $\frac{1}{2}$. This means

⁷In its minimal extension to the Standard Model supersymmetry does not incorporate gravity but many quantum gravity models are supersymmetric.

supersymmetry generators convert fermions to bosons and vice versa.

The superalgebra in eq. (3.1) is actually the smallest extension of the Poincare algebra as it is possible to introduce further anticommuting symmetry generators. Their maximal number is fixed to $N = 8$. Because the MSSM is a minimal extension of the Standard Model, it deals with only one set of anticommuting symmetry generators and is therefore referred to be a $N = 1$ supersymmetric theory.

A representation in the form of differential operators can be given by introducing superspace. Superspace is a manifold obtained by enlarging Minkowski space, whose coordinates are labeled with x^μ , with four anticommuting numbers: θ^α and $\bar{\theta}^{\dot{\alpha}}$, where $\alpha, \dot{\alpha} \in \{1, 2\}$ (see Appendix 10.4 for the definition of anticommuting numbers). A representation of the superalgebra reads

$$\begin{aligned} P^\mu &= i\partial^\mu, \\ J^{\mu\nu} &= i(x^\mu\partial^\nu - x^\nu\partial^\mu), \\ Q_\alpha &= i(\partial_\alpha + i\sigma_{\alpha\dot{\alpha}}^\mu\bar{\theta}^{\dot{\alpha}}\partial_\mu), \\ \bar{Q}_{\dot{\alpha}} &= i(-\bar{\partial}_{\dot{\alpha}} - i\theta^\alpha\sigma_{\alpha\dot{\alpha}}^\mu\partial_\mu). \end{aligned} \quad (3.2)$$

3.2 A Generic Supersymmetric Model in Superspace Formulation

This chapter outlines the generic ingredients and terms of a supersymmetric model. To this end it is practical to work in the language of superspace and superfields. Superfields are functions on superspace.

The superfields⁸ relevant for the MSSM are the chiral superfield $\hat{\Phi}$, the antichiral superfield $\hat{\bar{\Phi}}$ and the vector superfield \hat{V} . Chiral superfields are defined by the restriction $\bar{\mathcal{D}}_{\dot{\alpha}}\hat{\Phi} = 0$, antichiral superfields by $\mathcal{D}_\alpha\hat{\bar{\Phi}} = 0$ (see Appendix 10.4 for the definition of chiral covariant derivatives) and vector superfields by the condition of being real $\hat{V}^\dagger = \hat{V}$.

All superfields can be decomposed into component fields on Minkowski space. The component decomposition of the above fields read⁹

$$\begin{aligned} \hat{\Phi}(x, \theta, \bar{\theta}) &= A(x) + \sqrt{2}\theta\psi(x) + \theta\theta F(x) - i\theta\sigma^\mu\bar{\theta}\partial_\mu A(x) - \frac{1}{4}\theta\theta\bar{\theta}\bar{\theta}\partial_\mu\partial^\mu A(x) - \frac{i}{\sqrt{2}}\theta\theta\bar{\theta}\bar{\sigma}^\mu\partial_\mu\psi(x), \\ \hat{\bar{\Phi}}(x, \theta, \bar{\theta}) &= A^\dagger(x) + \sqrt{2}\bar{\theta}\bar{\psi}(x) + \bar{\theta}\bar{\theta}F^\dagger(x) + i\theta\sigma^\mu\bar{\theta}\partial_\mu A^\dagger(x) - \frac{1}{4}\theta\theta\bar{\theta}\bar{\theta}\partial_\mu\partial^\mu A^\dagger(x) - \frac{i}{\sqrt{2}}\bar{\theta}\bar{\theta}\theta\sigma^\mu\partial_\mu\bar{\psi}(x), \\ \hat{V}(x, \theta, \bar{\theta}) &= \theta\sigma^\mu\bar{\theta}v_\mu + i\theta\theta\bar{\theta}\bar{\lambda}(x) - i\bar{\theta}\bar{\theta}\theta\lambda(x) + \frac{1}{2}\theta\theta\bar{\theta}\bar{\theta}D(x), \end{aligned} \quad (3.3)$$

where $A(x)$ and $F(x)$ are complex scalar fields, $\psi(x)$ and $\lambda(x)$ are left-handed Weyl spinors, $D(x)$ is a real scalar field and v_μ is a vector field.

⁸Superfields are labeled with a hat throughout this thesis.

⁹For the vector superfield Wess-Zumino-gauge is applied.

The superfields transform under a generic gauge transformation as

$$\begin{aligned}\hat{\Phi} &\rightarrow e^{-2ig\hat{\Lambda}}\hat{\Phi}, \\ \hat{\bar{\Phi}} &\rightarrow \hat{\bar{\Phi}}e^{2ig\hat{\Lambda}}, \\ e^{2g\hat{V}} &\rightarrow e^{-2ig\hat{\Lambda}}e^{2g\hat{V}}e^{2ig\hat{\Lambda}},\end{aligned}\tag{3.4}$$

where $\hat{\Lambda} = \hat{\Lambda}^a T^a$ and $\hat{V} = \hat{V}^a T^a$. $\hat{\Lambda}^a$ is an arbitrary chiral superfield, the T^a are the generators of the gauge group in question and g is the gauge coupling constant of the gauge group.

One can therefore construct the important gauge invariant term $\int d^4\theta \hat{\bar{\Phi}}e^{2g\hat{V}}\hat{\Phi}$. If one introduces the gauge covariant derivative $D_\mu = \partial + igT^a v_\mu^a$ its component decomposition reads

$$\begin{aligned}\int d^4\theta \hat{\bar{\Phi}}e^{2g\hat{V}}\hat{\Phi} &= F^\dagger F + (D_\mu A)^\dagger (D^\mu A) + \bar{\psi}\bar{\sigma}^\mu i D_\mu \psi \\ &\quad - \sqrt{2}g \left(-i(A^\dagger T^a A)\lambda^a + i\bar{\lambda}^a (AT^a A^\dagger) \right) + g(A^\dagger T^a A)D^a.\end{aligned}\tag{3.5}$$

Therefore this term gives rise to the kinetic terms of the components of the chiral and antichiral superfields A , A^\dagger , ψ and $\bar{\psi}$ as well as their minimal coupling to the gauge fields v_μ^a and their superpartners λ^a and $\bar{\lambda}^a$ and terms involving the auxiliary fields F , F^\dagger and D .

With the field-strength chiral superfields $\hat{W}_\alpha := -\frac{1}{4}\overline{D}\overline{D}(e^{-2gV}\mathcal{D}_\alpha e^{2gV})$ one can write down a gauge invariant term yielding the kinetic terms of the gauge fields and their superpartners:

$$\int d^2\theta \frac{1}{16g^2} \hat{W}^{\alpha a} \hat{W}_\alpha^a + h.c. = \frac{1}{2} D^a D^a - \frac{1}{4} F_{\mu\nu}^a F^{a\mu\nu} + \frac{i}{2} \bar{\lambda}^a \bar{\sigma}^\mu (D_\mu \lambda^a) + \frac{i}{2} \lambda^a \sigma^\mu (D_\mu \bar{\lambda}^a).\tag{3.6}$$

A third generic term in a supersymmetric theory arises from the superpotential $W(\hat{\Phi})$ which is a holomorphic function in the chiral superfields:

$$\int d^2\theta W(\hat{\Phi}).\tag{3.7}$$

A renormalizable superpotential is given by $W(\hat{\Phi}) = c_i \hat{\Phi} + \frac{m_{ij}}{2} \hat{\Phi}_i \hat{\Phi}_j + \frac{g_{ijk}}{3!} \hat{\Phi}_i \hat{\Phi}_j \hat{\Phi}_k$. The component decomposition of the corresponding terms is

$$\begin{aligned}\int d^2\theta \hat{\Phi}_1 &= F_1, \\ \int d^2\theta \hat{\Phi}_1 \hat{\Phi}_2 &= A_1 F_2 + F_1 A_2 - \psi_1 \psi_2, \\ \int d^2\theta \hat{\Phi}_1 \hat{\Phi}_2 \hat{\Phi}_3 &= F_1 A_2 A_3 + A_1 F_2 A_3 + A_1 A_2 F_3 - A_1 \psi_2 \psi_3 - \psi_1 A_2 \psi_3 - \psi_1 \psi_2 A_3.\end{aligned}\tag{3.8}$$

The Lagrangian for a supersymmetric theory is therefore given by

$$\begin{aligned}\mathcal{L}_{\text{SUSY}} &= \mathcal{L}_{\text{matter}} + \mathcal{L}_{\text{gauge}} + \mathcal{L}_{\text{superpot}} \\ &= \int d^4\theta \hat{\Phi} e^{2g\hat{V}} \hat{\Phi} + \left(\int d^2\theta \frac{1}{16g^2} \hat{W}^{\alpha a} \hat{W}_\alpha^a + h.c. \right) + \left(\int d^2\theta W(\hat{\Phi}) + h.c. \right)\end{aligned}\quad (3.9)$$

Observing the component decomposition eq. (3.5), (3.6) and (3.8) of the three parts of this Lagrangian one observes that the F and D fields have no kinetic term and are therefore auxiliary fields which can be eliminated by their equation of motion $\frac{\partial \mathcal{L}}{\partial \phi} = \partial_\mu \frac{\partial \mathcal{L}}{\partial (\partial_\mu \phi)}$ with $\phi \in \{F, D\}$. Doing this one obtains

$$\begin{aligned}\mathcal{L}_D &= \frac{1}{2} D^a D^a + g A^\dagger T^a D^a A \quad \Rightarrow \quad D^a = -A^\dagger T^a A, \\ \mathcal{L}_D &= -\frac{1}{2} (A^\dagger T^a A)^2.\end{aligned}\quad (3.10)$$

and

$$\begin{aligned}\mathcal{L}_F &= F_i^\dagger F_i + \left(c_i F_i + m_{ij} F_i A_j + \frac{g_{ijk}}{2} F_i A_j A_k + h.c. \right) \quad \Rightarrow \quad F_i^\dagger = -\frac{\partial W(A)}{\partial A_i} \\ \mathcal{L}_F &= -\left| \frac{\partial W(A)}{\partial A_i} \right|^2\end{aligned}\quad (3.11)$$

3.3 The Minimal Supersymmetric Standard Model

After having introduced components of a generic supersymmetric model a possible realization of supersymmetry in nature - the Minimal Supersymmetric Standardmodel (MSSM) - is discussed in this section. The field content of the MSSM is summarized in table 3.1. In comparison to the Standard Model each particle has a superpartner which differs in its spin by $\frac{1}{2}$. The superpartners of fermions have Spin 0 and are referred to as sfermions. The name of each sfermion is given by the name of its Standard Model partner with an additional “s-” in front of it, e.g. selectron or up-squark. The superpartners of bosons have spin $\frac{1}{2}$ and get an additional “-ino” at the end of their name, e.g. Higgsino as the superpartner of the Higgs or bino as superpartner of the B -boson.

Apart from this doubling of the field content of the Standard Model, there is one modification within the Higgs sector, i.e. there are two instead of one Higgs superfield. These are necessary to avoid an anomaly in the electroweak gauge symmetry and to give masses to both up- and down-type quarks [20, page 8].

Note that the “chirality” of sfermions is understood to be the chirality of their superpartners. Of course scalar particles have no chirality.

Superfield	Components	$SU(3)_C \times SU(2)_L \times U(1)_Y$
$\hat{\Phi}$	A, ψ	
\hat{V}	λ, v_μ	
\hat{Q}	$\tilde{q}_L = \begin{pmatrix} \tilde{u}_L \\ \tilde{d}_L \end{pmatrix}, q_L = \begin{pmatrix} u_L \\ d_L \end{pmatrix}$	$(3, 2, \frac{1}{6})$
\hat{U}	\tilde{u}_R^\dagger, u_R	$(3^*, 1, -\frac{2}{3})$
\hat{D}	\tilde{d}_R^\dagger, d_R	$(3^*, 1, +\frac{1}{3})$
\hat{L}	$\tilde{l}_L = \begin{pmatrix} \tilde{\nu}_L \\ \tilde{e}_L \end{pmatrix}, l_L = \begin{pmatrix} \nu_L \\ e_L \end{pmatrix}$	$(1, 2, -\frac{1}{2})$
\hat{E}	\tilde{e}_R^\dagger, e_R	$(1, 1, 1)$
\hat{H}_d	H_d, \tilde{H}_d	$(1, 2, -\frac{1}{2})$
\hat{H}_u	H_u, \tilde{H}_u	$(1, 2, +\frac{1}{2})$
\hat{V}_Y	λ_Y, B_μ	$(1, 1, 0)$
\hat{V}_w^a	λ_w^a, W_μ^a	$(1, 3, 0)$
\hat{V}_s^a	λ_s^a, G_μ^a	$(8, 1, 0)$

Table 3.1: The table shows the field content of the MSSM in terms of the superfields and their components. The first two lines show the decomposition of the generic superfields (cf. eq. (3.3)).

The third column shows the representation in which the fields transform under $SU(3)_C$ and $SU(2)_L$ transformations and in which the generator in the covariant derivative needs to be inserted as well as the charges of the fields for $U(1)_Y$. For $SU(3)_C$ the “8” refers to the adjoint representation (see Appendix 10.2), the “3” to the fundamental and the “3*” to the antifundamental representation $T_{antifund}^a = -\frac{\lambda^a}{2}$. For $SU(2)_L$ “3” refers to the adjoint representation and “2” to the fundamental representation. For both $SU(2)_L$ and $SU(3)_C$ a “1” indicates the the trivial representation.

The Lagrangian¹⁰ for the MSSM reads

$$\begin{aligned}
\mathcal{L}_{\text{MSSM}} = & \int d^4\theta \left[\hat{Q} e^{2g_Y \hat{V}_Y + 2g_w \hat{V}_w + 2g_s \hat{V}_s} \hat{Q} + \hat{U} e^{2g_Y \hat{V}_Y + 2g_w \hat{V}_w - 2g_s \hat{V}_s^T} \hat{U} + \hat{D} e^{2g_Y \hat{V}_Y + 2g_w \hat{V}_w - 2g_s \hat{V}_s^T} \hat{D} \right. \\
& + \hat{L} e^{2g_Y \hat{V}_Y + 2g_w \hat{V}_w} \hat{L} + \hat{E} e^{2g_Y \hat{V}_Y + 2g_w \hat{V}_w} \hat{E} \\
& \left. + \hat{H}_d e^{2g_Y \hat{V}_Y + 2g_w \hat{V}_w} \hat{H}_d + \hat{H}_u e^{2g_Y \hat{V}_Y + 2g_w \hat{V}_w} \hat{H}_u \right] \\
& + \int d^2\theta \left[\frac{1}{16g_Y^2} \hat{W}_Y^\alpha \hat{W}_{Y\alpha} + \frac{1}{16g_w^2} \hat{W}_w^{a\alpha} \hat{W}_{w\alpha}^a + \frac{1}{16g_s^2} \hat{W}_s^{a\alpha} \hat{W}_{s\alpha}^a \right] + h.c. \\
& + \int d^2\theta W_{\text{MSSM}} + h.c. \\
& + \mathcal{L}_{\text{soft}}.
\end{aligned} \tag{3.12}$$

Apart from the kinetic and minimal coupling terms in the first four lines of eq. (3.12) and the

¹⁰This is the Lagrangian on the classical level, i.e. there are neither gauge fixing nor ghost terms.

soft breaking part of the Lagrangian in the last line of eq. (3.12) which will be discussed in section 3.3.1, there is a superpotential W_{MSSM} :

$$W_{\text{MSSM}} = y_d \hat{H}_d \hat{Q} \hat{D} + y_u \hat{H}_u \hat{Q} \hat{U} + y_e \hat{H}_d \hat{L} \hat{E} - \mu \hat{H}_d \hat{H}_u, \quad (3.13)$$

which will in regard of its form be justified in section 3.3.2. After eliminating auxiliary fields the Higgs potential is generated. In contrast to the Standard Model, the quadrilinear term in the Higgs potential is given in terms of the gauge couplings and is therefore no independent parameter. From the Higgs potential both H_u and H_d acquire a vacuum expectation value:

$$\langle H_u \rangle = \frac{1}{\sqrt{2}} \begin{pmatrix} 0 \\ v_u \end{pmatrix} \quad \langle H_d \rangle = \frac{1}{\sqrt{2}} \begin{pmatrix} v_d \\ 0 \end{pmatrix} \quad (3.14)$$

whose quotient is an important parameter of the electroweak MSSM.

$$\tan \beta := \frac{v_u}{v_d} \quad (3.15)$$

As in the Standard Model this spontaneous symmetry breaking and the presence of Yukawa-terms (first three terms of eq. (3.13)) lead to masses of the fermions.¹¹ Apart from that there are also other terms like quark-squark-Higgsino interactions. In addition there is the μ -term which is responsible for Higgsino and Higgs masses.

3.3.1 Supersymmetry Breaking and Mass Eigenstates

In order to explain why supersymmetric particles have not been found so far, supersymmetry has to be broken. Like in electroweak symmetry breaking supersymmetry is preserved at some high energy scale but its vacuum state is not supersymmetric. However there is no consensus on how supersymmetry is broken. But by ignoring the exact mechanism and parameterizing it by introducing appropriate terms in the Lagrangian one accounts for it in an absolutely viable way.

Terms which break supersymmetry should be soft, i.e. they should have coupling constants

¹¹Note the sum convention of $SU_L(2)$ doublets: $\hat{H}_u \hat{Q} = (\hat{H}_u)_\alpha \hat{Q}_\beta \epsilon^{\alpha\beta}$ to ensure gauge invariance (see Appendix 10.3 for the definition of $\epsilon^{\alpha\beta}$). This convention was not used in the Standard Model.

with positive mass dimension.

$$\begin{aligned}
\mathcal{L}_{\text{soft}} = & -M_Q^2 |\tilde{q}_L|^2 - M_U^2 |\tilde{u}_R|^2 - M_D^2 |\tilde{d}_R|^2 \\
& - M_L^2 |\tilde{l}_L|^2 - M_E^2 |\tilde{e}_R|^2 - M_{H_d}^2 |H_d|^2 - M_{H_u}^2 |H_u|^2 \\
& + \frac{1}{2} (M_1 \lambda_Y \lambda_Y + M_2 \lambda_w^a \lambda_w^a + M_3 \lambda_s^a \lambda_s^a) + h.c. \\
& - \left(A_d y_d H_d \tilde{q}_L \tilde{d}_R^\dagger + A_u y_u H_u \tilde{q}_L \tilde{u}_R^\dagger + A_e y_e H_d \tilde{l}_L \tilde{e}_R^\dagger - B \mu H_d H_u \right) + h.c.
\end{aligned} \tag{3.16}$$

The soft breaking terms in the MSSM comprise masses of the squarks, sleptons, Higgs-bosons and gauginos. The last line in eq. (3.16) resembles the superpotential in eq. (3.13). In fact the only two differences are that the superfields are replaced by their scalar components and that additional parameters with mass dimension one have been added. A_d , A_u , A_e are 3×3 matrices in family space.

There are fields in the MSSM which are no eigenstate of the mass operator $P^\mu P_\mu$ but have a mass matrix which is non-diagonal. This is true for neutral Higgsinos and gauginos which mix to neutralinos and charged Higgsinos and gauginos which mix to charginos to yield physical particles with definite mass. However, for this thesis only the mass matrix for electrically charged sfermions is given because this will change significantly when introducing R -symmetry in the next section. The Lagrangian describing these masses reads

$$\mathcal{L}_{m_{\tilde{q}}, m_{\tilde{e}}} = - \begin{pmatrix} \tilde{u}_L^\dagger & \tilde{u}_R^\dagger \end{pmatrix} M_u^2 \begin{pmatrix} \tilde{u}_L \\ \tilde{u}_R \end{pmatrix} - \begin{pmatrix} \tilde{d}_L^\dagger & \tilde{d}_R^\dagger \end{pmatrix} M_d^2 \begin{pmatrix} \tilde{d}_L \\ \tilde{d}_R \end{pmatrix} - \begin{pmatrix} \tilde{e}_L^\dagger & \tilde{e}_R^\dagger \end{pmatrix} M_e^2 \begin{pmatrix} \tilde{e}_L \\ \tilde{e}_R \end{pmatrix}. \tag{3.17}$$

where the mass matrix is given by

$$M_f^2 = \begin{pmatrix} M_{fLL}^2 & m_f X_f^* \\ m_f X_f & M_{fRR}^2 \end{pmatrix}. \tag{3.18}$$

The diagonal terms are given by the sum of the fermion mass squared m_f^2 , the appropriate soft breaking term (e.g. M_Q^2 for left handed squarks) and a contribution from the elimination of D -fields. In fact, this last term splits the masses of fermions and sfermions already without explicit supersymmetry breaking. This is because the generation of fermion masses requires the breaking of gauge symmetry which is not possible without breaking supersymmetry. However the off-diagonal terms are given by

$$X_f = A_f + \mu^* \{\cot \beta, \tan \beta\} \tag{3.19}$$

with $\cot \beta$ for up-type sfermions and $\tan \beta$ for down-type sfermions and $A_f \in \{A_d, A_u, A_e\}$.

3.3.2 R -Parity

The MSSM does not include any terms which violate baryon (B) or lepton number (L)¹² like

$$W_{\Delta B=1} = \lambda \hat{U} \hat{D} \hat{D} \quad \text{or} \quad W_{\Delta L=1} = \lambda' \hat{L} \hat{Q} \hat{D} \quad (3.20)$$

in the superpotential although this would be possible from the perspective of gauge invariance and renormalizability. However, this has not been observed experimentally. The most famous constraint on them is the non-observation of proton decay which restricts at least one of the parameters λ or λ' to be extremely small [20]. Forbidding these terms by postulating a conservation of B and L might not be the best solution since both B and L are known to be violated in nature by non-perturbative effects [24].

A possible way out is the postulation of the conservation of R -parity

$$P_R = (-1)^{3(B-L)+2s} \quad (3.21)$$

where s is the spin of the particle on which the R -parity operator is applied to. R -parity is a multiplicative quantum number which is constructed to be +1 for each Standard Model particle and -1 for each supersymmetric partner. Apart from the prohibition of the terms in eq. (3.20) this has important consequences:

- There has to be a lightest supersymmetric particle (LSP) which is absolutely stable. This is a candidate for dark matter.
- At colliders like the LHC there must always be an even number of supersymmetric particles be produced, if at all.

The superpotential of the MSSM (see, eq. (3.13)) is chosen in such a way that it is the only renormalizable and gauge invariant potential which respects R -parity.

¹²The chiral superfield \hat{Q} carries baryon number $\frac{1}{3}$, whereas $B = -\frac{1}{3}$ for \hat{D} , \hat{U} and $B = 0$ for all other superfields. The only multiplets carrying a non-zero lepton number are \hat{L} with $L = 1$ and \hat{E} with $L = -1$.

4 *R*-Symmetry

R-symmetry is an additional continuous symmetry which extends supersymmetry in a non-trivial way. This is actually covered in the Haag-Łopuszański-Sohnius theorem [23] but often concealed.

This section introduces *R*-symmetry and discusses briefly a minimal viable extension of the MSSM including *R*-symmetry, the MRSSM. Thereby some general features of the model are mentioned before the focus is laid on the strongly interacting sector which is the central topic of the thesis.

4.1 *R*-Symmetry Transformations

For a $N = 1$ supersymmetric theory, *R*-symmetry is a global $U(1)$ symmetry. It must not be confused with *R*-parity which is a discrete \mathbb{Z}_2 symmetry. A continuous global symmetry implies according to Noether's theorem a conserved charge. In the case of *R*-symmetry it is called *R*-charge and one therefore refers to *R*-symmetry as $U_R(1)$.

The defining property of $U_R(1)$ is that the anticommuting coordinates θ^α and $\bar{\theta}^{\dot{\alpha}}$ transform like

$$\theta \rightarrow e^{i\tau} \theta, \quad \bar{\theta} \rightarrow e^{-i\tau} \bar{\theta}, \quad (4.1)$$

where τ parametrizes the transformation. This in turn implies that the supersymmetry generators (see eq. (3.2)) transform like

$$Q \rightarrow e^{-i\tau} Q \quad \bar{Q} \rightarrow e^{i\tau} \bar{Q} \quad (4.2)$$

and *R*-symmetry does not commute with supersymmetry

$$[R, Q] = -Q \quad [R, \bar{Q}] = \bar{Q}, \quad (4.3)$$

meaning that superpartners do not have the same *R*-charge. The transformation of chiral and vector superfields reads

$$\begin{aligned} \hat{\Phi}(x, \theta, \bar{\theta}) &\rightarrow e^{ir_{\hat{\Phi}}\tau} \hat{\Phi}(x, e^{i\tau}\theta, e^{-i\tau}\bar{\theta}), \\ \hat{V}(x, \theta, \bar{\theta}) &\rightarrow \hat{V}(x, e^{i\tau}\theta, e^{-i\tau}\bar{\theta}), \end{aligned} \quad (4.4)$$

i.e. the chiral superfields transform with arbitrary *R*-charge where the *R*-charge of vector superfield is restricted to be zero by the condition that they are real. If one inserts the component decomposition eq. (3.3) of the superfields one can read off the *R*-charges of the component fields, see table 4.1.

Superfield		Boson		Fermion	
$\hat{\Phi}$	$r_{\hat{\Phi}}$	A	$r_{\hat{\Phi}}$	ψ	$r_{\hat{\Phi}} - 1$
\hat{V}	0	v^μ	0	λ	+1

Table 4.1: This table shows the R -charges of a generic chiral and vector superfield.

4.2 The Minimal R -Symmetric Supersymmetric Standard Model

If one imposes R -symmetry upon the MSSM one is faced with a certain arbitrariness, i.e. the choice of the R -charges of the chiral superfields. A minimal R -symmetric extension of the MSSM is the minimal R -symmetric supersymmetric Standard Model (MRSSM) [25]. In this model the R -charges are chosen in such a way, that every Standard Model particle has R -charge zero. Following this one obtains the R -charges of all particles which are summed up in table 4.2 [26].

Field	Superfield		Boson		Fermion	
gauge Vector matter	$\hat{V}_s^a, \hat{V}_w^a, \hat{V}_Y$	0	G_μ^a, W_μ^a, B_μ	0	$\lambda_s^a, \lambda_w^a, \lambda_Y$	+1
	\hat{L}, \hat{E}	+1	$\tilde{l}_l, \tilde{e}_R^\dagger$	+1	l_L, e_R	0
	$\hat{Q}, \hat{D}, \hat{U}$	+1	$\tilde{q}_L, \tilde{d}_R^\dagger, \tilde{u}_R^\dagger$	+1	q_L, d_R, u_R	0
H -Higgs	$\hat{H}_{d,u}$	0	$H_{d,u}$	0	$\tilde{H}_{d,u}$	-1
R -Higgs	$\hat{R}_{d,u}$	+2	$R_{d,u}$	+2	$\tilde{R}_{d,u}$	+1
adjoint chiral	$\hat{O}, \hat{T}, \hat{S}$	0	σ^a, ω^a, ρ	0	$\chi_s^a, \chi_w^a, \chi_Y$	-1

Table 4.2: This table lists the R -charges of all superfields and their components in the MRSSM. The fields of the R -Higgs and the adjoint chiral superfields are not present in the MSSM.

The gauge, matter and H -Higgs fields are the fields of the MSSM. Below the thin horizontal line, one finds the fields which are not present in the MSSM, i.e. the R -Higgs and adjoint chiral fields. These occur for the following reason.

In the MSSM the gauginos are Majorana particles. Their mass terms reads in two-spinor notation

$$\mathcal{L}_{\text{Majorana mass}} = -m\lambda\lambda + h.c. \quad (4.5)$$

which is not R -invariant because the Weyl fermion λ has R -charge +1. Giving no mass to the gauginos is phenomenologically not possible. The only way to account for a fermion mass is to write down a Dirac mass term

$$\mathcal{L}_{\text{Dirac mass}} = -m\chi\lambda + h.c., \quad (4.6)$$

where χ is another Weyl spinor. This means that the four-spinor of every gaugino is a Dirac instead of a Majorana spinor, e.g. for the gluino:

$$\tilde{g}_{\text{MSSM}} = \begin{pmatrix} -i\lambda_s \\ +i\bar{\lambda}_s \end{pmatrix} \quad \tilde{g}_{\text{MRSSM}} = \begin{pmatrix} -i\lambda_s \\ +i\bar{\chi}_s \end{pmatrix}. \quad (4.7)$$

In order to get a *R*-symmetric mass term one has to choose the *R*-charge of the new Weyl spinor χ to be the opposite of λ .

This explains the necessity of enlarging the field content if one imposes *R*-symmetry.

Of course the new Weyl-spinor χ must have also a superpartner. One chooses this superpartner to be a scalar, i.e. the additional Weyl fermion comes from a chiral superfield. In order to maintain gauge invariance, this chiral superfield has to transform in the adjoint representation, hence the name adjoint chiral in table 4.2. To fix notation the component decomposition of the eight chiral supermultiplets associated to the gluons is given by

$$\hat{O}^a(x, \theta, \bar{\theta}) = \sigma^a + \sqrt{2}\theta i\chi_s^a + \dots \quad a = 1, \dots, 8. \quad (4.8)$$

The scalar components σ^a are referred to as scalar gluons and the Weyl spinors χ^a are called octinos.

The same argument as for the adjoint chiral superfields explains the existence of additional Higgs-superfields which are referred to as *R*-Higgs fields.

Apart from these extensions *R*-symmetry also forbids terms which are allowed by supersymmetry. For the above choice of *R*-charges the μ -term in (3.13) and the *A*-terms in the last line of (3.16) are absent in the MRSSM. Inspecting eq. (3.19) implies that there is no squark mixing in the MRSSM. As a consequence terms which allow flavor violating processes like $\mu \rightarrow e\gamma$ in the MSSM are suppressed in the MRSSM [25]. Quite interestingly Dirac gauginos can be heavier than Majorana gauginos without being less natural in view of the hierarchy problem [27–30]. This is because the (one-loop) beta function of the squark mass does not depend on the gluino mass.¹³ Finally the production cross section of strongly interacting particles is suppressed [29, 31]. It is this last feature which is going to be observed further in this thesis. To this end the colored sector of the MRSSM is now considered in more detail.

4.3 The *R*-Symmetric Supersymmetric Quantum Chromodynamics

The subject of this thesis is the phenomenology of the strongly coupling sector of the MRSSM. The *R*-symmetric supersymmetric quantum chromodynamics (RSQCD) is therefore considered

¹³If $m_{\tilde{q}}$ is evolved via renormalization group equation to smaller energies, $m_{\tilde{g}}$ is in the MSSM responsible for an increase of $m_{\tilde{q}}$. At a high energy scale, all masses of supersymmetric particles are considered as equal, which forces $m_{\tilde{g}}$ in the MSSM to be “small” in order to ensure a not too high squark mass at the EWSB-scale. A too high $m_{\tilde{g}}$ would spoil the solution to the hierarchy problem. This $m_{\tilde{g}}$ dependence is absent in the MRSSM, which imposes no restriction on $m_{\tilde{g}}$, in this respect.

closer. Its Lagrangian for an arbitrary massless quark reads

$$\begin{aligned} \mathcal{L}_{\text{RSQCD}} = & \int d^4\theta \left(\hat{\bar{Q}}_L e^{2g_s \hat{V}_s} \hat{Q}_L + \hat{\bar{Q}}_R e^{-2g_s \hat{V}_s^T} \hat{Q}_R + \hat{\bar{O}} e^{2g_s \hat{V}_s^{\text{fund}}} \hat{O} \right) \\ & + \left(\int d^2\theta \frac{1}{16g_s^2} \hat{W}_s^{a\alpha} \hat{W}_{s\alpha}^a + h.c. \right) + \mathcal{L}_{\text{soft}} \end{aligned} \quad (4.9)$$

where \hat{Q}_L and \hat{Q}_R refer to the left- and right-handed superfield of the quark. Note that each field in the first line of eq. (4.9) transforms in a different representation of $SU_C(3)$, i.e. the fundamental, the antifundamental and the adjoint one. From now on T^a stands for the fundamental representation of the generators of $SU(3)_C$. In terms of components fields these expressions are given by

$$\begin{aligned} \int d^4\theta \hat{\bar{Q}}_L e^{2g_s \hat{V}_s} \hat{Q}_L = & F_L^\dagger F_L + (D_\mu \tilde{q}_L)^\dagger (D^\mu \tilde{q}_L) + \bar{q}_L \bar{\sigma}^\mu i D_\mu q_L \\ & - \sqrt{2}g_s \left(-i(\tilde{q}_L^\dagger T^a q_L) \lambda^a + i\bar{\lambda}^a (\bar{q}_L T^a \tilde{q}_L) \right) + g_s \tilde{q}_L^\dagger T^a D^a \tilde{q}_L, \end{aligned} \quad (4.10)$$

$$\begin{aligned} \int d^4\theta \hat{\bar{Q}}_R e^{-2g_s \hat{V}_s^T} \hat{Q}_R = & F_R^\dagger F_R + (D_\mu \tilde{q}_R)^\dagger (D^\mu \tilde{q}_R) + \bar{q}_R \bar{\sigma}^\mu i D_\mu q_R \\ & + \sqrt{2}g_s \left(-i(\tilde{q}_R T^{*a} q_R) \lambda^a + i\bar{\lambda}^a (\bar{q}_R T^{*a} \tilde{q}_R^\dagger) \right) - g_s \tilde{q}_R T^{*a} D^a \tilde{q}_R^\dagger, \end{aligned} \quad (4.11)$$

$$\begin{aligned} \int d^4\theta \hat{\bar{O}} e^{2g_s \hat{V}_s^{\text{fund}}} \hat{O} = & F_O^\dagger F_O + (D_\mu \sigma^a)^\dagger (D^\mu \sigma^a) + \bar{\chi} \bar{\sigma}^\mu i D_\mu \chi \\ & - \sqrt{2}g_s \left(-i(\sigma_b^\dagger (-if_{abc})(-i\chi^c)) \lambda^a + i\bar{\lambda}^a (i\bar{\chi}_b (+if_{abc}) \sigma^{c\dagger}) \right) \\ & - ig_s \sigma^{b\dagger} f^{abc} D^a \sigma^c, \end{aligned} \quad (4.12)$$

where in the gauge covariant derivative $D_\mu = \partial_\mu + ig_s T^a G_\mu^a$ the generator T^a needs to be replaced by $-T^{*a}$ or $-if^{abc}$ if applied to a field transforming in the antifundamental or adjoint representation respectively.

The soft breaking Lagrangian accounts for the squark, gaugino and scalar gluon masses. These mass terms arise from a hidden sector spurion. For gauginos the D-type spurion is given by $\hat{W}'_\alpha = \theta_\alpha D$ and mediates super symmetry breaking at the mediation scale M : $\int d\theta^2 \frac{\hat{W}'_\alpha}{M} W_s^\alpha \hat{O}$. After integrating out the spurion one obtains [26, 27]

$$\begin{aligned} \mathcal{L}_{\text{soft}} = & -\frac{m_{\tilde{q}}^2}{2} (|\tilde{q}_L|^2 + |\tilde{q}_R|^2), \\ & -m_\sigma^2 |\sigma^a|^2 - m_g (\lambda\chi - \sqrt{2} D^a \sigma^a + h.c.) \end{aligned} \quad (4.13)$$

where the complex scalar gluons which are also referred to as sgluons

$$\sigma = \frac{\phi_0 + i\sigma_0}{\sqrt{2}}, \quad (4.14)$$

constitute of two real ones with different masses. The equations of motion for the auxiliary fields are

$$D^a = -g_s \tilde{q}_L^\dagger T^a \tilde{q}_L + g_s \tilde{q}_R T^{*a} \tilde{q}_R^\dagger + i g_s \sigma^{\dagger b} f^{abc} \sigma^c - \sqrt{2} m_g (\sigma^a + \sigma^{\dagger a}), \quad (4.15)$$

$$F_i = 0 \quad \text{for} \quad i = L, R, O \quad (4.16)$$

where D^a is still real as the purely imaginary parts do not contribute by virtue of the antisymmetry of the structure constants. After eliminating the auxiliary fields the complete Lagrangian reads in four-spinor notation¹⁴

$$\begin{aligned} \mathcal{L}_{\text{RSQCD}} = & |D_\mu \sigma|^2 + |D_\mu \tilde{q}_R|^2 + |D_\mu \tilde{q}_L|^2 + \bar{q} i \not{D} q + \bar{g}^a i \not{D} P_L \tilde{g}^a + \bar{g}^a i \not{D} P_R \tilde{g}^a - \frac{1}{4} (F_a^{\mu\nu})^2 \\ & - \sqrt{2} g_s \left(\bar{g}^a P_R (q^C T^a \tilde{q}_L) + (\tilde{q}_L^\dagger T^a \bar{q}^C) P_L \tilde{g}^a \right) \\ & + \sqrt{2} g_s \left(\bar{g}^a P_R (q T^{*a} \tilde{q}_R^\dagger) + (\tilde{q}_R T^{*a} \bar{q}) P_L \tilde{g}^a \right) \\ & - \sqrt{2} g_s \left(\bar{g}^a P_R (\tilde{g}^b (i f^{abc}) \sigma^c) + (\sigma^{\dagger b} (-i f^{abc}) \bar{g}^c) P_L \tilde{g}^a \right) \\ & - \frac{m_{\tilde{q}}^2}{2} (|\tilde{q}_L|^2 + |\tilde{q}_R|^2) - m_\sigma^2 |\sigma^a|^2 - m_{\tilde{g}} \bar{g}^a \tilde{g}^a \\ & - \frac{1}{2} \left(g_s \tilde{q}_L^\dagger T^a \tilde{q}_L - g_s \tilde{q}_R T^{*a} \tilde{q}_R^\dagger - i g_s \sigma^{\dagger b} f^{abc} \sigma^c + \sqrt{2} m_{\tilde{g}} (\sigma^a + \sigma^{\dagger a}) \right)^2 \end{aligned} \quad (4.17)$$

Observe that there is no three sgluon vertex, because of the antisymmetry of the structure constants f^{abc} . As already alluded to there are two distinct sgluons with different masses. The mass of the pseudoscalar σ_0^a is given by the soft breaking parameter $m_{\sigma_0} = m_\sigma$ whereas the mass of the scalar ϕ_0 is given by

$$m_{\phi_0} = \sqrt{m_{\sigma_0}^2 + 4m_{\tilde{g}}^2}. \quad (4.18)$$

The Feynman rules inferred from this Lagrangian are given in Appendix 10.5.

¹⁴How a four-spinor is composed of Weyl-spinors is given in the Appendix 10.3.

5 Squark and Gluino Production at Tree Level

This chapter considers the production of strongly interacting supersymmetric particles in the MRSSM.¹⁵ The various processes and their associated cross sections are compared to their analogues in the MSSM.

The production of sgluons is not included in the following analysis. However, there are two possible channels for sgluon production at tree-level: a quark-antiquark and a gluon-gluon initiated process:

$$q\bar{q} \rightarrow \phi_0\phi_0 \ (\sigma_0\sigma_0), \quad GG \rightarrow \phi_0\phi_0 \ (\sigma_0\sigma_0). \quad (5.1)$$

To give a reasonable and consistent prediction of hadronic cross sections, a scenario with large sgluon mass, i.e. soft breaking parameter $m_\sigma = 5 \text{ TeV}$, is considered. This validates the negligence of sgluon production as in this case they are too heavy to produce them significantly at the LHC with $\sqrt{S} = 13 \text{ TeV}$. See [32–34] for a calculation of the sgluon production cross section. Section 5.1 gives analytic results for the parton reaction before the next section describes how the hadronic cross section is obtained. Section 5.3 presents the hadronic cross section of all considered processes for various choices of squark and gluino mass. In particular, squark production is considered in detail. This includes the statement of uncertainties of the calculation.

5.1 Partonic Processes and their Cross Section

The tree-level Feynman diagrams for squark and gluino production in the MRSSM are shown in fig. 5.1. On the partonic level there are six different channels. For squark-antisquark and gluino-antigluino production there are two possible partonic reactions respectively.

¹⁵In fact only the RSQCD is considered as contribution coming from the electroweak sector scale with $\mathcal{O}(\alpha_w^2)$ where $\alpha_w = \frac{g_w^2}{4\pi}$ or $\mathcal{O}(\alpha_{\text{em}}^2)$ where $\alpha_{\text{em}} = \frac{e^2}{4\pi}$ and are therefore significantly smaller than contribution from the strongly interacting sector which scale with $\mathcal{O}(\alpha_s^2)$ where $\alpha_s = \frac{g_s^2}{4\pi}$.

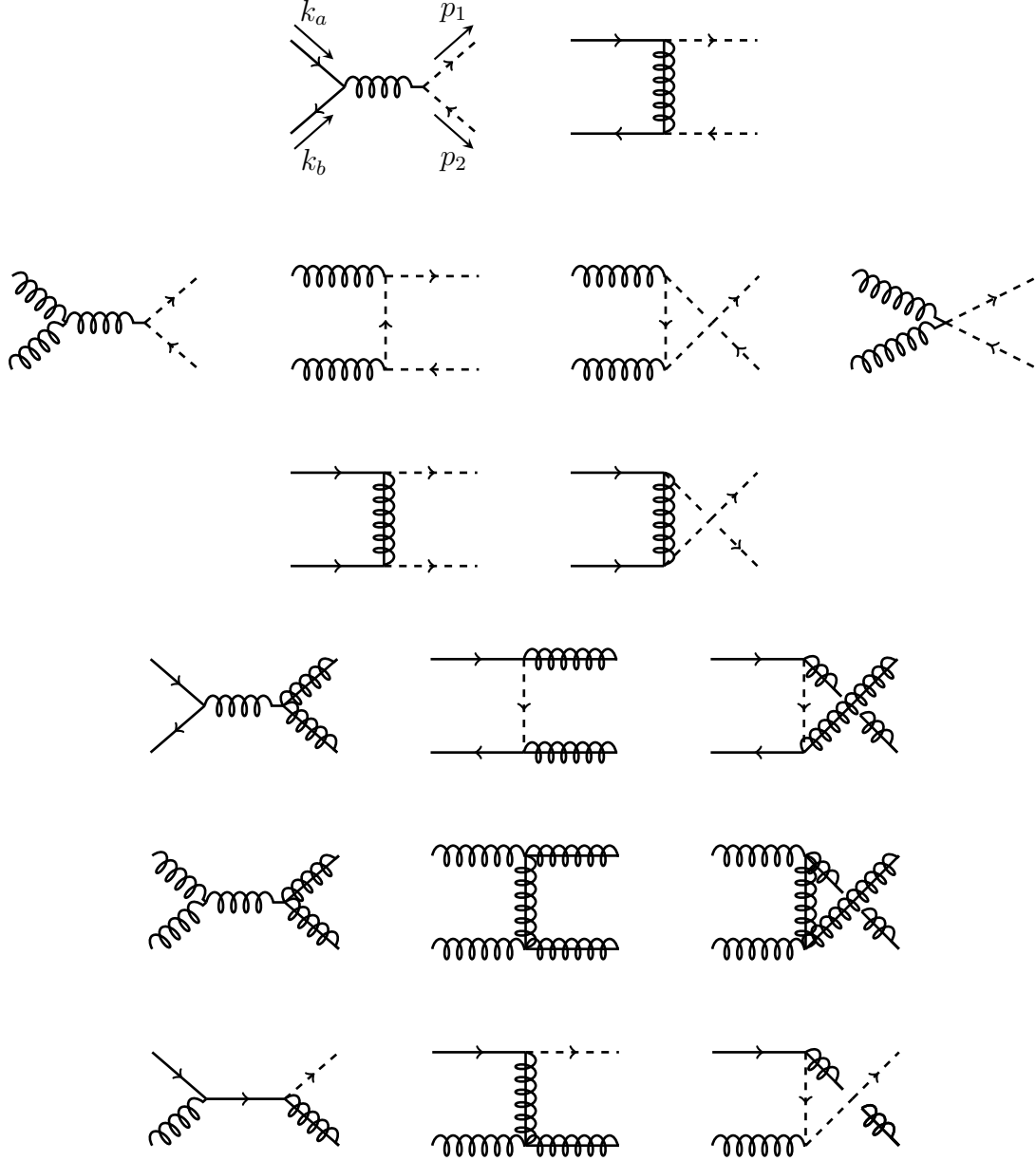


Figure 5.1: Tree level diagrams for squark and gluino production at tree level in the MRSSM. The processes $GG \rightarrow \tilde{q}\tilde{q}^*$ and $qG \rightarrow \tilde{q}\tilde{g}$ are identical to those in the MSSM. The processes $q\bar{q} \rightarrow \tilde{q}\tilde{q}^*$ and $qq \rightarrow \tilde{q}\tilde{q}^*$ involve the production of less “chiralities” than in the MSSM. Also in the $q\bar{q} \rightarrow \tilde{g}\tilde{g}^*$ channel only half of the t-channel squark “chiralities” occur in the MRSSM. (Anti-)Gluino production via initial gluons $GG \rightarrow \tilde{g}\tilde{g}^*$ proceeds via the same diagrams like in the MSSM but its cross section is twice as much in the MRSSM for gluino and antigluino are distinguishable particles.

For the following calculation the top quark is excluded from the initial state as it is too heavy to be significantly present in protons. For consistency reasons also the stop is excluded from the final states. One therefore deals with $n_f - 1 = 5$ quark flavors. In view of the renormalization and mass factorization to be performed at the one-loop level, the results are calculated in (conventional) dimensional regularization (see section 7.1) and are therefore given in $D = 4 - 2\epsilon$ dimensions. Furthermore it has been distinguished between the gauge coupling g_s from the gluon-quark-quark vertex and its supersymmetric analogue \hat{g}_s from the gluino-squark-quark vertex. So far, it has not been distinguished between them because supersymmetry dictates them to be identical. However, the loop corrections to their corresponding vertex differ in dimensional regularization by a finite amount, as will be shown in section 7. To rectify this, an additional finite (supersymmetry restoring) counterterm needs to be added to one of the renormalization constants of g_s or \hat{g}_s . This will be done in section 7.6.

To parametrize results, the usual Mandelstam variables s, t, u and the following modifications of them are used¹⁶

$$\begin{aligned}
s &= (k_a + k_b)^2 = (p_1 + p_2)^2, \\
t &= (k_a - p_1)^2 = (k_b - p_2)^2, \\
u &= (k_a - p_2)^2 = (k_b - p_1)^2, \\
t_{\tilde{g}} &= t - m_{\tilde{g}}^2, & t_{\tilde{q}} &= t - m_{\tilde{q}}^2, \\
u_{\tilde{g}} &= u - m_{\tilde{g}}^2, & u_{\tilde{q}} &= u - m_{\tilde{q}}^2.
\end{aligned} \tag{5.2}$$

¹⁶The kinematics of the process is denoted in fig. 5.1.

Applying the Feynman rules in the Appendix 10.5, one obtains the following sums¹⁷ over absolute squared Feynman amplitudes:

$$\begin{aligned} \sum |\mathcal{M}^B|^2(q_i \bar{q}_j \rightarrow \tilde{q} \tilde{q}^\dagger) &= \delta_{ij} \left[8N_c C(F) g_s^4 \frac{(n_f - 1)}{s^2} + 4N_c C(F) \hat{g}_s^4 \frac{1}{t_{\tilde{g}}^2} - 8C(F) g_s^2 \hat{g}_s^2 \frac{1}{t_{\tilde{g}} s} \right] (tu - m_{\tilde{q}}^4) \\ &\quad + (1 - \delta_{ij}) 4N_c C(F) \hat{g}_s^4 \frac{tu - m_{\tilde{q}}^4}{t_{\tilde{g}}^2}, \end{aligned} \quad (5.3)$$

$$\begin{aligned} \sum |\mathcal{M}^B|^2(GG \rightarrow \tilde{q} \tilde{q}^\dagger) &= 4(n_f - 1) g_s^4 \left[2N_c^2 C(F) \left(1 - 2 \frac{t_{\tilde{q}} u_{\tilde{q}}}{s^2} \right) - 2C(F) \right] \\ &\quad \left[1 - \epsilon - 2 \frac{s m_{\tilde{q}}^2}{t_{\tilde{q}} u_{\tilde{q}}} \left(1 - \frac{s m_{\tilde{q}}^2}{t_{\tilde{q}} u_{\tilde{q}}} \right) \right], \end{aligned} \quad (5.4)$$

$$\begin{aligned} \sum |\mathcal{M}^B|^2(q_i q_j \rightarrow \tilde{q} \tilde{q}) &= \delta_{ij} 2 \hat{g}_s^4 N_c C(F) \left[\frac{1}{t_{\tilde{g}}^2} + \frac{1}{u_{\tilde{g}}^2} \right] (tu - m_{\tilde{q}}^4) \\ &\quad + (1 - \delta_{ij}) 4 \hat{g}_s^4 N_c C(F) \frac{tu - m_{\tilde{q}}^4}{t_{\tilde{g}}^2}, \end{aligned} \quad (5.5)$$

$$\begin{aligned} \sum |\mathcal{M}^B|^2(q \bar{q} \rightarrow \tilde{g} \tilde{g}) &= 8N_c^2 C(F) g_s^4 \left[\frac{2m_{\tilde{g}}^2 s + t_{\tilde{g}}^2 + u_{\tilde{g}}^2}{s^2} - \epsilon \right] \\ &\quad + 4N_c^2 C(F) g_s^2 \hat{g}_s^2 \left[\frac{m_{\tilde{g}}^2 s + t_{\tilde{g}}^2}{s t_{\tilde{q}}} + \frac{m_{\tilde{g}}^2 s + u_{\tilde{g}}^2}{s u_{\tilde{q}}} + \epsilon \left(\frac{t_{\tilde{g}}}{t_{\tilde{q}}} + \frac{u_{\tilde{g}}}{u_{\tilde{q}}} \right) \right] \\ &\quad + 2C(F) (N_c^2 - 1) \hat{g}_s^4 \left(\frac{t_{\tilde{g}}^2}{t_{\tilde{q}}^2} + \frac{u_{\tilde{g}}^2}{u_{\tilde{q}}^2} \right) \end{aligned} \quad (5.6)$$

$$\begin{aligned} \sum |\mathcal{M}^B|^2(GG \rightarrow \tilde{g} \tilde{g}) &= 16N_c^3 C(F) g_s^4 \left(1 - \frac{t_{\tilde{g}} u_{\tilde{g}}}{s^2} \right) \\ &\quad \left[\frac{s^2}{t_{\tilde{g}} u_{\tilde{g}}} (1 - \epsilon)^2 - 2(1 - \epsilon) + 4 \frac{m_{\tilde{g}}^2 s}{t_{\tilde{g}} u_{\tilde{g}}} \left(1 - \frac{m_{\tilde{g}}^2 s}{t_{\tilde{g}} u_{\tilde{g}}} \right) \right], \end{aligned} \quad (5.7)$$

$$\begin{aligned} \sum |\mathcal{M}^B|^2(qG \rightarrow \tilde{q} \tilde{g}) &= 2g_s^2 \hat{g}_s^2 \left[2N_c^2 C(F) \left(1 - 2 \frac{s u_{\tilde{q}}}{t_{\tilde{g}}^2} \right) - 2C(F) \right] \\ &\quad \left[(-1 + \epsilon) \frac{t_{\tilde{g}}}{s} + \frac{2(m_{\tilde{g}}^2 - m_{\tilde{q}}^2) t_{\tilde{g}}}{s u_{\tilde{q}}} \left(1 + \frac{m_{\tilde{q}}^2}{u_{\tilde{q}}} + \frac{m_{\tilde{g}}^2}{t_{\tilde{g}}} \right) \right]. \end{aligned} \quad (5.8)$$

The constants $C(A)$, $C(F)$ of the color algebra $SU(N_c)$ with $N_c = 3$ are given in Appendix 10.2.

The absolute squared amplitudes have been checked with the **Mathematica** output generated by the packages **FeynArts** [35] and **FormCalc** [36, 37] which used a model file for the MRSSM generated by **SARAH** [38–41].

Having calculated the absolute squared Feynman amplitudes one obtains the partonic cross

¹⁷The sum \sum denotes the summation over all external spins and colors.

sections (see Appendix 10.7) via

$$\frac{d^2\sigma^B}{dt\,du} = \frac{K_{ab}}{s^2} \frac{\pi S_\epsilon}{\Gamma(1-\epsilon)} \left[\frac{tu - m_1^2 m_2^2}{\mu^2 s} \right]^{-\epsilon} \Theta(tu - m_1^2 m_2^2) \Theta(s - 4m^2) \delta(s + t + u - m_1^2 - m_2^2) \sum |\mathcal{M}^B|^2, \quad (5.9)$$

where m_1 (m_2) is the mass of the first (second) final state particle and m is their arithmetic mean. The leading order cross sections then evaluate to

$$\begin{aligned} \sigma^B(q_i \bar{q}_j \rightarrow \tilde{q} \tilde{q}^\dagger) &= \delta_{ij} \frac{g_s^4}{16\pi s} (n_f - 1) \left[\frac{4}{27} - \frac{16m_{\tilde{q}}^2}{27s} \right] \beta_{\tilde{q}} \\ &\quad + \delta_{ij} \frac{g_s^2 \hat{g}_s^2}{16\pi s} \left[\left(\frac{4}{27} + \frac{8m_-^2}{27s} \right) \beta_{\tilde{q}} + \left(\frac{8m_{\tilde{g}}^2}{27s} + \frac{8m_-^4}{27s^2} \right) L_1 \right] \\ &\quad + \frac{\hat{g}_s^4}{16\pi s} \left[-\frac{8}{9} \beta_{\tilde{q}} + \left(-\frac{4}{9} - \frac{8m_-^2}{9s} \right) L_1 \right], \end{aligned} \quad (5.10)$$

$$\sigma^B(GG \rightarrow \tilde{q} \tilde{q}^\dagger) = \frac{(n_f - 1)g_s^4}{16\pi s} \left[\left(\frac{5}{24} + \frac{31m_{\tilde{q}}^2}{12s} \right) \beta_{\tilde{q}} + \left(\frac{4m_{\tilde{q}}^2}{3s} + \frac{m_{\tilde{q}}^4}{3s^2} \right) \ln \frac{1 - \beta_{\tilde{q}}}{1 + \beta_{\tilde{q}}} \right], \quad (5.11)$$

$$\sigma^B(q_i q_j \rightarrow \tilde{q} \tilde{q}) = \frac{\hat{g}_s^4}{16\pi s} \left[-\frac{8}{9} \beta_{\tilde{q}} + \left(-\frac{4}{9} - \frac{8m_-^2}{9s} \right) L_1 \right], \quad (5.12)$$

$$\begin{aligned} \sigma^B(q\bar{q} \rightarrow \tilde{g} \tilde{g}) &= \frac{g_s^4}{16\pi s} \left[\frac{16}{9} + \frac{32m_{\tilde{g}}^2}{9s} \right] \beta_{\tilde{g}} \\ &\quad + \frac{\hat{g}_s^2 g_s^2}{16\pi s} \left[\left(-\frac{4}{3} - \frac{8m_-^2}{3s} \right) \beta_{\tilde{g}} + \left(\frac{8m_{\tilde{g}}^2}{3s} + \frac{8m_-^4}{3s^2} \right) L_2 \right] \\ &\quad + \frac{\hat{g}_s^4}{16\pi s} \left[\left(\frac{32}{27} + \frac{32m_-^4}{27(m_-^4 + m_{\tilde{q}}^2 s)} \right) \beta_{\tilde{g}} - \frac{64m_-^2}{27s} L_2 \right], \end{aligned} \quad (5.13)$$

$$\sigma^B(GG \rightarrow \tilde{g} \tilde{g}) = \frac{g_s^4}{16\pi s} \left[\left(-6 - \frac{51m_{\tilde{g}}^2}{2s} \right) \beta_{\tilde{g}} + \left(-\frac{9}{2} - \frac{18m_{\tilde{g}}^2}{s} + \frac{18m_{\tilde{g}}^4}{s^2} \right) \ln \frac{1 - \beta_{\tilde{g}}}{1 + \beta_{\tilde{g}}} \right], \quad (5.14)$$

$$\begin{aligned} \sigma^B(qG \rightarrow \tilde{q} \tilde{g}) &= \frac{g_s^2 \hat{g}_s^2}{16\pi s} \left[\frac{\kappa}{s} \left(-\frac{7}{9} - \frac{32m_-^2}{9s} \right) + \left(-\frac{8m_-^2}{9s} + \frac{2m_{\tilde{q}}^2 m_-^2}{s^2} + \frac{8m_-^4}{9s^2} \right) L_3 \right. \\ &\quad \left. + \left(-1 - \frac{2m_-^2}{s} + \frac{2m_{\tilde{q}} m_-^2}{s^2} \right) L_4 \right], \end{aligned} \quad (5.15)$$

where the abbreviations [42]

$$\begin{aligned} \beta_{\tilde{q}} &= \sqrt{1 - \frac{4m_{\tilde{q}}^2}{s}}, & \beta_{\tilde{g}} &= \sqrt{1 - \frac{4m_{\tilde{g}}^2}{s}}, \\ m_-^2 &= m_{\tilde{g}}^2 - m_{\tilde{q}}^2, & \kappa &= \sqrt{(s - m_{\tilde{g}}^2 - m_{\tilde{q}}^2)^2 - 4m_{\tilde{g}}^2 m_{\tilde{q}}^2}, \\ L_1 &= \ln \frac{s + 2m_-^2 - s\beta_{\tilde{q}}}{s + 2m_-^2 + s\beta_{\tilde{q}}}, & L_2 &= \ln \frac{s - 2m_-^2 - s\beta_{\tilde{g}}}{s - 2m_-^2 + s\beta_{\tilde{g}}}, \\ L_3 &= \ln \frac{s - m_-^2 - \kappa}{s - m_-^2 + \kappa}, & L_4 &= \ln \frac{s + m_-^2 - \kappa}{s + m_-^2 + \kappa} \end{aligned} \quad (5.16)$$

have been used. In the following, the considered processes of the MRSSM are compared to those of the MSSM.

The Process $q_i \bar{q}_j \rightarrow \tilde{q} \tilde{q}^\dagger$

The production of a squark and an antisquark through a quark and an antiquark in the initial state originates from two types of Feynman diagrams, see fig. 5.2. The first one has an s -channel gluon and is the same in the MSSM and in the MRSSM. The second one exhibits a difference due to the t -channel gluino which is no Majorana particle in the MRSSM. To see



Figure 5.2: Tree level diagrams for $q\bar{q} \rightarrow \tilde{q}\tilde{q}^\dagger$

this one can either just apply the Feynman rules in Appendix 10.5 or think of the conservation of R -charge: Left handed squarks have R -charge $+1$ and right handed squarks have R -charge -1 . Antiparticles have the opposite R -charge of their corresponding particles. The final state particles have to meet the total R -charge zero from the initial state. Because of this, one only has $\tilde{q}_L \tilde{q}_L^\dagger$ and $\tilde{q}_R \tilde{q}_R^\dagger$ as the final states in the MRSSM whereas in the MSSM one actually has four instead of two t -channel diagrams: The corresponding final states are $\tilde{q}_L \tilde{q}_L^\dagger$, $\tilde{q}_R \tilde{q}_R^\dagger$, $\tilde{q}_L \tilde{q}_R^\dagger$ and $\tilde{q}_R \tilde{q}_L^\dagger$. Consequently contributions from the t -channel diagrams are suppressed in the MRSSM in comparison to the MSSM. As shown in fig. 5.5 this suppression grows with the masses. The reason for this lies in the gluino mass dependence of the t -channel diagrams which is explained in the discussion of squark production.

If the initial state quarks are of different flavor, the s -channel diagram is absent.

The Process $G G \rightarrow \tilde{q} \tilde{q}^\dagger$

This process has the same cross section as in the MSSM for also in the MSSM only “chirality” like squark and antisquark $\tilde{q}_A \tilde{q}_A^\dagger$ with $A \in \{L, R\}$ can be produced.

The Process $q_i q_j \rightarrow \tilde{q} \tilde{q}$

In the MRSSM only the production of “chirality” unlike squarks $\tilde{q}_L \tilde{q}_R$ is allowed whilst in the MSSM also “chirality” like squarks can be produced. This is again a consequence of the conservation of R -charge. The upshot of this is a suppression of squark production in the MRSSM in comparison to the MSSM. To be more explicit the suppression of squark production in the MRSSM grows with the gluino mass. This can be understood as follows: As in the MRSSM a left handed squark needs to be produced with a right handed squark, one can read off, from the Feynman rules given in Appendix 10.5, that the gluino propagator

$i \frac{p+m_{\tilde{g}}}{p^2-m_{\tilde{g}}^2}$ is sandwiched between the projectors P_L and P_R which leads to the cancellation of the gluino mass in the numerator. Therefore for small momenta of the gluino compared to the gluino mass one gets $\mathcal{M} \sim m_{\tilde{g}}^{-2}$ in the MRSSM while in the MSSM one finds a suppression proportional to $m_{\tilde{g}}^{-1}$.

When considering the total cross section, one has to sum $|\mathcal{M}|^2$ over all helicities. The diagrams for those different final state helicities are shown for flavor like squark production in tab. 5.1 and for flavor unlike squark production in tab. 5.2 for the MSSM and the MRSSM. To avoid double counting, one needs to weight $|\mathcal{M}|^2(qq \rightarrow \tilde{q}_L \tilde{q}_L)$ and $|\mathcal{M}|^2(qq \rightarrow \tilde{q}_R \tilde{q}_R)$ with a statistical factor of $\frac{1}{2}$ as one integrates over the momenta of both particles in t - and u -channel diagrams to arrive at the cross section.

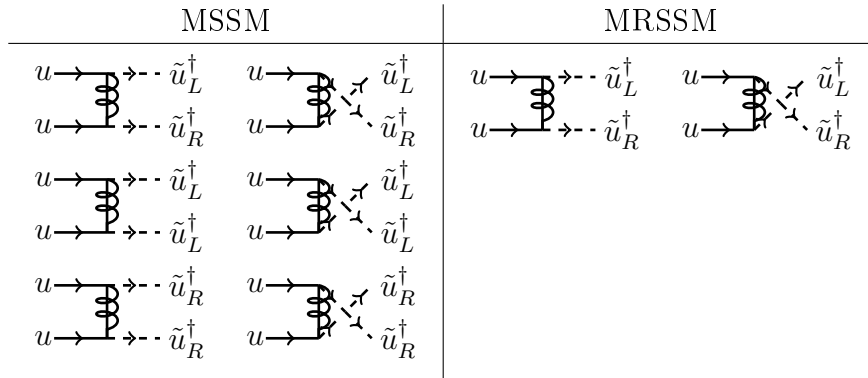


Table 5.1: All Feynman diagrams contributing to flavor like squark production in the MSSM and the MRSSM for the example of u -quarks. For the MSSM the absolute squared Feynman amplitudes from the diagrams with “chirality” like squarks need to be weighted with a factor of $\frac{1}{2}$.

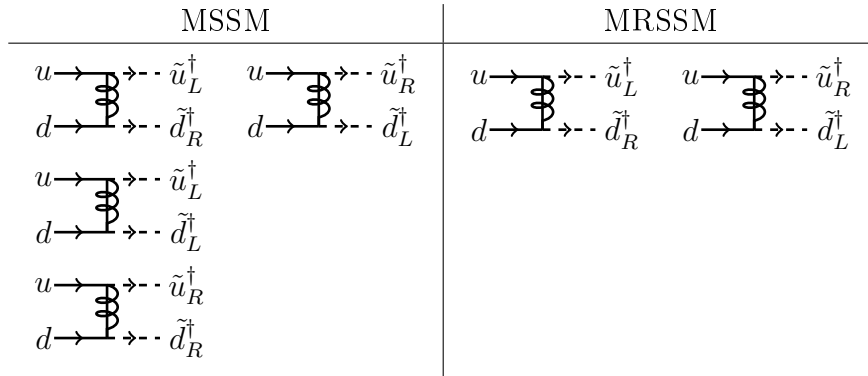


Table 5.2: All Feynman diagrams contributing to flavor unlike squark production in the MSSM and the MRSSM for the example of the initial state with u - and d -quarks.

Because of the absence of “chirality” like squarks in the final state in the MRSSM (and a missing interference of the two diagrams in tab. 5.1 in the column of the MRSSM), the partonic cross

section of flavor like and unlike squarks is the same in the MRSSM, i.e. on the partonic level:

$$\sigma_{\text{Part, MRSSM}}^{\text{B}}(uu \rightarrow \tilde{u}_L \tilde{u}_R) = \sigma_{\text{Part, MRSSM}}^{\text{B}}(ud \rightarrow \tilde{u}_L \tilde{d}_R) + \sigma_{\text{Part, MRSSM}}^{\text{B}}(ud \rightarrow \tilde{u}_R \tilde{d}_L). \quad (5.17)$$

That is however not true in the MSSM because for flavor like squarks, there is a non vanishing interference of the t - and u -channel diagram of the processes $qq \rightarrow \tilde{q}_L \tilde{q}_L$ and $qq \rightarrow \tilde{q}_R \tilde{q}_R$. This term is given in [42, p.7].

The Process $q\bar{q} \rightarrow \tilde{g}\tilde{g}$

In contrast to the MSSM no statistical factor of $\frac{1}{2}$ is taken into account when turning from $|\mathcal{M}|^2$ to σ . This is because gluino and antigluino are distinguishable particles. Still in comparison to the MSSM cross section [42, p.9] only the first line in eq. (5.13) is doubled up as the other two lines originate from an t or u channel squark which occurs in only one instead of two “chiralities”. Furthermore an interference term from the t and u channel diagram which occurs in the MSSM is absent in the MRSSM.

The Process $GG \rightarrow \tilde{g}\tilde{g}$

As in the previous process, the MRSSM cross section for $GG \rightarrow \tilde{g}\tilde{g}$ receives no statistical factor of $\frac{1}{2}$ like in the MSSM. As there are no further differences between MSSM and MRSSM in this channel, the MRSSM cross section is simply twice as large as in the MSSM.

The Process $qG \rightarrow \tilde{q}\tilde{g}$

This process is exactly the same in the MSSM and MRSSM for there are two differences between the models which exactly cancel each other: Firstly in the MRSSM there is not only the production of a squark and a gluino but also the production of a squark and an antigluino. But on the other hand R-charge needs to be conserved which dictates that a “left-handed” squark can only be produced with an antigluino and a “right-handed” squark can only be produced with a gluino (see table 4.2).

In order to account for the confinement of quarks and gluons within hadrons, the next section describes how to obtain the hadronic cross sections for the considered processes.

5.2 Hadronic Cross Section

Quarks, antiquarks and gluons are no free particles but are confined within hadrons. As hadrons consist of a variety of the just mentioned partons which share the hadron’s momentum, one does not have a definite initial state in hadron collisions which is assumed in the previous

section. Fortunately the hadronic cross section for the production of a final state X , e.g. $X = \tilde{q}\tilde{q}$, can be obtained by convolving the partonic cross section with parton density functions of the initial hadrons:

$$\sigma_{\text{Had}}^B(P_1 P_2 \rightarrow X) = \int dx_1 dx_2 f_{P_1/H_1}(x_1) f_{P_2/H_2}(x_2) \sigma_{\text{Part}}^B(P_1 P_2 \rightarrow X, s = x_1 x_2 S). \quad (5.18)$$

The parton density functions $f_{P_i/H_j}(x)$ and the momentum fractions x_i are explained below. The hadrons center-of-mass energy is denoted with \sqrt{S} where $\sqrt{s} = \sqrt{S x_1 x_2}$ denotes the partons center-of-mass energy.

As the production of the final state X may proceed via various initial partons, one has to sum over all possibilities arising from the initial hadrons H_1 and H_2 :

$$\sigma_{\text{Had}}^B(H_1 H_2 \rightarrow X) = \sum_{i,j} \sigma_{\text{Had}}^B(P_i P_j \rightarrow X) \quad (5.19)$$

where the sum runs over all partons P_i (P_j) which are in the hadron H_1 (H_2).

To get an intuitive idea of this factorization, regard the hadrons as extended objects consisting of partons¹⁸ which are permanently interacting with each other. Now consider two colliding hadrons at high energies in their center-of-mass frame. Due to Lorentz contraction the hadrons appear as thin discs and the parton's mutual interactions are time-delayed within this frame. This effectively means that a hadron at the time of collision is virtually frozen in the approximate infinite momentum frame.

This in turn implies that the hadron consists, at the time of collision, of a definite number of partons which can be thought of as carrying a definite fraction of the hadron's momentum $p_{\text{Part}} = x p_{\text{Had}}$ with $x \in (0, 1)$. The parton density function $f_{P/H}(x)$ can (at tree-level) therefore be understood as the probability of finding a parton P within the hadron H carrying x of its momentum fraction.

They actually depend on an arbitrary energy scale referred to as the factorization scale μ_F . The μ_F evolution is given within the scope of perturbation theory by coupled integro-differential equations named after Gribov, Lipatov [44], Dokshitzer [45], Altarelli and Parisi [46]: the DGLAP-equations. For further reading on parton density functions and factorization see [47] and [48]. See [49] for how to determine parton density functions.

Fig. 5.3 shows a parton density function set for the proton. One can see that the partons most probable to carry a high fraction of momentum are the valence quarks. For lower values of x , gluons constitute the major component of the proton.

Fig. 5.5 shows the hadronic cross section for the production of various squarks in the MRSSM. These can only be produced by their Standard Model partner, e.g. two up-squarks can only be produced by two up-quarks. Because the partonic cross section for these processes are the

¹⁸The proton is considered as composed of three valence quarks: Two up-quarks and one down-quark. In addition there are gluons and seaquarks, i.e. virtual quark-antiquark pairs.

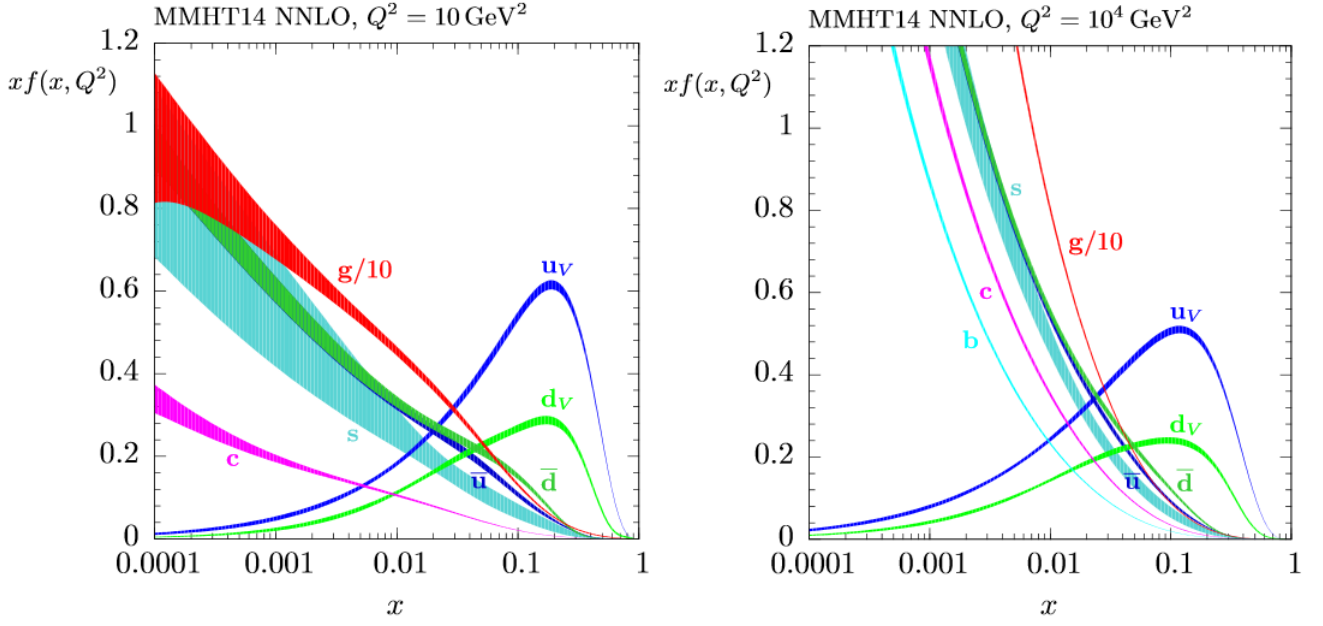


Figure 5.3: Parton density function of the proton, taken from MMHT2014 [43] with 68% confidence level. The parton density function is multiplied by x in order to counteract its peak at $x \rightarrow 0$. The parton density function is given at two different factorisation scales $\mu_F = Q$.

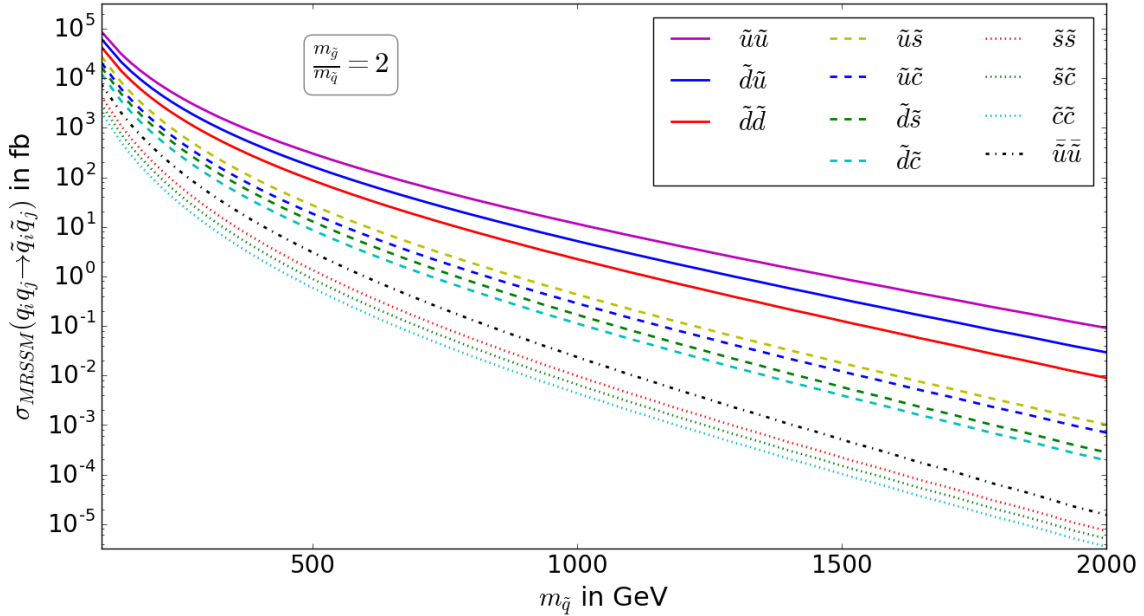


Figure 5.4: Hadronic cross section for squark production in the MRSSM at the LHC at $\sqrt{S} = 13 \text{ GeV}$. The ratio of the gluino and squark mass is fixed to 2. The parton densities used are MMHT2014L0 (LHAPDFID:25000) with $\alpha_s(M_Z) = 0.135$ in the 5-flavor scheme [43]. As renormalization and factorization scale $\mu_R = \mu_F = \frac{m_1 + m_2}{2}$ has been chosen, where m_i are the final state particle masses.

same, cf. eq. (5.17), one can see the influence of the parton density functions quite nicely: The up-squark production is the dominant contribution to squark production. Apart from the solid lines in fig. 5.5 which correspond to the production of first generation squarks, also the cross section of mixed first and second generation (dashed lines) and second generation (dotted lines) squarks is shown. The dashed dotted line shows the cross section of the charged conjugated particles of the dominant channel.

5.3 Results for Squark and Gluino Production at Tree-Level

This section presents hadronic tree-level (Born) cross sections of squark and gluino production for two colliding protons in both, the MSSM and the MRSSM.

Note that in the following all possible production channels are taken into account. This is, for squark and squark-gluino production, also the charged conjugated processes, i.e. $\tilde{q}^\dagger \tilde{q}^\dagger$ and $\tilde{q}^\dagger \tilde{g} (\tilde{\bar{g}})$, are included. In addition, squark production counts those processes twice which involve flavor unlike quarks, e.g. $ud \rightarrow \tilde{u} \tilde{d}$ is counted twice as the d -quark may come from either proton. This applies also to squark-antisquark production through a quark-antiquark pair.

The calculations have been performed by a C++ code which uses a library containing the absolute squared amplitudes for the processes in question. Note that the author has opted for the absolute squared amplitudes and not the partonic cross sections because this allows also for the calculation of partial differential cross sections, for possible future use. To perform the integration over the Mandelstam variable t and x_1 and x_2 , the routine “Cuhre” which is part of the CUBA library [50] is used.

The following paragraph discusses fig. 5.5, 5.6 and 5.7, i.e. the hadronic cross section of all considered processes for three successive mass ratios of gluino and squark: $\frac{m_{\tilde{g}}}{m_{\tilde{q}}} = 0.9, 2$ and 5 . Also, the corresponding fraction of final states is shown.

For the small mass ratio $\frac{m_{\tilde{g}}}{m_{\tilde{q}}} = 0.9$ and small squark masses, the dominant contribution comes from gluino-squark production. The subdominant channel is represented by gluino (antigluino) production which is much more pronounced in the MRSSM, which can be explained by the above mentioned factor of two difference in the $GG \rightarrow \tilde{g} \tilde{g} (\tilde{\bar{g}})$ channel which comes from the distinguishable gluino and antigluino in the MRSSM. Furthermore there is the above mentioned destructive interference term in the $q\bar{q} \rightarrow \tilde{g} \tilde{g} (\tilde{\bar{g}})$ channel which makes the cross section for this process in the MRSSM dominant over the one in the MSSM.

A salient difference between the MSSM and the MRSSM is that squark production is strongly suppressed in the MRSSM. While in the MSSM it becomes dominant above ≈ 2000 GeV it is at least subsubdominant for the whole displayed squark mass in the MRSSM. This suppression has already been explained above.

Turning from $\frac{m_{\tilde{g}}}{m_{\tilde{q}}} = 0.9$ to $\frac{m_{\tilde{g}}}{m_{\tilde{q}}} = 2$ suppresses quite strongly the production of gluinos in all

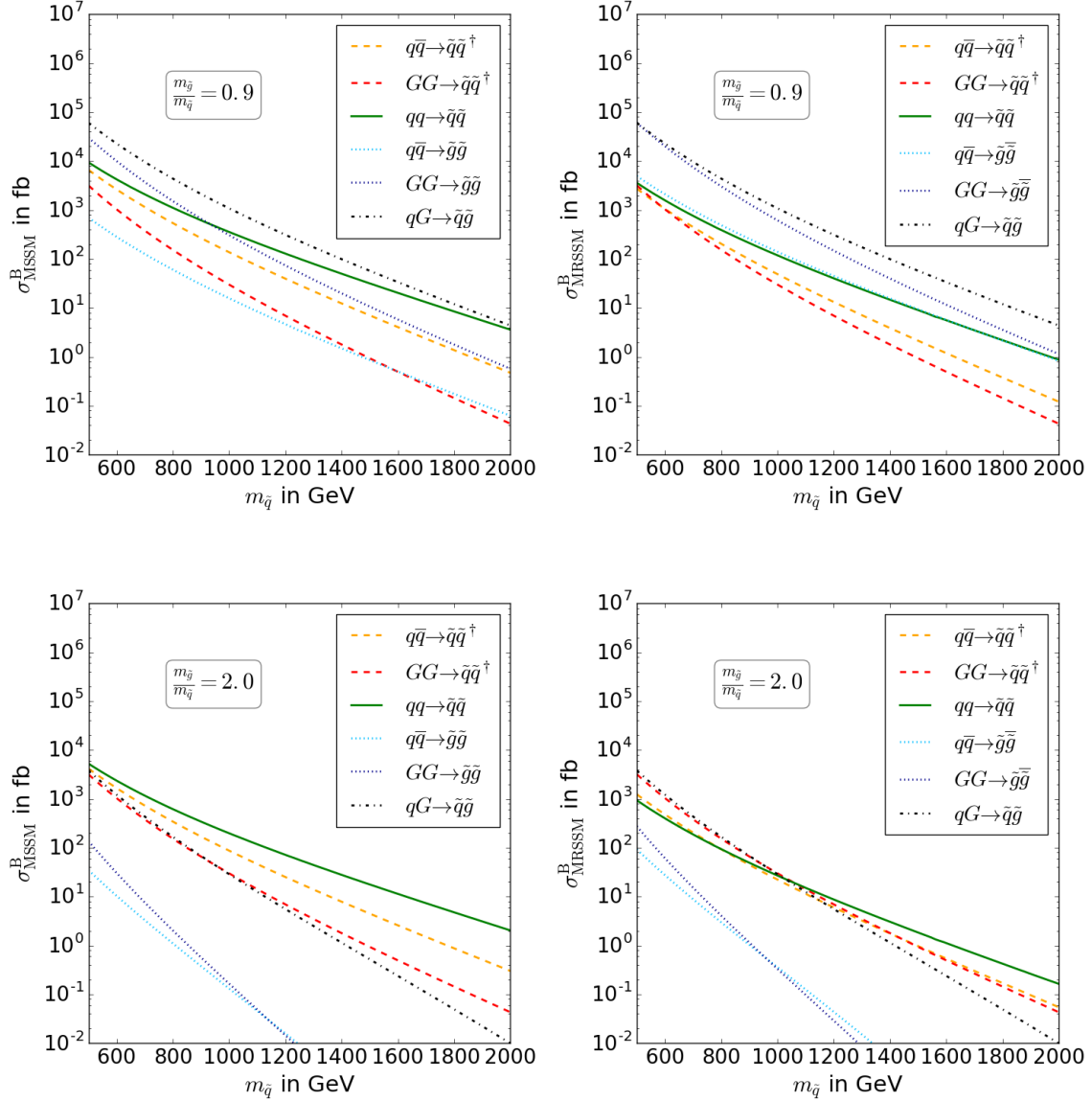


Figure 5.5: Hadronic cross section for squark and gluino production in the MSSM (left-hand side) and MRSSM (right-hand side) at the LHC with $\sqrt{S} = 13$ GeV. The ratio of gluino and squark mass is fixed to 0.9 (first row) and 2 (second row). In the final state it has been summed over all squark flavors except for t -squarks. For the channels $qq \rightarrow \tilde{q}\tilde{q}$ and $qG \rightarrow \tilde{q}\tilde{G}$ also the charge conjugated process is included. The parton densities used are **MMHT2014LO** (LHAPDFID:25000) with $\alpha_s(M_Z) = 0.135$ in the 5-flavor scheme [43]. As renormalization and factorization scale $\mu_R = \mu_F = \frac{m_1 + m_2}{2}$ has been chosen, where m_i are the final state particle masses.

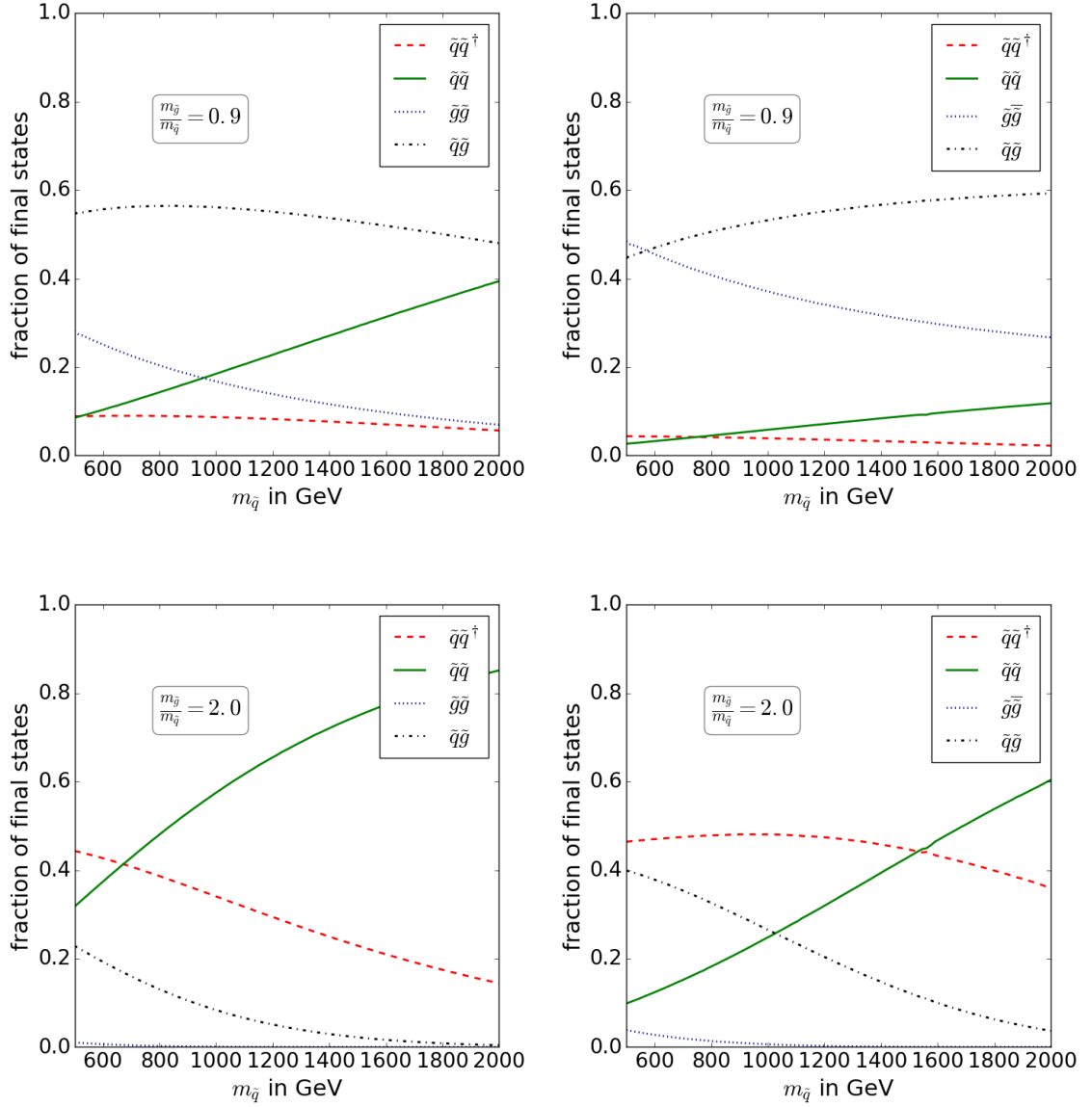


Figure 5.6: Relative contributions of the indicated final states on the total hadronic cross section in the MSSM (left-hand side) and MRSSM (right-hand side) at the LHC with $\sqrt{S} = 13$ GeV. The ratio of gluino and squark mass is fixed to 0.9 (first row) and 2 (second row). In the final state it has been summed over all squark flavors except for t -quarks. For the channels $q\bar{q} \rightarrow \tilde{q}\tilde{q}$ and $qG \rightarrow \tilde{q}\tilde{G}$ also the charge conjugated process is included. The parton densities and the renormalization and factorization scale are chosen as in fig. 5.5.

pertaining channels. For the MSSM one finds above 500 GeV a growing dominance of squark production. The same happens in the MRSSM but for a significantly higher squark mass of about 1200 GeV. This suppression of squark production in the MRSSM increases with a growing gluino masses which can be seen when going from $\frac{m_{\tilde{g}}}{m_{\tilde{q}}} = 0.9$ to $\frac{m_{\tilde{g}}}{m_{\tilde{q}}} = 2$ or even $\frac{m_{\tilde{g}}}{m_{\tilde{q}}} = 5$ depicted in fig. 5.7. This reflects the gluino mass dependence explained in detail in section 5.1. See also 5.9 for a visualization of this behavior.

Note also, that for sufficiently large squark masses, squark production becomes the dominant process, see fig. 5.5 and 5.6. This is because the production of heavy particles requires large longitudinal momenta of the colliding partons, i.e. large x . Looking at the parton density functions in fig. 5.3 one sees that within the proton the partons most likely to carry large momentum are quarks. So looking at large x the proton basically consists of quarks and because the only process involving only quarks in the initial state is squark production, this channel dominates for high masses.

The total cross section in the MRSSM is increasingly smaller than in the MSSM, which can be seen for $\frac{m_{\tilde{g}}}{m_{\tilde{q}}} = 2$ when taking the $GG \rightarrow \tilde{q}\tilde{q}^\dagger$ channel, which is the same for both models, as a benchmark.

When raising the gluino squark mass ratio further to $\frac{m_{\tilde{g}}}{m_{\tilde{q}}} = 5$ the above described tendency continues. This is, all processes including a gluino get even more negligible and squark production gets further suppressed. While in the MSSM it becomes dominant over $GG \rightarrow \tilde{q}\tilde{q}^\dagger$ at $m_{\tilde{q}} \approx 700$ GeV, it is subdominant in the MRSSM within the whole displayed mass range, even though it does not fall that steeply as the dominant channel.

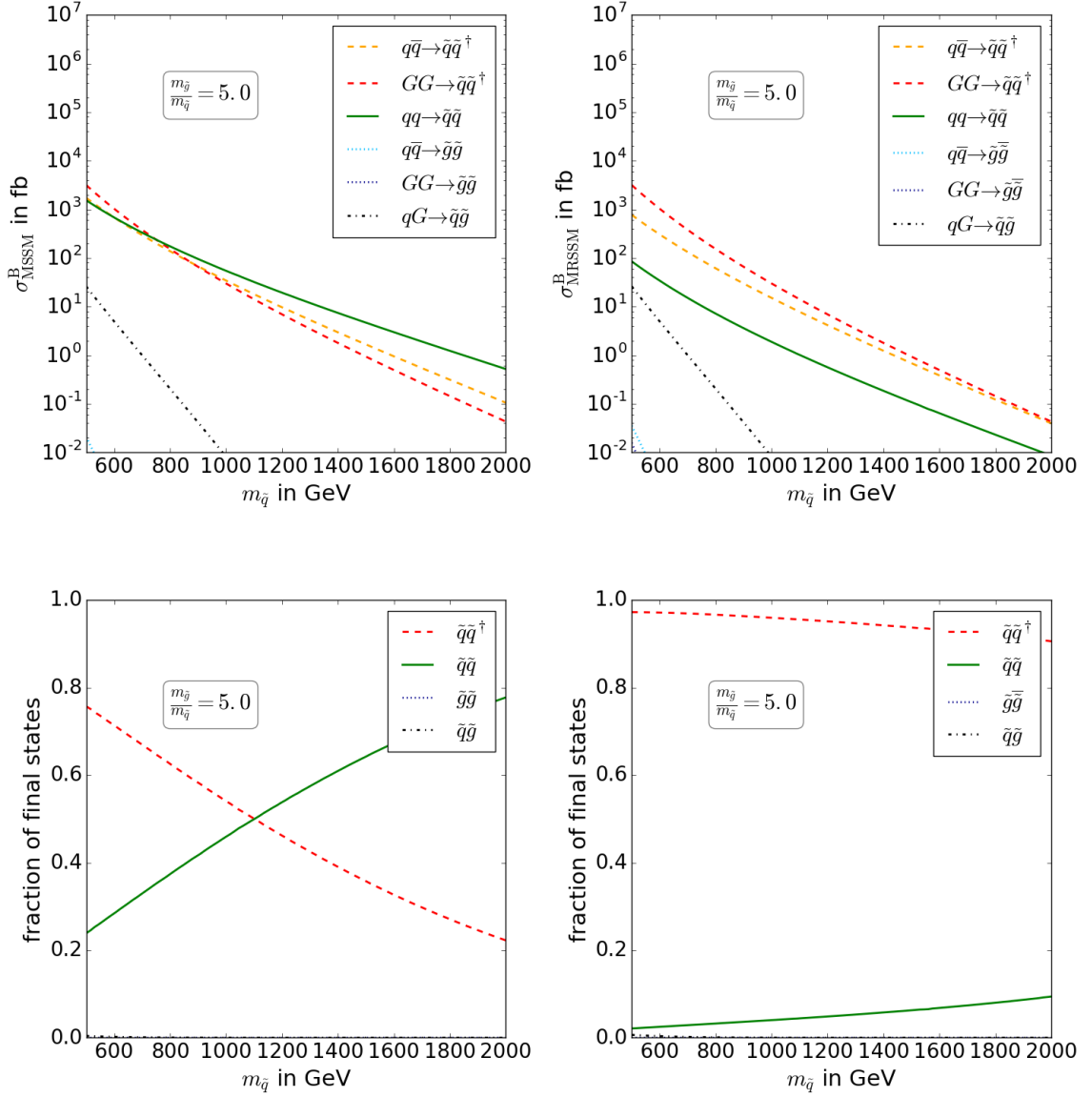


Figure 5.7: Hadronic cross section for squark and gluino production (in the first row) and relative contributions of the indicated final states to the total hadronic cross section (in the second row) in the MSSM (left-hand side) and MRSSM (right-hand side) at the LHC with $\sqrt{S} = 13$ GeV. The ratio of gluino and squark mass is fixed to 5. In the final state it has been summed over all squark flavors except for staus. For the channels $qq \rightarrow \tilde{q}\tilde{q}$ and $qG \rightarrow \tilde{q}\tilde{g}$ also the charge conjugated process is included. The parton density functions and the renormalization and factorization scale are chosen as in fig. 5.5.

The contour plots in fig. 5.8 underline the already mentioned difference between squark production in the MRSSM and the MSSM. While the cross sections for small gluino masses resemble each other closely, the cross section in the MRSSM gets increasingly suppressed with rising gluino mass.

Fig.5.9 shows the Born cross section of squark production including all possible flavors for a fixed mass of the gluino $m_{\tilde{g}} = 2000 \text{ GeV}$ (top) and the squark $m_{\tilde{q}} = 1000 \text{ GeV}$ (bottom). The figure includes uncertainty of the calculation which come from the parton density functions and the renormalization and factorization scale.

The 68% uncertainty from the central value pdf-set is obtained by performing the calculation with all eigenvector sets of the central value and taking the minimum and maximum at each point as deviations from the calculation with the central set.

The uncertainty from the renormalization scale μ_R and the factorization scale μ_F is obtained by varying both parameters with a factor of $\frac{1}{2}$ and two. For each parameter combination the cross section has been calculated. The uncertainty originating from the scale has then been determined by taking the minimum and maximum of these nine numbers for each point.

The total uncertainty is then obtained by Gauß's propagation of uncertainties:

$$\Delta\sigma = \sqrt{(\Delta\sigma_{\text{pdf}})^2 + (\Delta\sigma_{\text{scale}})^2}. \quad (5.20)$$

The uncertainty coming from the scale variation has been found much greater than the one from the parton density functions. The uncertainty from the phase space integration is negligible, i.e. $\Delta\sigma_{\text{int}} < 1\%$.

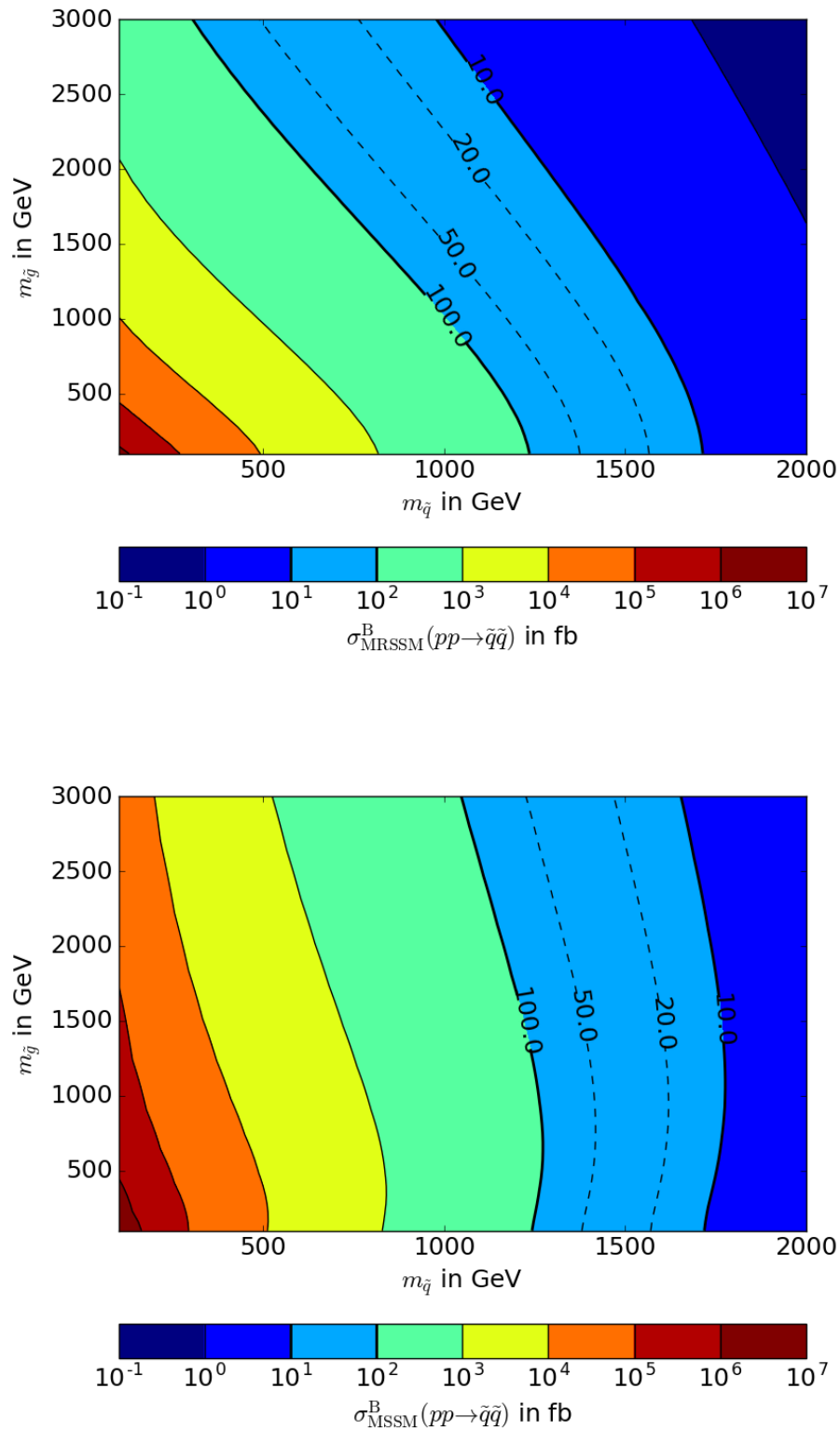


Figure 5.8: The squark (and antisquark) production cross section including five flavors in the MRSSM (top) and MSSM (bottom) at the LHC with $\sqrt{S} = 13$ GeV. The parton density functions and the renormalization and factorization scale are chosen as in fig. 5.5.

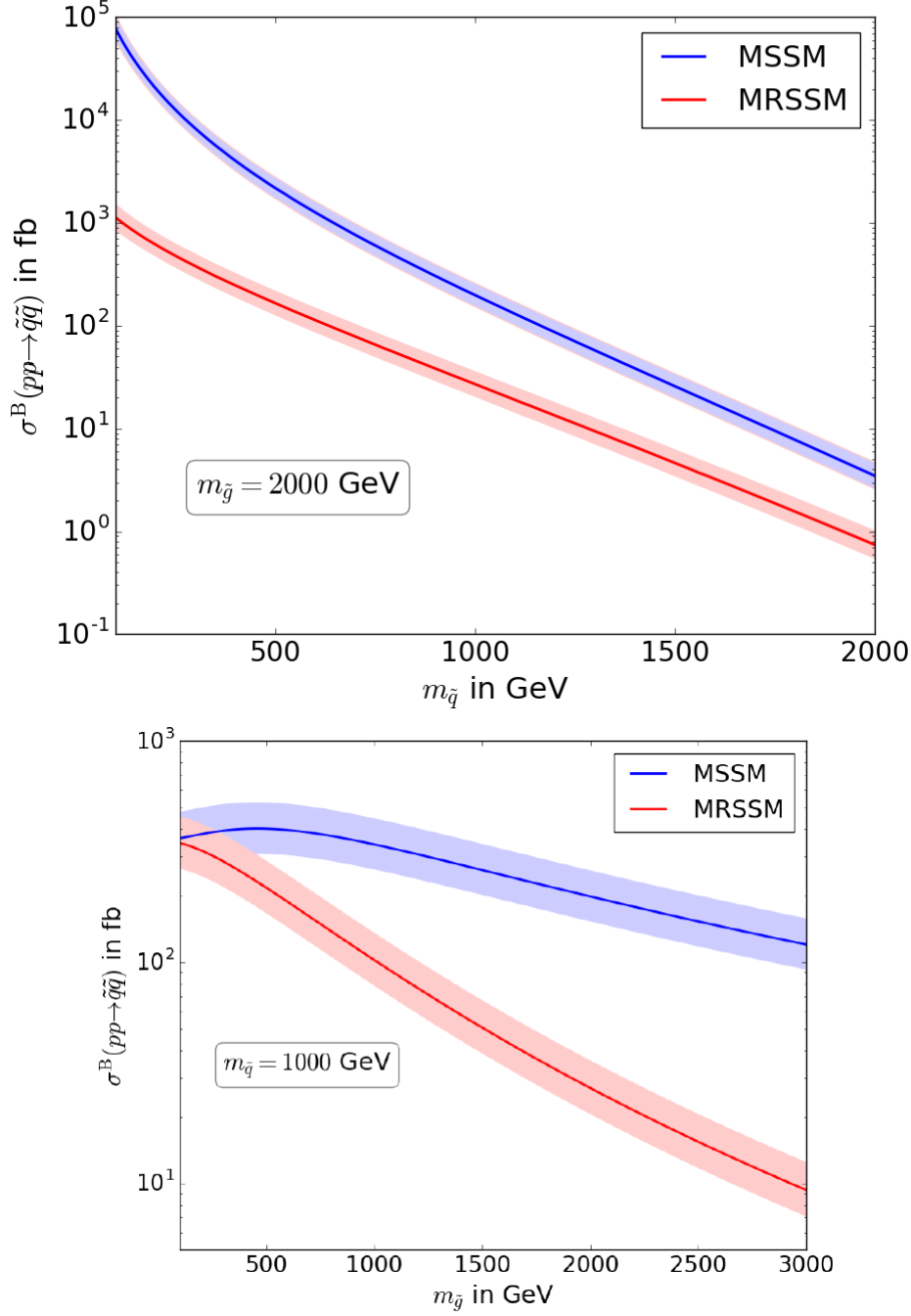


Figure 5.9: Comparison of squark (and antisquark) production cross section including five flavors in the MSSM and MRSSM at the LHC with $\sqrt{S} = 13$ GeV for fixed gluino mass (top) and fixed squark mass (bottom). The parton density functions and the renormalization and factorization scale are chosen as in fig. 5.5.

$m_{\tilde{g}} \backslash m_{\tilde{q}}$	500 GeV	1000 GeV	1500 GeV
1000 GeV	934.9 fb $^{+30.0\%+1.2\%}_{-27.2\%-2.1\%}$	102.1 fb $^{+31.2\%+1.9\%}_{-29.2\%-2.1\%}$	13.12 fb $^{+34.1\%+2.1\%}_{-31.6\%-1.7\%}$
1500 GeV	360.9 fb $^{+30.5\%+1.1\%}_{-30.0\%-2.2\%}$	50.52 fb $^{+32.4\%+1.7\%}_{-29.5\%-1.9\%}$	7.712 fb $^{+34.9\%+2.4\%}_{-31.8\%-2.8\%}$
2000 GeV	165.5 fb $^{+30.5\%+0.9\%}_{-28.2\%-2.1\%}$	26.97 fb $^{+32.6\%+1.5\%}_{-29.8\%-2.1\%}$	4.625 fb $^{+34.5\%+1.8\%}_{-31.8\%-1.6\%}$

Table 5.3: Squark production cross section at tree-level (including five flavors and also the production of antisquarks) in the MRSSM for various squark and gluino masses. The parton density functions and the renormalization and factorization scale are chosen as in fig. 5.5. The uncertainty of the numerical integration is lower than one permille. The first relative uncertainty comes from the variation of μ_R and μ_F as described in the text. The second uncertainty corresponds to the parton density function uncertainty.

$m_{\tilde{g}} \backslash m_{\tilde{q}}$	500 GeV	1000 GeV	1500 GeV
1000 GeV	5257 fb $^{+28.4\%+1.8\%}_{-24.6\%-1.2\%}$	340.4 fb $^{+31.0\%+1.6\%}_{-28.4\%-1.9\%}$	33.97 fb $^{+33.6\%+2.3\%}_{-30.6\%-1.2\%}$
1500 GeV	3263 fb $^{+27.9\%+1.2\%}_{-25.4\%-1.8\%}$	260.7 fb $^{+30.8\%+1.3\%}_{-28.4\%-2.2\%}$	30.46 fb $^{+33.2\%+1.8\%}_{-30.7\%-1.9\%}$
2000 GeV	2179 fb $^{+27.9\%+1.1\%}_{-25.6\%-1.9\%}$	198.1 fb $^{+30.7\%+1.5\%}_{-28.6\%-2.1\%}$	25.75 fb $^{+33.2\%+1.5\%}_{-30.7\%-2.0\%}$

Table 5.4: Same content as in table 5.3 but for the MSSM.

The cross sections for the production of squarks (and antisquarks) including five flavors are given for a representative set of masses in table 5.3 for the MRSSM and in table 5.4 for the MSSM. In addition to the cross section, the relative uncertainty of the scale variation and the parton density functions are given.

As a summary of the comparison between MSSM and MRSSM, one can say, that the gluino production is enhanced in the MRSSM due to distinguishable gluino and antigluino. In order to meet missing experimental evidence for supersymmetry, this suggests that in the MRSSM gluinos might be heavier than squarks. Focusing on $\frac{m_{\tilde{g}}}{m_{\tilde{q}}} \geq 2$ the most significant change between the considered models is the growing suppression of squark production for an increasing gluino mass. This is why this channel is going to be investigated at next-to-leading order within this thesis. The ensuing sections provide the prerequisites for this calculation.

6 Virtual and Real Corrections

The results calculated in the previous chapter are not the complete theoretical predictions for the cross sections of the various processes but only the first term in a perturbation series of α_s .

To provide accurate predictions, it is necessary that corrections to the leading order are small. This implies that α_s , which is strongly dependent on the energy scale, needs to fulfill $\alpha_s < 1$. It is known that α_s becomes of $\mathcal{O}(1)$ and larger when the energy scale is of $\mathcal{O}(200 \text{ MeV})$ and smaller [47]. Fortunately, squark production is a process which involves large enough energy to maintain the validity of perturbation theory, as the typical energy scale involved, is the mass of squarks which certainly fulfills $m_{\tilde{q}} > 500 \text{ GeV}$.

This section describes the necessary steps in the calculation of the squark production cross section at next-to-leading order, i.e. its $\mathcal{O}(\alpha_s)$ -correction.

6.1 Virtual Corrections

According to quantum field theory the $\mathcal{O}(\alpha_s)$ correction to a tree-level process includes the computation of one-loop diagrams such as shown in fig. 6.1.

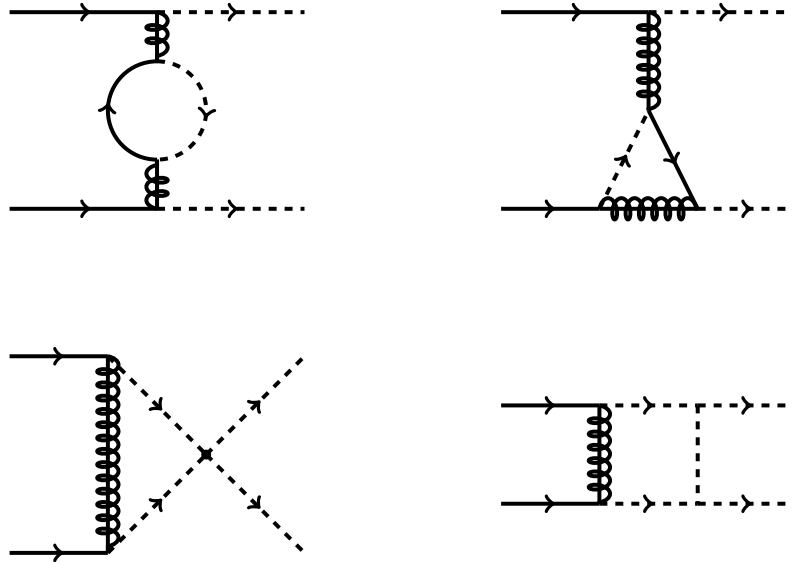


Figure 6.1: A selection of diagrams contributing to the 1-loop matrix element for squark production. Each diagram is a representative of a certain topology. In the first line, an example for a self-energy and a vertex-correction diagram is shown. The second line lists typical box-diagrams: a three-point box and a four-point box.

There are no loop corrections of external particles, which is explained in section 8.1.

To yield $\mathcal{O}(\alpha_s)$ corrections in the cross section, the interference term between the one-loop

amplitude \mathcal{M}^{1L} and the Born amplitude \mathcal{M}^B needs to be considered:

$$\begin{aligned} |\mathcal{M}^B + \mathcal{M}^{1L}|^2 &= |\mathcal{M}^B|^2 + \mathcal{M}^B \mathcal{M}^{1L*} + \mathcal{M}^{1L} \mathcal{M}^{B*} + |\mathcal{M}^{1L}|^2 \\ &= |\mathcal{M}^B|^2 + 2\Re(\mathcal{M}^B \mathcal{M}^{1L*}) + \mathcal{O}(2\text{-loop}). \end{aligned} \quad (6.1)$$

However, this term contains divergences. These come from integrals over undetermined momentum and energy of particles running in loops. Due to their origin these divergences are referred to as ultraviolet (UV) or infrared (IR) divergences. Ultraviolet divergences occur when loop momenta and energy tend to infinity which corresponds to arbitrary short distance interactions. However, these divergences are cured by first regularizing them and then introducing appropriate counterterms¹⁹ in the Lagrangian to cancel the extracted singularities. The second step is called renormalization and can be understood as a redefinition or rescaling of parameters and fields in the Lagrangian in the first place:

$$\begin{aligned} \phi^0/\sigma^0 &\rightarrow \sqrt{Z_{\phi^0/\sigma^0}} \phi^0/\sigma^0, & \tilde{q}_{L/R} &\rightarrow \sqrt{Z_{\tilde{q}_{L/R}}} \tilde{q}_{L/R}, \\ P_L \tilde{g} &\rightarrow \sqrt{Z_{\tilde{g}}^L} P_L \tilde{g}, & P_R \tilde{g} &\rightarrow \sqrt{Z_{\tilde{g}}^R} P_R \tilde{g}, \\ q &\rightarrow \sqrt{Z_q} q, & G_\mu &\rightarrow \sqrt{Z_G} G_\mu, \end{aligned} \quad (6.2)$$

$$\begin{aligned} g_s &\rightarrow g_{s \text{ bare}}, & m_{\tilde{q}}^2 &\rightarrow m_{\tilde{q}}^2 \text{ bare}, \\ m_\sigma^2 &\rightarrow m_\sigma^2 \text{ bare}, & m_{\tilde{g}} &\rightarrow m_{\tilde{g}} \text{ bare}. \end{aligned} \quad (6.3)$$

In this thesis the computation of amplitudes is performed in $D = 4 - 2\epsilon$ dimensions in order to regularize infinities. Ultraviolet divergences then show up as single poles in ϵ . The renormalization will be discussed in detail in section 7 and 8.1.

Having removed the ultraviolet divergences the matrix element is not free of divergences as it still comprises infrared divergences. These split into soft and collinear (or mass) singularities²⁰ which cannot be removed by means of renormalization. These additional singularities show up as single and double poles in ϵ in the matrix element \mathcal{M}^{1L} and the virtual cross section which is obtained after performing the 2-body phase space integration as in eq. (5.9) but over $2\Re(\mathcal{M}^B \mathcal{M}^{1L*})$:

$$\begin{aligned} \frac{d^2\sigma^V}{dt du} &= \frac{K_{ab}}{s^2} \frac{\pi S_\epsilon}{\Gamma(1-\epsilon)} \left[\frac{tu - m_1^2 m_2^2}{\mu^2 s} \right]^{-\epsilon} \Theta(tu - m_1^2 m_2^2) \\ &\quad \Theta(s - 4m^2) \delta(s + t + u - m_1^2 - m_2^2) \sum 2\Re(\mathcal{M}^B \mathcal{M}^{1L*}). \end{aligned} \quad (6.4)$$

The single poles correspond to soft and collinear divergences whereas the double poles correspond to the coincidence of soft and collinear divergences.

¹⁹These counterterms have to be of the same $\mathcal{O}(\hbar)$ as the loop diagrams they are constructed to cancel [51].

²⁰The names differ in the literature. Often infrared divergences are used as a synonym for soft divergences. The name soft and collinear divergences is explained within the next section.

6.2 Real Corrections

A crucial thing to recognize in the calculation of the $\mathcal{O}(\alpha_s)$ correction to the squark production cross section is that not only virtual corrections but also real corrections give rise to this physical observable. This is because one does not measure final state partons but jets, which consist of hadrons which in turn consist of partons. This means that the radiation of a massless particle whose energy tends to zero or the radiation of a particle which is collinear to one of the final state partons of the tree-level process can not be distinguished from the tree-level process in experiment, for both processes may give rise to the same number of jets. Ergo, the cross section of squark production at $\mathcal{O}(\alpha_s^3)$ is given by

$$\sigma^{\text{NLO}} = \sigma^{\text{B}} + \sigma^{\text{V}} + \sigma^{\text{R}}, \quad (6.5)$$

where σ^{R} denotes the cross section arising from real corrections. However, real corrections also contain divergences. To see how these arise, consider the second diagram in fig. 6.2.

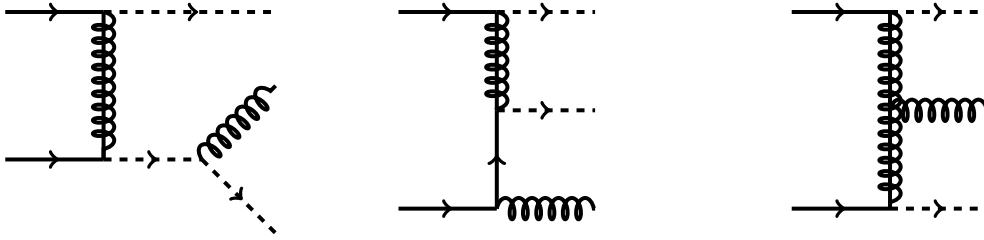


Figure 6.2: A selection of real gluon emission diagrams contributing to squark production. Each diagram is a representative of a certain diagram type. The first one is final state gluon emission, the second one initial state gluon radiation and the third one is the radiation of a gluon from a virtual particle within the diagram.

The propagator of the quark which radiates off a gluon gives a contribution of the form

$$\frac{1}{(p_q + p_g)^2 - m_q^2} = \frac{1}{p_q \cdot p_g} = \frac{1}{2E_q E_g (1 - \beta_q \cos \theta_{qg})} \quad \text{with } \beta_q = \frac{|\vec{p}_q|}{E_q} \quad (6.6)$$

to the diagram in question. Here, p_q, p_g (E_q, E_g) are the quark's and gluon's four-momentum (energy) and θ_{qg} is the angle between the quark's and gluon's three-momentum. One observes two potentially singular limits

$$\text{soft gluon :} \quad E_g \rightarrow 0 \quad (6.7)$$

$$\text{collinear particles :} \quad \theta_{qg} \rightarrow 0 \quad \text{if } m_q \rightarrow 0. \quad (6.8)$$

Including these singularities into the cross section causes the cancellation of single poles coming from the virtual cross section and the soft divergences coming from the real cross section as well as the cancellation of double poles. At this point the only singularities which are left in

the sum of real and virtual cross section are collinear ones, coming from the real correction. To see how these are removed, consider the collinear limit in (6.8). Within this limits the inner quark can almost be considered as on-shell which means that it may travel a long distance between the emission of a gluon and taking part in the actual interaction. This suggests that some divergences may come from the incoming hadron and are actually not associated with the hard interaction. In fact this turns out to be true: The remaining collinear divergences have a generic form and can be absorbed into the parton density functions. Within the $\overline{\text{MS}}$ -scheme, the redefinition of parton density functions is given by [52]:

$$f_{P_i/H}(x, \mu_f) = f(x) + \left(-\frac{1}{\epsilon}\right) \left[\frac{\alpha_s}{2\pi} \frac{\Gamma(1-\epsilon)}{\Gamma(1-2\epsilon)} \left(\frac{4\pi\mu_R^2}{\mu_F^2} \right)^\epsilon \right] \int_1^x \frac{dz}{z} P_{P_i P_j}(z) f_{P_j/H}\left(\frac{x}{z}\right). \quad (6.9)$$

Here, the indices P_i label partons, i.e. quarks or the gluon, and H labels the hadron in which the partons are confined. $\Gamma(\dots)$ is the Gamma function and $P_{P_i P_j}(x)$ are the Altarelli-Parisi-kernels [46] which are a measure for the propability of finding a parton P_i with momentum fraction x within a parton P_j . This procedure of removing collinear divergences is referred to as mass factorization [47].

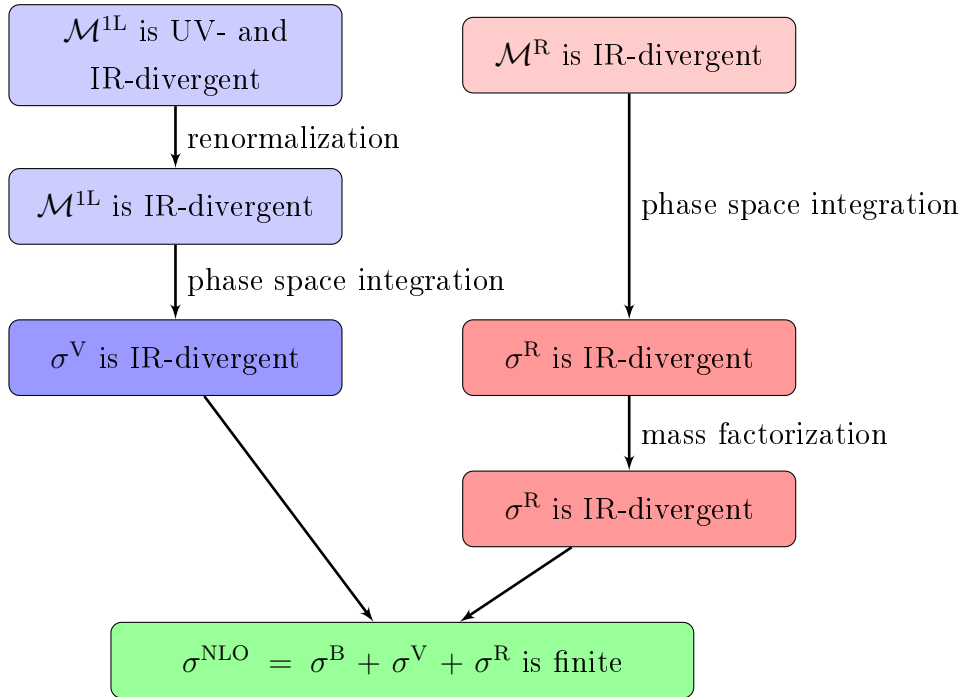


Figure 6.3: This scheme illustrates the necessary steps in the computation of the next-to-leading order cross section which are required to render it finite. Within the virtual corrections, UV-divergences of the loop diagrams are removed on the level of the matrix element. The matrix element of the real corrections become singular within certain regions of phase space. Collinear divergences can be removed by mass factorization. After this, the poles of virtual and real corrections add up to zero.

In fact, apart from this removal of collinear divergences, the Kinoshita-Lee-Naunberg-Theorem

[53, 54] guarantees the finiteness of sufficiently inclusive observables, i.e. the cancellation of soft divergences between virtual and real corrections.

Figure 6.3 summarizes the required steps to render the next-to-leading order cross section finite.

6.2.1 Real Gluon Radiation

A representative set of Feynman-diagrams for real gluon emission are shown in fig. 6.2. In order to extract the singularities the so called “two cut phase space slicing method” [52] has been adopted. Within this approach, the phase space has been divided into different regimes: a soft part (S), a hard collinear part (HC) and a hard non-collinear part ($H\bar{C}$):

$$\sigma^R = \int_S d\sigma^R + \int_H d\sigma^R = \int_S d\sigma^R + \int_{HC} d\sigma^R + \int_{H\bar{C}} d\sigma^R. \quad (6.10)$$

In the soft part, the energy of the outgoing gluon is only integrated up to $\delta_s \frac{\sqrt{s}}{2}$ where δ_s is a cut on which the final result must not depend on and \sqrt{s} is the center of mass energy of the colliding partons. A second cut δ_c is introduced to separate the collinear from the non-collinear region. After dividing the phase space into the three mentioned parts, each integration is performed separately. In the parts containing divergences, i.e. the soft and hard collinear part, the integration over the gluons four-momentum is performed analytically in $D = 4 - 2\epsilon$ dimensions. After performing mass factorization and adding up all three contributions, the real corrections do not depend on the two cut parameters δ_s and δ_c . Furthermore the $\frac{1}{\epsilon^2}$ and $\frac{1}{\epsilon}$ poles have exactly the opposite sign of the ones extracted from the virtual corrections.

6.2.2 Real Quark Radiation

As already mentioned before, adding up virtual and real gluon emission contributions results in the cancellation of divergences. However, there is a further contribution to squark production at next-to-leading order. This involves the radiation of an additional antiquark in the final state. To meet color conservation, the initial state has to be composed of a quark and a gluon, see fig. 6.4. These contributions do not comprise soft divergences, as they are associated with a different initial state and the factorization theorem guarantees the absences of soft divergences in each initial state separately [47]. This can be seen by inspecting eq. (5.18) with the leading order parton density function replaced by the renormalized parton density function from eq. (6.9). As the left hand side of eq. (5.18) is free of soft (and collinear) divergences, also the right hand side has to be infrared finite. Furthermore, the renormalized parton density functions are free of soft divergences, that is why the partonic cross section in eq. (5.18) also needs to be free of soft divergences. In other words, real corrections, coming from an initial state with quark and gluon, cannot contribute to the cancellation of soft divergences with virtual corrections which are associated with two quarks in the initial state.

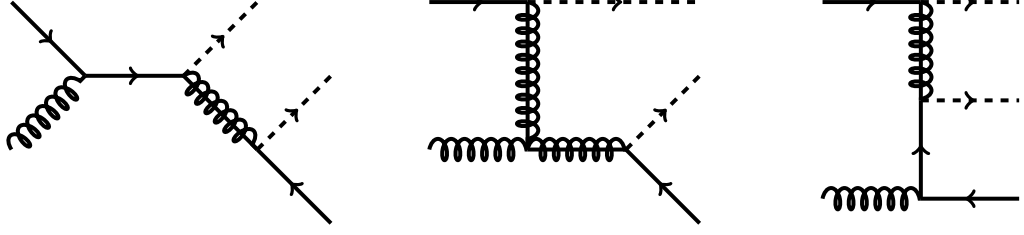


Figure 6.4: A selection of real quark emission diagrams contributing to squark production. The first two diagrams have a gluino propagator which may go on-shell. In this regime of phase space these diagrams should not be included in the correction to squark-production but to a tree-level contribution to squark-gluino-production.

A split-up of phase space in a soft and a hard part is therefore not needed. However, there are collinear singularities, originating from initial state radiation like shown in the last diagram of fig. 6.4, which again have to be removed by means of mass factorization.

But there is another complication: The first and second diagram in fig. 6.4 include a gluino which subsequently decays into a squark-antiquark pair. If the squared gluino's four-momentum approaches its mass-shell $p^2 = m_{\tilde{g}}^2$ the amplitude of this diagram hits a singularity. Of course, this can only happen if $m_{\tilde{g}} > m_{\tilde{q}}$.

These singularities are treated by introducing a non-zero width $\Gamma_{\tilde{q}}$ for the gluino as a regulator, i.e. modifying the propagator to the Breit-Wigner form

$$\frac{1}{p^2 - m_{\tilde{q}}^2} \rightarrow \frac{1}{p^2 - m_{\tilde{q}}^2 + im_{\tilde{q}}\Gamma_{\tilde{q}}}. \quad (6.11)$$

Integrating over the regime of phase space, where the gluino approaches its mass-shell, actually gives the tree-level contribution of the process $qG \rightarrow \tilde{q}\tilde{g}$ weighted by the branching ratio $\frac{\Gamma_{\tilde{q} \rightarrow q\tilde{g}}}{\Gamma_{\tilde{q}}}$. To avoid double counting, one has to cut this very regime of phase space out and subtract it from the total contribution originating from those diagrams. For a detailed prescription on how to deal with this issue, see [42, 55].

7 Renormalization of the MRSSM

This section discusses the removal of ultraviolet divergences in the amplitude of squark production at 1-loop level in the RSQCD. After a very brief introduction and discussion of the regularization schemes, field and mass renormalization constants are calculated in the on-shell scheme, using dimensional regularization. After that, the renormalization constant of the strong gauge coupling g_s is computed in a mixture of $\overline{\text{MS}}$ - and zero-momentum subtraction scheme. This is done because the gauge coupling of the parton density functions `MMHT2014` is given in the $\overline{\text{MS}}$ -scheme but does not include heavy particles, such as the top-quark or supersymmetric particles in its β -function. However renormalizing these heavy particles in the zero-momentum subtraction, implies that the β -function of g_s is exactly the one from QCD. This is shown in section 7.5. Afterwards, the fact that dimensional regularization breaks supersymmetry, which is already discussed in section 7.2, is revisited. Section 7.6 describes the calculation of an additional counterterm which restores supersymmetry within the renormalization. Finally, the UV-divergent parts of all renormalization constants in the RSQCD are given. These might prove useful in checks for UV-finiteness of a Green-function or a physical observable. The chapter closes with a discussion of the renormalized matrix amplitude.

7.1 Regularization Schemes

Dimensional Regularization (DREG)

Dimensional regularization (DREG) is a very common procedure for regularizing infinities which was devised by t'Hooft and Veltman [56]. In this scheme, loop momenta, gamma- and epsilon-tensors, phase space and fields are defined in D dimensions [57]. As in every regularization scheme, a parameter with mass dimension needs to be introduced. In DREG, that is the μ parameter which ensures that the loop integrals still have mass dimension four:

$$\int \frac{d^4 p}{(2\pi)^4} \rightarrow \mu^{4-D} \int \frac{d^D p}{(2\pi)^D}. \quad (7.1)$$

If one writes $D = 4 - 2\epsilon$, the divergences of the loop integrals manifest in $\frac{1}{\epsilon}$ poles.

However DREG suffers a flaw in supersymmetry. As the degrees of freedom of a massless gauge boson are $D - 2$ but the degrees of freedom of its superpartner are two, there is a mismatch if $D \neq 4$. As a consequence, there are 2ϵ degrees of freedom associated with the gluon²¹ which do not have a supersymmetric partner. Therefore DREG violates supersymmetry.

²¹These degrees of freedom are identified with scalars and are therefore referred to as ϵ scalars.

Dimensional Reduction (DRED)

Dimensional reduction (DRED) was introduced to rectify the imperfections of DREG, i.e. it introduces no mismatch of degrees of freedom.²² DRED promotes only momenta to D dimensions. All other quantities which are D dimensional in DREG stay in four dimensions. The most important difference is that the contraction of the metric tensor with itself equals four

$$g_{\mu\nu}g^{\mu\nu} = 4, \quad (7.2)$$

instead of D in dimensional regularization. It has been shown in [60] that DRED can be defined in a mathematically consistent way.

7.2 Regularization Scheme Dependences

To discuss the subject of this section, it is useful to introduce the effective action Γ . A formal introduction of Γ can be found in [2]. In short, Γ can be viewed as a generalization of the classical action $\Gamma_{\text{cl}} = \int \mathcal{L}_{\text{cl}}$ by quantum effects:

$$\Gamma = \Gamma_{\text{cl}} + \mathcal{O}(\hbar). \quad (7.3)$$

This means that in addition to the vertices in the classical Lagrangian, new vertices arise due to loop effects. As already alluded to, loop corrections might a priori not be finite and then need to be rendered ultraviolet finite by the addition of counterterms. For $\mathcal{O}(\hbar)$ corrections one writes

$$\Gamma^{(\leq 1)} \rightarrow \Gamma^{(\leq 1)} + \Gamma^{(1),\text{ct}}. \quad (7.4)$$

These counterterms depend on the regularization (and renormalization) scheme. If one chooses to work with DREG, which is done in this thesis, supersymmetry will not be preserved at 1-loop order, i.e. $\Gamma_{\text{DREG}}^{(\leq 1)}$ is not supersymmetric. To maintain supersymmetry invariance of the renormalized effective action, the counterterms will not only consist of supersymmetric counterterms $\Gamma_{\text{DREG}}^{(1),\text{ct,sym}}$ but also of counterterms restoring supersymmetry $\Gamma_{\text{DREG}}^{(1),\text{ct,trans}}$.

$$\Gamma_{\text{DREG}}^{(1),\text{ct}} = \Gamma_{\text{DREG}}^{(1),\text{ct,sym}} + \Gamma_{\text{DREG}}^{(1),\text{ct,trans}} \quad (7.5)$$

²²It is not clear whether DRED preserves supersymmetry at all orders in perturbation theory [58] but it does preserve supersymmetry at 1-loop level [59].

Fortunately, a supersymmetry conserving regularization scheme (at 1-loop level) is given by DRED [59]. One way to acquire supersymmetry restoring counterterms is therefore given by

$$\Gamma_{\text{DRED}}^{(\leq 1)} + \Gamma_{\text{DRED}}^{(1),\text{ct}} \stackrel{!}{=} \Gamma_{\text{DREG}}^{(\leq 1)} + \Gamma_{\text{DREG}}^{(1),\text{ct}}. \quad (7.6)$$

Equating also the finite terms in $\Gamma^{(1),\text{ct},\text{sym}}$ in DRED and DREG the choice of the supersymmetry restoring counterterms is fixed by [61–63]:

$$\Gamma_{\text{DREG}}^{(1),\text{ct},\text{trans}} = \Gamma_{\text{DRED}}^{(\leq 1)} - \Gamma_{\text{DREG}}^{(\leq 1)}. \quad (7.7)$$

This equation justifies the label “trans” at the supersymmetry restoring counterterm because it actually describes the transition counterterm from DREG to DRED or vice versa.

In the case of the MRSSM it will turn out that the only supersymmetry violation comes from corrections associated with the gluon, as already alluded to in section 7.1. However, supersymmetry restoring will always already be included in δZ^{DREG} . Referring to the field renormalization constants from eq. (6.2), this is

$$\delta Z^{\text{DREG}} = \delta Z^{\text{DREG},\text{sym}} + \delta Z^{\text{trans}} \quad (7.8)$$

where

$$\delta Z^{\text{trans}} = \delta Z^{\text{DREG}} - \delta Z^{\text{DRED}} \quad (7.9)$$

is the supersymmetry restoring renormalization constant. Note the sign within this definition in comparison to eq. (7.7). The only point where particular care is required is the coupling: The gauge coupling g_s and the Yukawa coupling \hat{g}_s receive different supersymmetry restoring counterterms:

$$\delta g_s^{\text{trans}} \neq \delta \hat{g}_s^{\text{trans}}. \quad (7.10)$$

This is due to different loop diagrams, i.e.²³

$$i\Gamma_{\text{DREG}, q_i \bar{q}_j G_\mu^a}^{(1),\text{ct},\text{trans}} \quad \text{and} \quad i\Gamma_{\text{DREG}, \tilde{q}_L i \bar{q}_j \tilde{g}^a}^{(1),\text{ct},\text{trans}} \quad (7.11)$$

are proportional to a different combination of $C(A)$ and $C(F)$. Furthermore there are different fields on the vertices, which also come with different supersymmetry restoring counterterms. Therefore one has to distinguish between these couplings at 1-loop level. In order to match g_s to the experimentally measured coupling from the parton density functions, it is renormal-

²³The fields as subscript on the effective action denote the derivative with respect to them. The quantity $i\Gamma_{\phi_1 \dots \phi_N}^{(n)}$ labels the one-particle irreducible Green function of the $\phi_1 \dots \phi_N$ vertex at n -loop-level.

ized in the $\overline{\text{MS}}$ -scheme (with an additional manipulation for heavy particles, which will be explained in section 7.4). One therefore needs to add the difference of $\delta\hat{g}_s^{\text{trans}}$ and $\delta g_s^{\text{trans}}$ to the renormalization constant of the Yukawa coupling \hat{g}_s in order to renormalized g_s and \hat{g}_s in the same way.

7.3 On-Shell Renormalization

One part of the computation of the cross section at next-to-leading order is the calculation of renormalization constants. Field renormalization constants δZ and parameter renormalization constants δo with $o \in \{g, m\}$ are defined by

$$Z = 1 + \delta Z \qquad o_{\text{bare}} = o + \delta o \qquad (7.12)$$

where Z and o_{bare} are defined by the multiplicative renormalization transformation, introduced in eq. (6.2) and (6.3). The field and mass renormalization constants have been calculated in DREG in the on-shell scheme. The advantage of this is that when turning to the cross section no modification of the Green function to the S-matrix element has to be done. This is discussed in more detail in section 8.1.

The calculation has partially been performed by hand but was always checked with the mathematica output generated by the packages **FeynArts** [35] and **FormCalc** [36, 37] which used a model file generated by **SARAH** [38–41].

The renormalization constants are given in terms of Passarino-Veltman integrals whose definition can be found in Appendix 10.6.

The Quark Self-Energy

The quark self-energy (depicted in fig. 7.1) splits into contribution from the Standard Model as well as a supersymmetric analogue which is already present in the MSSM.

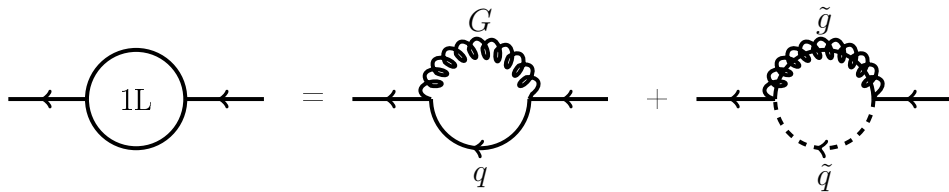


Figure 7.1: Feynman diagrams contributing to the self-energy of the quark at 1-loop level.

The one-particle-irreducible diagrams evaluate to

$$i\Gamma_{q_i\bar{q}_j}^{\text{1L}} = i\frac{g_s^2}{16\pi^2}\delta_{ij}C(F)\left[2\left(B_0(p^2, 0, 0) + B_1(p^2, 0, 0) - \frac{1}{2}\right)\not{p} - 2B_1(p^2, m_{\tilde{g}}^2, m_{\tilde{q}}^2)\not{p}\right]. \quad (7.13)$$

The left-handed part λ^a is associated with the superpartner of the gluon and therefore the “actual” gluino whereas the right-handed part $\bar{\chi}^a$ was introduced to assign a Dirac-mass to the gluino and may be referred to as the octino.

From the Lagrangian in eq. (4.17) one can see that the couplings of the two particles are quite distinct. This is reflected by different field renormalization constants of the left- and right-handed part of the gluino (see eq. (6.2)). As for the quarks, the fermion (and momentum) flow

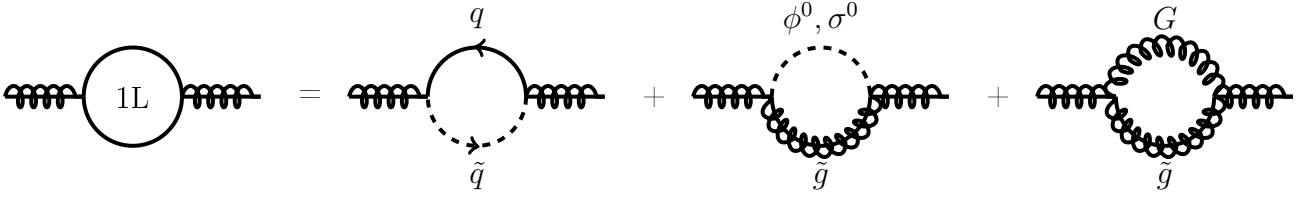


Figure 7.3: Diagrammatic contributions to the self-energy of the gluino at 1-loop level

in a diagram is from the right to the left. The Feynman diagrams for the gluino self-energy are shown in 7.3. The one-particle irreducible Green function is given by

$$i\Gamma_{\tilde{g}^a \tilde{g}^b}^{1L} = i \frac{g_s^2}{16\pi^2} \delta_{ab} \left[-4T(F) \left((n_f - 1)B_1(p^2, 0, m_{\tilde{q}}^2) + B_1(p^2, m_t^2, m_{\tilde{q}}^2) \right) P_L \not{p} \right. \\ \left. + C(A) \left((B_0(p^2, m_{\tilde{g}}^2, m_{\phi^0}^2) - B_0(p^2, m_{\tilde{g}}^2, m_{\sigma^0}^2))m_{\tilde{g}} - (B_1(p^2, m_{\tilde{g}}^2, m_{\phi^0}^2) + B_1(p^2, m_{\tilde{g}}^2, m_{\sigma^0}^2))\not{p} \right) \right. \\ \left. + C(A) \left((2 - 4B_0(p^2, 0, m_{\tilde{g}}^2))m_{\tilde{g}} - (1 - 2(B_0(p^2, 0, m_{\tilde{g}}^2) + B_1(p^2, 0, m_{\tilde{g}}^2)))\not{p} \right) \right], \quad (7.23)$$

where $n_f = 6$ is the number of quark flavors.

The counterterm Feynman rule derived from multiplicative renormalization reads

$$i\Gamma_{\tilde{g}^a \tilde{g}^b}^{1L,ct} \hat{=} a \text{ (crossed-out diagram) } b \hat{=} i\delta_{ab} \left[(\delta Z_{\tilde{g}}^L P_L + \delta Z_{\tilde{g}}^R P_R) \not{p} - \left(\frac{\delta Z_{\tilde{g}}^L + \delta Z_{\tilde{g}}^R}{2} m_{\tilde{g}} + \delta m_{\tilde{g}} \right) \right].$$

The on-shell renormalization conditions for the fields are

$$\frac{\partial}{\partial(P_L \not{p})} \left[\Re(\Gamma_{\tilde{g}^a \tilde{g}^b}^{1L}) + \Gamma_{\tilde{g}^a \tilde{g}^b}^{1L,ct} \right]_{\not{p}=m_{\tilde{g}}} = 0, \quad \frac{\partial}{\partial(P_R \not{p})} \left[\Re(\Gamma_{\tilde{g}^a \tilde{g}^b}^{1L}) + \Gamma_{\tilde{g}^a \tilde{g}^b}^{1L,ct} \right]_{\not{p}=m_{\tilde{g}}} = 0, \quad (7.24)$$

where the derivative of $\Sigma = \Sigma^{VL} P_L \not{p} + \Sigma^{VR} P_R \not{p} + \Sigma^{SL} P_L + \Sigma^{SR} P_R$ with respect to $P_A \not{p}$ ($A \in \{L, R\}$) is defined by [64]

$$\frac{\partial}{\partial(P_A \not{p})} \Sigma \Big|_{\not{p}=m} = \Sigma^{VA} + \frac{\partial}{\partial p^2} (m^2 \Sigma^{VL} + m^2 \Sigma^{VR} + m \Sigma^{SL} + m \Sigma^{SR}). \quad (7.25)$$

This leads to the following renormalization constants

$$\begin{aligned}
\delta Z_{\tilde{g}}^L = & \frac{g_s^2}{16\pi^2} \Re \left[4T(F) \left((n_f - 1) B_1(m_{\tilde{g}}^2, 0, m_{\tilde{q}}^2) + B_1(m_{\tilde{g}}^2, m_t^2, m_{\tilde{q}}^2) \right) \right. \\
& + C(A) (B_1(m_{\tilde{g}}^2, m_{\tilde{g}}^2, m_{\phi^0}^2) + B_1(m_{\tilde{g}}^2, m_{\tilde{g}}^2, m_{\sigma^0}^2)) \\
& + C(A) (1 - 2(B_0(m_{\tilde{g}}^2, 0, m_{\tilde{g}}^2) + B_1(m_{\tilde{g}}^2, 0, m_{\tilde{g}}^2))) \\
& + 4T(F) m_{\tilde{g}}^2 \frac{\partial}{\partial p^2} \left((n_f - 1) B_1(p^2, 0, m_{\tilde{q}}^2) + B_1(p^2, m_t^2, m_{\tilde{q}}^2) \right) \\
& - 2C(A) m_{\tilde{g}} \frac{\partial}{\partial p^2} \left(B_0(p^2, m_{\tilde{g}}^2, m_{\phi^0}^2) - B_0(p^2, m_{\tilde{g}}^2, m_{\sigma^0}^2) - B_1(p^2, m_{\tilde{g}}^2, m_{\phi^0}^2) - B_1(p^2, m_{\tilde{g}}^2, m_{\sigma^0}^2) \right) \\
& \left. - 4C(A) m_{\tilde{g}}^2 \frac{\partial}{\partial p^2} \left(-B_0(p^2, 0, m_{\tilde{g}}^2) + B_1(p^2, 0, m_{\tilde{g}}^2) \right) \right]_{p^2=m_{\tilde{g}}^2} \quad (7.26)
\end{aligned}$$

and

$$\begin{aligned}
\delta Z_{\tilde{g}}^R = & \frac{g_s^2}{16\pi^2} \Re \left[C(A) (B_1(m_{\tilde{g}}^2, m_{\tilde{g}}^2, m_{\phi^0}^2) + B_1(m_{\tilde{g}}^2, m_{\tilde{g}}^2, m_{\sigma^0}^2)) \right. \\
& + C(A) (1 - 2(B_0(m_{\tilde{g}}^2, 0, m_{\tilde{g}}^2) + B_1(m_{\tilde{g}}^2, 0, m_{\tilde{g}}^2))) \\
& + 4T(F) m_{\tilde{g}}^2 \frac{\partial}{\partial p^2} \left((n_f - 1) B_1(p^2, 0, m_{\tilde{q}}^2) + B_1(p^2, m_t^2, m_{\tilde{q}}^2) \right) \\
& - 2C(A) m_{\tilde{g}} \frac{\partial}{\partial p^2} \left(B_0(p^2, m_{\tilde{g}}^2, m_{\phi^0}^2) - B_0(p^2, m_{\tilde{g}}^2, m_{\sigma^0}^2) - B_1(p^2, m_{\tilde{g}}^2, m_{\phi^0}^2) - B_1(p^2, m_{\tilde{g}}^2, m_{\sigma^0}^2) \right) \\
& \left. - 4C(A) m_{\tilde{g}}^2 \frac{\partial}{\partial p^2} \left(-B_0(p^2, 0, m_{\tilde{g}}^2) + B_1(p^2, 0, m_{\tilde{g}}^2) \right) \right]_{p^2=m_{\tilde{g}}^2} . \quad (7.27)
\end{aligned}$$

As for the quark there are constant terms amid the Passarino-Veltman integrals. These arise only in DREG but not in DRED. The transition counterterms are

$$\delta Z_{\tilde{g}}^{A \text{ trans}} = \delta Z_{\tilde{g}}^{A \text{ DREG}} - \delta Z_{\tilde{g}}^{A \text{ DRED}} = C(A) \frac{g_s^2}{16\pi^2} \quad (7.28)$$

for $A \in \{L, R\}$. The gluino mass counterterm is ascertained by the condition

$$\left[\Re(\Gamma_{\tilde{g}^a \tilde{g}^b}^{1L}) + \Gamma_{\tilde{g}^a \tilde{g}^b}^{1L, \text{ct}} \right]_{p=m_{\tilde{g}}} = 0 \quad (7.29)$$

which is equivalent to

$$\delta m_{\tilde{g}} = \Re \left(m_{\tilde{g}} \frac{\Sigma^{VL} + \Sigma^{VR}}{2} + \frac{\Sigma^{SL} + \Sigma^{SR}}{2} \right) \quad (7.30)$$

and yields

$$\begin{aligned} \delta m_{\tilde{g}} = & \frac{g_s^2}{16\pi^2} m_{\tilde{g}}^2 \Re \left[-2T(F) \left((n_f - 1) B_1(m_{\tilde{g}}^2, 0, m_{\tilde{q}}^2) + B_1(m_{\tilde{g}}^2, m_t^2, m_{\tilde{q}}^2) \right) \right. \\ & + C(A) \left(B_0(m_{\tilde{g}}^2, m_{\tilde{g}}^2, m_{\phi_0}^2) - B_0(m_{\tilde{g}}^2, m_{\tilde{g}}^2, m_{\sigma_0}^2) - B_1(m_{\tilde{g}}^2, m_{\tilde{g}}^2, m_{\phi_0}^2) - B_1(m_{\tilde{g}}^2, m_{\tilde{g}}^2, m_{\sigma_0}^2) \right) \\ & \left. + C(A) \left(1 - 2B_0(m_{\tilde{g}}^2, 0, m_{\tilde{g}}^2) + 2B_1(m_{\tilde{g}}^2, 0, m_{\tilde{g}}^2) \right) \right]. \end{aligned} \quad (7.31)$$

Again there is a transition counterterm

$$\delta m_{\tilde{g}}^{\text{trans}} = \delta m_{\tilde{g}}^{\text{DREG}} - \delta m_{\tilde{g}}^{\text{DRED}} = C(A) \frac{g_s^2}{16\pi^2} m_{\tilde{g}}. \quad (7.32)$$

Apart from the renormalization constant of the gauge coupling and the supersymmetry restoring counterterm these are all renormalization constants needed from squark production at next to leading order. In fact the field renormalization constants of the gluino are not needed as they drop out when summing up all three counterterm Feynman diagrams.

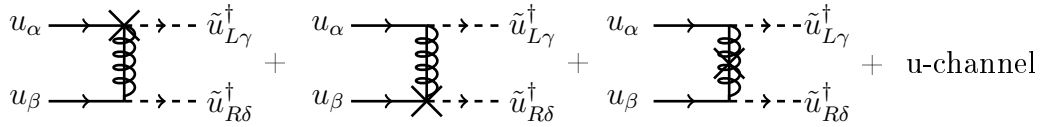


Figure 7.4: 1-Loop-level counterterm Feynman diagrams for squark production in the MRSSM. The Greek letters label the particle's color.

This can be seen when writing down the matrix amplitudes for the counterterm Feynman diagrams shown in fig. 7.4:

$$\mathcal{M}^B = -2g_s^2 \frac{\langle v_2 | P_R \not{k}_3 | u_1 \rangle}{t_{\tilde{g}}} T_{\delta\beta}^a T_{\gamma\alpha}^a + 2g_s^2 \frac{\langle v_2 | P_L \not{k}_3 | u_1 \rangle}{u_{\tilde{g}}} T_{\gamma\beta}^a T_{\delta\alpha}^a \quad (7.33)$$

$$\mathcal{M}_{\text{vertex}}^{\text{1L,ct}} = 2\mathcal{M}^B \left(\frac{\delta \hat{g}_s}{\hat{g}_s} + \frac{\delta Z_q}{2} + \frac{\delta Z_{\tilde{g}}^L}{2} + \frac{\delta Z_{\tilde{q}}}{2} \right) \quad (7.34)$$

$$\begin{aligned} \mathcal{M}_{\text{self-energy}}^{\text{1L,ct}} = & 2g_s^2 \left\langle v_2 \left| P_R i \frac{\not{p} + m_{\tilde{g}}}{t_{\tilde{g}}} \left[i(\delta Z_{\tilde{g}}^L P_L + \delta Z_{\tilde{g}}^R P_R) \not{p} \right. \right. \right. \\ & \left. \left. - i \left(\frac{\delta Z_{\tilde{g}}^L + \delta Z_{\tilde{g}}^R}{2} m_{\tilde{g}} + \delta m_{\tilde{g}} \right) \right] i \frac{\not{p} + m_{\tilde{g}}}{t_{\tilde{g}}} P_L \right| u_1 \right\rangle \Big|_{p=p_1-p_3} + \text{u-channel} \\ = & -\mathcal{M}^B \delta Z_{\tilde{g}}^L + 2 \frac{m_{\tilde{g}}}{t_{\tilde{g}}} \left(-2g_s^2 \frac{\langle v_2 | P_R \not{k}_3 | u_1 \rangle}{t_{\tilde{g}}} T_{\delta\beta}^a T_{\gamma\alpha}^a \right) \delta m_{\tilde{g}} \\ & + 2 \frac{m_{\tilde{g}}}{u_{\tilde{g}}} \left(2g_s^2 \frac{\langle v_2 | P_L \not{k}_3 | u_1 \rangle}{u_{\tilde{g}}} T_{\gamma\beta}^a T_{\delta\alpha}^a \right) \delta m_{\tilde{g}}. \end{aligned} \quad (7.35)$$

$\delta Z_{\tilde{g}}^R$ drops out already in $\mathcal{M}_{\text{self-energy}}^{\text{1L,ct}}$ as the octino does neither couple to quarks nor to squarks. The renormalization constant of the actual gluino $\delta Z_{\tilde{g}}^L$ drops out when $\mathcal{M}_{\text{self-energy}}^{\text{1L,ct}}$

and $\mathcal{M}_{\text{vertex}}^{\text{1L,ct}}$ are added. This is also true in a more general case, i.e. the renormalization constants of virtual particles do always drop out. This may be understood in the path integral approach of quantum field theory [2]: When considering a certain process, the Green function corresponding to this process, can be expressed as a path integral over fields within the theory. The field of virtual particles occurs only in the exponential, in contrast to the fields of external particles. This means that rescaling a field of an inner particle has no influence on the Green function. Ergo the field renormalization constants of any virtual particle must always drop out when considering a certain process.

7.4 Renormalization of the Gauge Coupling

The gauge coupling g_s is renormalized in the $\overline{\text{MS}}$ -scheme with the modification that additional logarithms are subtracted, i.e. light particles are treated in the $\overline{\text{MS}}$ -scheme and heavy particles in the zero-momentum subtraction scheme. This is to decouple heavy particles from the running of $\alpha_s = \frac{g_s^2}{4\pi}$. This renormalization procedure allows to adopt the experimental values of α_s from the parton density functions. The running due to effects of heavy particles is then encoded in the logarithms of δg_s .

Extracting δg_s from the quark-quark-gluon vertex requires not only the computation of $i\Gamma_{q_i\bar{q}_j}^{\text{1L}} G_a^\mu$ but also the (re)evaluation of auxiliary field renormalization constants δZ_q^{aux} and δZ_G^{aux} in the above mentioned scheme. These will not be the same as in the on-shell scheme.

The Quark Self-Energy Revisited

The quark self-energy has two contributions which are shown in figure 7.1. The first one corresponds to light particles and the second one to heavy particles: $i\Gamma_{q_i\bar{q}_j}^{\text{1L}} = i\Gamma_{q_i\bar{q}_j}^{\text{1L,light}} + i\Gamma_{q_i\bar{q}_j}^{\text{1L,heavy}}$. For light particles only the UV-divergent²⁴ part is kept. The self energy corresponding to the heavy particles is evaluated at zero momentum $p^2 = 0$

$$i\Gamma_{q_i\bar{q}_j}^{\text{1L,light}} \Big|_{\text{UV-div}} = iC(F) \frac{g_s^2}{16\pi^2} \Delta_\epsilon \not{p} \delta_{ij}, \quad (7.36)$$

$$i\Gamma_{q_i\bar{q}_j}^{\text{1L,heavy}}(p^2 = 0) = -iC(F) \frac{g_s^2}{16\pi^2} 2B_1(0, m_g^2, m_q^2) \not{p} \delta_{ij}. \quad (7.37)$$

The renormalization constant for the evaluation of δg_s is determined by the condition

$$\frac{\partial}{\partial \not{p}} \left[\Gamma_{q_i\bar{q}_j}^{\text{1L,light}} \Big|_{\text{UV-div}} + \Gamma_{q_i\bar{q}_j}^{\text{1L,heavy}}(p^2 = 0) + \Gamma_{q_i\bar{q}_j}^{\text{1L,ct}} \right] = 0 \quad (7.38)$$

²⁴In contrast to the MS -scheme in the $\overline{\text{MS}}$ -scheme not only the pure ultraviolet divergence but also two additional transcendent numbers are subtracted. It is therefore common to define $\Delta_\epsilon = \frac{1}{\epsilon} - \gamma_E + \ln 4\pi$.

and computes to

$$\delta Z_q^{\text{aux}} = \frac{g_s^2}{16\pi^2} C(F) [-\Delta_\epsilon + 2B_1(0, m_{\tilde{g}}^2, m_{\tilde{q}}^2)]. \quad (7.39)$$

The Gluon Self-Energy

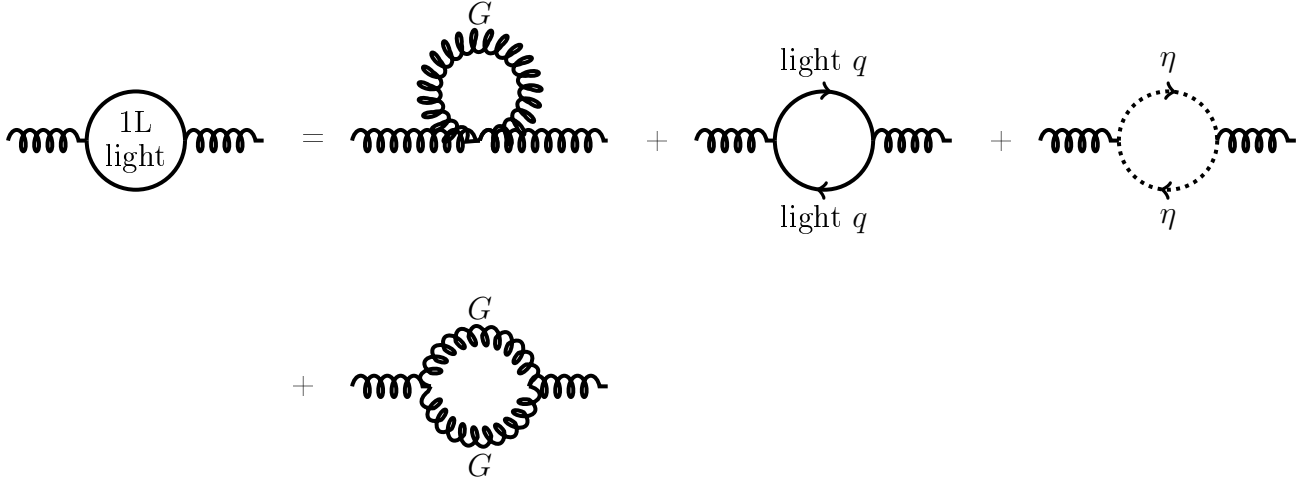


Figure 7.5: Contribution to the self-energy of the gluon originating from light particles.

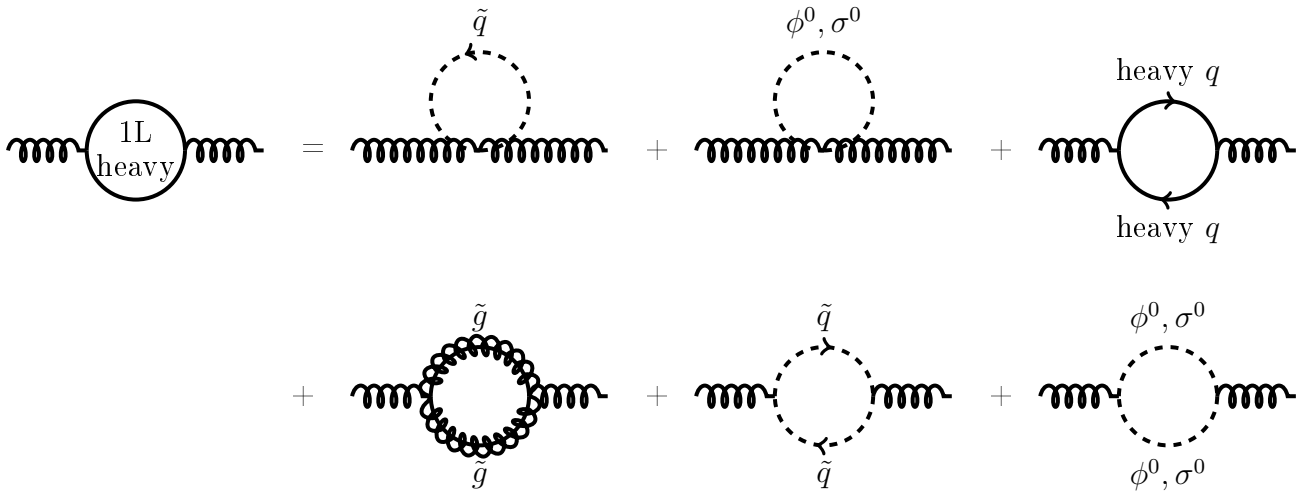


Figure 7.6: Contribution to the self-energy of the gluon originating from heavy particles, in the last diagram either ϕ^0 or σ^0 are running in the loop.

As for the quark self-energy, there are again contributions to the self-energy of the gluon originating from light and heavy particles. Again these are differently dealt with. The ultraviolet

divergent one-particle irreducible Green function is given by

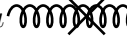
$$\begin{aligned}
i\Gamma_{G_\mu^a G_\nu^b}^{\text{1L,light}} \Big|_{\text{UV-div}} &= i \frac{g_s^2}{16\pi^2} \Delta_\epsilon \left[0 - \frac{4(n_f - 1)}{3} T(F) (p^2 g^{\mu\nu} - p^\mu p^\nu) + \frac{C(A)}{12} (p^2 g^{\mu\nu} + 2p^\mu p^\nu) \right. \\
&\quad \left. + \frac{C(A)}{12} (19p^2 g^{\mu\nu} - 22p^\mu p^\nu) \right] \delta_{ab} \\
&= i \frac{g_s^2}{16\pi^2} \Delta_\epsilon \left[-\frac{4(n_f - 1)}{3} T(F) + \frac{5}{3} C(A) \right] (p^2 g^{\mu\nu} - p^\mu p^\nu) \delta_{ab}. \tag{7.40}
\end{aligned}$$

Both the contribution from the gluon loop and the one from the ghost loop are not proportional to $(p^2 g^{\mu\nu} - p^\mu p^\nu)$ but their sum is. This transversal form is an implication of gauge invariance [47].

The heavy particle contributions are calculated in the zero-momentum subtraction:

$$\begin{aligned}
i\Gamma_{G_\mu^a G_\nu^b}^{\text{1L,heavy}}(p^2 = 0) &= i \frac{g_s^2}{16\pi^2} \delta_{ab} \left[-4T(F)n_f \left(\Delta_\epsilon - \ln \frac{m_{\tilde{q}}^2}{\mu^2} \right) m_{\tilde{q}}^2 g^{\mu\nu} - C(A) \left(\Delta_\epsilon - \ln \frac{m_{\phi^0}^2}{\mu^2} \right) m_{\phi^0}^2 g^{\mu\nu} \right. \\
&\quad - C(A) \left(\Delta_\epsilon - \ln \frac{m_{\sigma^0}^2}{\mu^2} \right) m_{\sigma^0}^2 g^{\mu\nu} - \frac{4}{3} T(F) \left(\Delta_\epsilon - \ln \frac{m_{\tilde{g}}^2}{\mu^2} \right) (p^2 g^{\mu\nu} - p^\mu p^\nu) \\
&\quad - \frac{4}{3} C(A) \left(\Delta_\epsilon - \ln \frac{m_{\tilde{g}}^2}{\mu^2} \right) (p^2 g^{\mu\nu} - p^\mu p^\nu) \\
&\quad - \frac{2}{3} T(F)n_f \left(\Delta_\epsilon - \ln \frac{m_{\tilde{q}}^2}{\mu^2} \right) (p^2 g^{\mu\nu} - p^\mu p^\nu) + 4T(F)n_f \left(\Delta_\epsilon - \ln \frac{m_{\tilde{q}}^2}{\mu^2} \right) m_{\tilde{q}}^2 g^{\mu\nu} \\
&\quad - \frac{1}{6} C(A) \left(\Delta_\epsilon - \ln \frac{m_{\phi^0}^2}{\mu^2} \right) (p^2 g^{\mu\nu} - p^\mu p^\nu) + C(A) \left(\Delta_\epsilon - \ln \frac{m_{\phi^0}^2}{\mu^2} \right) m_{\phi^0}^2 g^{\mu\nu} \\
&\quad \left. - \frac{1}{6} C(A) \left(\Delta_\epsilon - \ln \frac{m_{\phi^0}^2}{\mu^2} \right) (p^2 g^{\mu\nu} - p^\mu p^\nu) + C(A) \left(\Delta_\epsilon - \ln \frac{m_{\phi^0}^2}{\mu^2} \right) m_{\phi^0}^2 g^{\mu\nu} \right] \\
&= i \frac{g_s^2}{16\pi^2} \delta_{ab} \left[-\frac{4}{3} T(F) \left(\Delta_\epsilon - \ln \frac{m_{\tilde{t}}^2}{\mu^2} \right) (p^2 g^{\mu\nu} - p^\mu p^\nu) \right. \\
&\quad - \frac{4}{3} C(A) \left(\Delta_\epsilon - \ln \frac{m_{\tilde{g}}^2}{\mu^2} \right) (p^2 g^{\mu\nu} - p^\mu p^\nu) \\
&\quad - \frac{2}{3} T(F)n_f \left(\Delta_\epsilon - \ln \frac{m_{\tilde{q}}^2}{\mu^2} \right) (p^2 g^{\mu\nu} - p^\mu p^\nu) \\
&\quad - \frac{1}{6} C(A) \left(\Delta_\epsilon - \ln \frac{m_{\phi^0}^2}{\mu^2} \right) (p^2 g^{\mu\nu} - p^\mu p^\nu) \\
&\quad \left. - \frac{1}{6} C(A) \left(\Delta_\epsilon - \ln \frac{m_{\phi^0}^2}{\mu^2} \right) (p^2 g^{\mu\nu} - p^\mu p^\nu) \right]. \tag{7.41}
\end{aligned}$$

The counterterm Feynman rule for the gluon propagator is

$$i\Gamma_{G_\mu^a G_\nu^b}^{\text{1L,ct}} \hat{=} a, \mu \text{  b, \nu \hat{=} -i\delta Z_G (p^2 g^{\mu\nu} - p^\mu p^\nu) \delta_{ab}.$$

The renormalization condition for δZ_G^{aux} reads

$$\Gamma_{G_\mu^a G_\nu^b}^{\text{1L,light}} \Big|_{\text{UV-div}} + \Gamma_{G_\mu^a G_\nu^b}^{\text{1L,heavy}}(p^2 = 0) - \delta Z_G^{\text{aux}} (p^2 g^{\mu\nu} - p^\mu p^\nu) \delta_{ab} = 0 \quad (7.42)$$

and yields

$$\begin{aligned} \delta Z_G^{\text{aux}} = \frac{g_s^2}{16\pi^2} \Bigg\{ & \left[-\frac{4}{3}T(F)(n_f - 1) + \frac{5}{3}C(A) \right] \Delta_\epsilon + \left[-\frac{4}{3}T(F) \left(\Delta_\epsilon - \ln \frac{m_t^2}{\mu^2} \right) \right. \\ & - \frac{4}{3}C(A) \left(\Delta_\epsilon - \ln \frac{m_g^2}{\mu^2} \right) - \frac{2}{3}T(F)n_f \left(\Delta_\epsilon - \ln \frac{m_{\tilde{q}}^2}{\mu^2} \right) \\ & \left. - \frac{1}{6}C(A) \left(\Delta_\epsilon - \ln \frac{m_{\phi^0}^2}{\mu^2} \right) - \frac{1}{6}C(A) \left(\Delta_\epsilon - \ln \frac{m_{\sigma^0}^2}{\mu^2} \right) \right] \Bigg\} \end{aligned} \quad (7.43)$$

where the first squared bracket comes from light and the second one from heavy particles running in the loop.

The $q\bar{q}G$ Vertex Correction

Like the self-energies, the vertex corrections are composed of loops from light particles from the Standard Model and additional heavy particle loops. The contributions from Standard

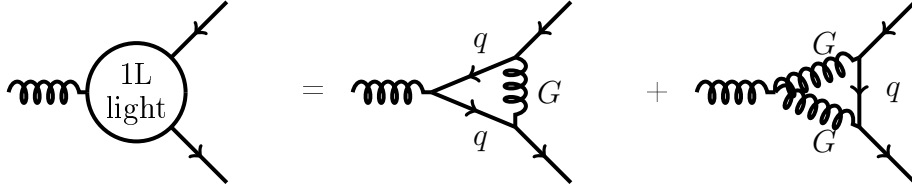


Figure 7.7: Contribution from light (Standard Model) particles to the $q\bar{q}G$ vertex correction.

Model particles (shown in fig. 7.7) to the $q\bar{q}G$ yield

$$\begin{aligned} i\Gamma_{q_i \bar{q}_j G_\mu^a}^{\text{1L,light}} \Big|_{\text{UV-div}} &= -ig_s T_{ij}^a \gamma^\mu \frac{g_s^2}{16\pi^2} \left[\left(C(F) - \frac{C(A)}{2} \right) 2(B_0(0, 0, 0) - 2C_{00}(0, 0, 0, 0, 0)) \right. \\ &\quad \left. + C(A)(B_0(0, 0, 0) + 2C_{00}(0, 0, 0, 0, 0)) \right] \\ &= -ig_s T_{ij}^a \gamma^\mu \frac{g_s^2}{16\pi^2} \Delta_\epsilon \left[\left(C(F) - \frac{C(A)}{2} \right) + \frac{3}{2}C(A) \right]. \end{aligned} \quad (7.44)$$

The term in the curved brackets of eq. (7.44) corresponds to the first diagram in fig. 7.7 whereas the term with the prefactor $C(A)$ corresponds to the second diagram. The three-point-function with only heavy particles running in the loop (displayed in fig. 7.8) evaluates

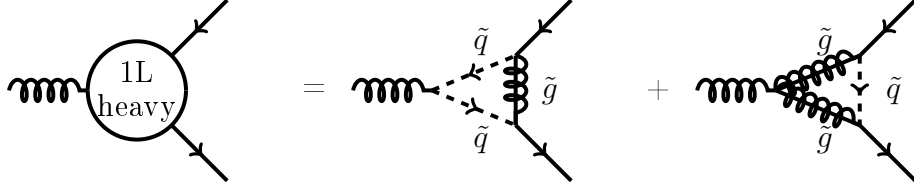


Figure 7.8: Contribution from heavy particles to the $q\bar{q}G$ vertex correction.

to

$$\begin{aligned}
 i\Gamma_{q_i\bar{q}_j G_\mu^a}^{1L, \text{heavy}}(p_i^2 = 0) &= -ig_s T_{ij}^a \gamma^\mu \frac{g_s^2}{16\pi^2} \left[\left(C(F) - \frac{C(A)}{2} \right) 4C_{00}(0, 0, 0, m_{\tilde{g}}^2, m_{\tilde{q}}^2, m_{\tilde{q}}^2) \right. \\
 &\quad \left. + C(A) (B_0(0, m_{\tilde{g}}^2, m_{\tilde{q}}^2) - 2C_{00}(0, 0, 0, m_{\tilde{g}}^2, m_{\tilde{g}}^2, m_{\tilde{q}}^2)) \right] \\
 &= ig_s T_{ij}^a \gamma^\mu \frac{g_s^2}{16\pi^2} 2C(F) B_1(0, m_{\tilde{g}}^2, m_{\tilde{q}}^2). \tag{7.45}
 \end{aligned}$$

The argument $p_i^2 = 0$ of the vertex function denotes that all external particles are taken on shell, i.e. at zero momentum.

In the second line of eq. (7.45) identities from section 10.6 have been used. The renormalization condition for the counterterm of the gauge coupling δg_s reads

$$i\Gamma_{q_i\bar{q}_j G_\mu^a}^{1L, \text{light}} \Big|_{\text{UV-div}} + i\Gamma_{q_i\bar{q}_j G_\mu^a}^{1L, \text{heavy}}(p_i^2 = 0) + \left[-ig_s T_{ij}^a \gamma^\mu \left(\frac{\delta g_s}{g_s} + \delta Z_q^{\text{aux}} + \frac{\delta Z_G^{\text{aux}}}{2} \right) \right] = 0. \tag{7.46}$$

Finally one can read off $\frac{\delta g_s}{g_s}$

$$\begin{aligned}
 \frac{\delta g_s}{g_s} &= \frac{g_s^2}{16\pi^2} \left[\left(\frac{2}{3} T(F)(n_f - 1) - \frac{11}{6} C(A) \right) \Delta_\epsilon + \left(\frac{5}{6} C(A) + \frac{2}{3} T(F) + \frac{1}{3} T(F)n_f \right) \Delta_\epsilon \right. \\
 &\quad \left. - \frac{2}{3} C(A) \ln \frac{m_{\tilde{g}}^2}{\mu^2} - \frac{1}{3} T(F)n_f \ln \frac{m_{\tilde{q}}^2}{\mu^2} - \frac{2}{3} T(F) \ln \frac{m_t^2}{\mu^2} - \frac{1}{12} C(A) \left(\ln \frac{m_{\phi^0}^2}{\mu^2} + \ln \frac{m_{\sigma^0}^2}{\mu^2} \right) \right]. \tag{7.47}
 \end{aligned}$$

Note the only difference to the MSSM [42] is the appearance of the sgluon masses as well as a factor of two in front of the logarithm of the gluino mass which is due to twice as much degrees of freedom of the gluino in the MRSSM.

7.5 The Beta Function

The beta function describes the dependence of the gauge coupling g_s upon the energy scale μ . Writing down the action of a theory in D dimensions, one needs to introduce an energy scale μ in order to keep the action dimensionless. For μ not being a physical parameter it can be

absorbed into the fields and parameters. To this end, one defines the bare coupling

$$g_{sB}(g_s, \mu) = \mu^\epsilon g_s \left(1 + \frac{\delta g_s}{g_s} \right), \quad (7.48)$$

which must not depend upon the unphysical scale μ , ergo

$$0 = \frac{dg_{sB}}{d \ln \mu} = \frac{\partial g_{sB}}{\partial \ln \mu} + \beta \frac{\partial g_{sB}}{\partial g_s} \quad (7.49)$$

where the definition of the beta function $\frac{\partial g_s}{\partial \ln \mu}$ has been inserted. Equation (7.49) serves to calculate $\beta(g_s, \epsilon)$. By equating coefficients and using the shortcuts

$$\begin{aligned} \frac{\beta_0^L}{2} &= \frac{2}{3}T(F)(n_f - 1) - \frac{11}{6}C(A) \\ \frac{\beta_0^H}{2} &= \frac{5}{6}C(A) + \frac{2}{3}T(F) + \frac{1}{3}T(F)n_f \\ L &= -\frac{2}{3}C(A) \ln \frac{m_{\tilde{g}}^2}{\mu^2} - \frac{1}{3}T(F)n_f \ln \frac{m_{\tilde{q}}^2}{\mu^2} - \frac{2}{3}T(F) \ln \frac{m_t^2}{\mu^2} - \frac{1}{12}C(A) \left(\ln \frac{m_{\phi^0}^2}{\mu^2} + \ln \frac{m_{\sigma^0}^2}{\mu^2} \right) \end{aligned}$$

for contributions from light and heavy particles, so that

$$\frac{\delta g_s}{g_s} = \frac{g_s^2}{16\pi^2} \left(\frac{\beta_0^L}{2\epsilon_{UV}} + \frac{\beta_0^H}{2\epsilon_{UV}} + L \right) \quad (7.50)$$

one finds

$$\beta(g_s, \epsilon) = -\epsilon g_s \left(1 + \frac{g_s^2}{16\pi^2} L \right) + \beta(g_s) + \mathcal{O}(2\text{-loop}) \quad (7.51)$$

$$\beta(g_s) = \frac{g_s^3}{16\pi^2} \beta_0^L + \mathcal{O}(2\text{-loop}). \quad (7.52)$$

This is the β function of QCD first found by Politzer [65], Gross and Wilczek [66]. This means that renormalizing g_s in the way it is decouples heavy particles from the β function and allows to adopt $\alpha_s = \frac{g_s^2}{4\pi}$ from the parton density functions.

7.6 Supersymmetry Restoring Counterterm

As already discussed in section 7.2, care is required in terms of supersymmetry restoring when renormalizing the gauge coupling g_s and the Yukawa coupling \hat{g}_s . In doing so one needs the already calculated transition counterterms of the quark, squark and gluino from eq. (7.16), (7.21) and (7.28) as well as the transition counterterm of the gluon.

The Gluon Self-Energy Revisited

The only regularization dependence of the gluon self-energy arises from the gluon loop, i.e. the last diagram in figure 7.5. With the definition of $\Gamma_{\text{DREG}}^{(1),\text{ct,trans}}$ in eq. (7.7) one obtains

$$i\Gamma_{\text{DREG},G_\mu^a G_\nu^b}^{(1),\text{ct,trans}} = -i\frac{1}{3}C(A)\frac{g_s^2}{16\pi^2}(p^2 g^{\mu\nu} - p^\mu p^\nu)\delta_{ab} \quad (7.53)$$

which translates to the transition counterterm

$$\delta Z_G^{\text{trans}} = \frac{C(A)}{3} \frac{g_s^2}{16\pi^2}. \quad (7.54)$$

The $q\bar{q}G$ Vertex Correction Revisited

The diagrams from which the supersymmetry restoring contributions to the $q\bar{q}G$ vertex come from are shown in figure 7.7 and evaluate to

$$i\Gamma_{\text{DREG},q_i\bar{q}_j G_\mu^a}^{(1),\text{ct,trans}} = -ig_s T_{ij}^a \gamma^\mu \frac{g_s^2}{16\pi^2} \left[\left(C(F) - \frac{C(A)}{2} \right) + \frac{C(A)}{2} \right] \quad (7.55)$$

$$= -ig_s T_{ij}^a \gamma^\mu \left[\frac{\delta g_s^{\text{trans}}}{g_s} + \delta Z_q^{\text{trans}} + \frac{\delta Z_G^{\text{trans}}}{2} \right] \quad (7.56)$$

where the second line shows the supersymmetry restoring counterterms to which they have to be equated to. Using the transition counterterms of the field yields

$$\frac{\delta g_s^{\text{trans}}}{g_s} = -\frac{C(A)}{6} \frac{g_s^2}{16\pi^2}. \quad (7.57)$$

The $\tilde{q}_L\bar{q}\tilde{g}$ Vertex Correction

The supersymmetry restoring corrections to the $\tilde{q}_L\bar{q}\tilde{g}$ vertex originate from the diagram in figure 7.9. The supersymmetry restoring part is given by

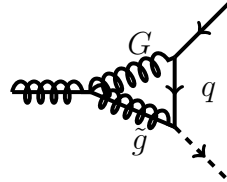


Figure 7.9: Diagram of the supersymmetry restoring correction of the $q\bar{q}\tilde{g}$ vertex

$$i\Gamma_{\text{DREG},\tilde{q}_L i \bar{q}_j \tilde{g}^a}^{(1),\text{ct,trans}} = -ig_s \sqrt{2} P_L T_{ij}^a \frac{g_s^2}{16\pi^2} C(A) \quad (7.58)$$

$$= -ig_s \sqrt{2} P_L T_{ij}^a \left[\frac{\delta \hat{g}_s^{\text{trans}}}{g_s} + \frac{\delta Z_q^{\text{trans}} + \delta Z_{\tilde{q}}^{\text{trans}} + \delta Z_{\tilde{g}}^{\text{trans}}}{2} \right]. \quad (7.59)$$

Again, using the transition counterterms of the respective fields, one obtains

$$\frac{\delta \hat{g}_s^{\text{trans}}}{g_s} = -\frac{C(F) - C(A)}{2} \frac{g_s^2}{16\pi^2}. \quad (7.60)$$

As a consequence of the two different supersymmetry restoring parts of the coupling renormalization constants an additional renormalization constant $\delta g_s^{\text{restore}}$ needs to be introduced. As described in section 7.2 it is given by

$$\frac{\delta g_s^{\text{restore}}}{g_s} = \frac{\delta \hat{g}_s^{\text{trans}}}{g_s} - \frac{\delta g_s^{\text{trans}}}{g_s} = \frac{g_s^2}{16\pi^2} \left(\frac{2C(A)}{3} - \frac{C(F)}{2} \right). \quad (7.61)$$

In short, this means that the gauge coupling g_s is renormalized with δg_s given in eq. (7.47) and the Yukawa coupling \hat{g}_s is renormalized with $\delta \hat{g}_s = \delta g_s + \delta g_s^{\text{restore}}$.

The finite correction $\delta g_s^{\text{restore}}$ is the same as in supersymmetric QCD which should not surprise too much as all its contributions originate from loops with gluons.

7.7 $\overline{\text{MS}}$ - Renormalization

To check quickly for UV-finiteness of a Greenfunction or a physical observable it is useful to have the extracted UV-divergences of the renormalization constants at hand. How these are obtained is described in section 10.6. They evaluate to:

$$\begin{aligned} \delta Z_{\tilde{g}}^L &= -\frac{g_s^2}{16\pi^2\epsilon_{\text{UV}}} 2 [T(F)n_f + C(A)], & \delta Z_{\tilde{g}}^R &= -\frac{g_s^2}{16\pi^2\epsilon_{\text{UV}}} 2C(A), \\ \delta m_{\tilde{g}} &= \frac{g_s^2}{16\pi^2\epsilon_{\text{UV}}} [T(F)n_f - 2C(A)] m_{\tilde{g}}, \\ \delta Z_{\tilde{q}} &= 0, & \delta m_{\tilde{q}}^2 &= 0, \\ \frac{\delta g_s}{g_s} &= \frac{g_s^2}{16\pi^2\epsilon_{\text{UV}}} [T(F)n_f - C(A)] = 0, \\ \delta Z_{\phi^0} &= 0, & \delta m_{\phi^0}^2 &= -\frac{g_s^2}{16\pi^2\epsilon_{\text{UV}}} [8T(F)n_f - 16C(A)] m_{\tilde{g}}^2, \\ \delta Z_{\sigma^0} &= 0, & \delta m_{\sigma^0}^2 &= 0, \\ \delta Z_G &= -\frac{g_s^2}{16\pi^2\epsilon_{\text{UV}}} 2T(F)n_f. \end{aligned} \quad (7.62)$$

The results have been checked with the `FormCalc` function `UVDivergentPart[expr]` which replaces the loop integrals in `expr` with its UV divergent part.

Note that the renormalization constants $\delta m_{\tilde{g}}$, $\delta m_{\phi^0}^2$ and $\delta m_{\sigma^0}^2$ are not independent from each other as the masses of the gluino and the two sgluons arise from only two parameters, i.e. $m_{\tilde{g}}$ and m_{σ}^2 from the soft breaking part of the Lagrangian, eq. (4.17). In addition, it happens that the particle content of RSQCD is such that $\frac{\delta g_s}{g_s} = 0$. This means that the β function of g_s

equals zero at 1-loop-level if one does not choose to decouple heavy particles from the running as it is done in this thesis. However at 2-loop-level there is a non-zero β function of g_s , which has been calculated by SARAH.

7.8 The Renormalization of the Matrix Element

This section explains how the renormalization of the matrix element of squark production is implemented in the framework of the automated calculation and gives intermediate results in form of the renormalized matrix element.

7.8.1 Implementation into the Model File

Within the automated calculation, the renormalization of the matrix element of squark production has been achieved by extending the model file generated by SARAH with counterterm Feynman rules and renormalization constants.

The derivation of the counterterm Feynman rules has been performed by the author whereas the implementation into the model file was mainly done by Philip Dießner, another member of the group. To explain the implementation, the code extract describing the quark-squark-gluino vertex is considered as an example.

```
C[F[3, {gt1, ct1}], F[15, {ct2}], -S[13, {gt3, ct3}]] == {{
((-I)*g3*Lam[ct2, ct3, ct1]*(Conjugate[ZUL[gt1, 1]]*ZU[gt3, 1] + \
  Conjugate[ZUL[gt1, 2]]*ZU[gt3, 2] + Conjugate[ZUL[gt1, 3]]*ZU[gt3, \
  3]))/Sqrt[2],
((-I)*(dZFu1[gt1]/2+dZSu1[gt3]/2+dZG1L1/2+dZgs1+dZgs1restore)*g3*Lam[ct2, \
  ct3, ct1]*(Conjugate[ZUL[gt1, 1]]*ZU[gt3, 1] + Conjugate[ZUL[gt1, \
  2]]*ZU[gt3, 2] + Conjugate[ZUL[gt1, 3]]*ZU[gt3, 3]))/Sqrt[2]
}, {0,0}}
```

The syntax of the vertex, also described in [67], is like $\{\{L, L^{ct}\}, \{R, R^{ct}\}\}$, where the shortcuts are explained in table 7.1. The names of the particles within the model are given in the FeynArts manual [67] when MSSMQCD.mod, the QCD extension of the MSSM model file, is explained.

However, $F[3, \{gt1, ct1\}]$ is an up-type quark of the $gt1$ 'th generation with color $ct1$ and $F[15, \{ct2\}]$ is a gluino with color $ct2$. In comparison to [67], there is a slight difference in the definition of squarks. Whereas the MSSM model file, MSSMQCD.mod, has three indices to label squarks, the model file generated by SARAH uses only two: $-S[13, \{gt3, ct3\}]$ denotes an anti up-type squark of mass eigenstate $gt3$ and color $ct3$. This means more specifically that $gt3 \in \{1, 2, 3\}$ labels the “left-handed” squarks with increasing mass and $gt3 \in \{4, 5, 6\}$ the “right-handed” squarks with increasing mass.

Shortcut	Meaning
L	coupling proportional to the projector P_L
L ^{ct}	counterterm for L
R	coupling proportional to the projector P_R
R ^{ct}	counterterm for R

Table 7.1: Explanation of the shortcuts describing the vertex structure in the above given mode extract.

Within the above given extract of the model file, **Lam** are the Gell-Mann matrices and **ZU** and **ZUL** are mixing matrices which are equated to the unit matrix, as there is no squark mixing in the MRSSM and the CKM-matrix is also approximated with the unit matrix.

Equipped with that knowledge, one sees that this Feynman rule is the Feynman rule (16b) from Appendix 10.5.

The renormalization constants for masses and fields are calculated by the **FormCalc** functions **MassRC** and **FieldRC** [64].

```

RenConst[dZFu1[gen_]] := FieldRC[F[3,{gen}]] [[1]]
RenConst[dZFd1[gen_]] := FieldRC[F[4,{gen}]] [[1]]

RenConst[dZSu1[gen_]] := FieldRC[S[13,{gen}]]
RenConst[dMSu1[gen_]] := MassRC[S[13,{gen}]]
RenConst[dZSd1[gen_]] := FieldRC[S[14,{gen}]]
RenConst[dMSd1[gen_]] := MassRC[S[14,{gen}]]

RenConst[dZG1L1] := FieldRC[F[15]] [[1]]
RenConst[dZG1R1] := FieldRC[F[15]] [[2]]
RenConst[dZbarG1L1] := dZG1R1
RenConst[dZbarG1R1] := dZG1L1
RenConst[dMG11] := MassRC[F[15]]

RenConst[dZgs1] := 0 - FiniteGs * g3*g3/(16*Pi*Pi)*(2*Log[(MassGlu/mu)^2]
+Log[(MassSq/mu)^2]+1/3*Log[(MassFu[3]/mu)^2]
+1/4*Log[(Masssigma0/mu)^2]
+1/4*Log[(Massphi0/mu)^2])
dZgs1restore := FiniteGs * g3*g3/(12*Pi*Pi)

RenConst[dZGG1] := FieldRC[V[5]]

```

The first two lines encode the field renormalization constant of up- and down-type quarks. The function **FieldRC** actually calculates two renormalization constants when the argument is a

fermion field: the left- and right-handed part. But these terms are identical since electroweak interactions are not considered within the model file. It therefore suffices to just pick the first element of the list by adding `[[1]]` to the two-component list.

The next block of the code provides the renormalization constants of up- and down-type squarks and the ensuing block deals with the gluino. Here it is important to separate the calculation of the field renormalization constant of the left- and right-handed component of the Dirac-spinor by adding `[[1]]` or `[[2]]` at the end of `FieldRC[F[15]]` to pick the appropriate element of the list.

Finally, the gauge coupling renormalization and the supersymmetry restoring counterterm are implemented, before the gluon field is renormalized. The necessity of the parameter `FiniteGs` will be explained in the next section.

These renormalization constants have been checked with the above calculated renormalization constants.

7.8.2 The Renormalized Matrix Element

After providing the model file with renormalization constants and counterterm Feynman rules, the matrix element for squark production can be renormalized. For more details on how the renormalization works within `FormCalc`, see the manual [64]. To check whether all UV-divergences have been removed, the `FormCalc` function `UVDivergentPart` has been used.

However, the matrix element still contains IR-divergences. To keep track of these divergences, the calculation in `FormCalc` has been performed with the option: `Dimension → 0` which is the only opportunity to really work in D dimensions, i.e. the result contains a quantity `Dminus4` which equals -2ϵ in DREG. The expression $\sum 2\Re(\mathcal{M}^B \mathcal{M}^{IL*})$ coming from `FormCalc` is then given in terms of scalar integrals, like defined in Appendix 10.6. To display how the `FormCalc` output looks like, the following box shows the off-shell amplitude of the up-quark self-energy in terms of loop integrals and `Dminus4`.

```
Amp[{{F[3, {1, Col1}], k[1], 0, {}}} -> {{F[3, {1, Col2}], k[2], 0, {}}}]
[(1/([Pi]^2)) g3^2 ((1/6 + Dminus4/12) (B0i[bb0, Pair[k[1], k[1]], 0, 0]
+ B0i[bb1, Pair[k[1], k[1]], 0, 0])
- 1/6 B0i[bb1, Pair[k[1], k[1]], MassGlu^2, MassSu[1]^2])
Mat[(u2|6 k[1]|u1>)] SUNT[Col1, Col2]]
+ (1/([Pi]^2)) g3^2 ((1/6 + Dminus4/12) (B0i[bb0, Pair[k[1], k[1]], 0, 0]
+ B0i[bb1, Pair[k[1], k[1]], 0, 0])
- 1/6 B0i[bb1, Pair[k[1], k[1]], MassGlu^2, MassSu[4]^2])
Mat[(u2|7 k[1]|u1>)] SUNT[Col1, Col2]]
```

Here, `k[1]` and `k[2]` are the momenta of the in- and outgoing quark, `Col1` and `Col2` their respective color, `B0i[bb0,...]` denotes the loop integral $B_0(\dots)$ and `B0i[bb1,...]` the loop integral $B_1(\dots)$, `Pair[k[1], k[1]]` labels the scalar product of the four vector `k[1]` with

itself, `MassGlu` is the gluino mass, `MassSu[i]` with $i \in \{1, 4\}$ names the degenerate squark mass, `Mat[...]` marks a container which stores the helicity and color matrix element, $|u1\rangle$ and $|u2\rangle$ are the spinors of the in- and outgoing quark, `6` labels the right-handed projector P_R and `SUNT` with only two indices is a Kronecker delta in color space.

To extract infrared divergences, `LoopTools` [68] is used. This package provides the function `SetLambda` which can be set to 0, -1 or -2 to extract the finite part, $\frac{1}{\epsilon}$ pole or $\frac{1}{\epsilon^2}$ pole of scalar integrals in dimensional regularisation. This means, when all arguments of a scalar integral are provided numerically, the integral is replaced with the coefficient of ϵ^i , where $i \in \{0, -1, -2\}$ is set by `SetLambda`. The so extracted divergences include both, UV and IR poles. In fact, the function `SetUVDiv` controls whether UV divergences are kept (`SetUVDiv` \rightarrow 1) or discarded (`SetUVDiv` \rightarrow 0), which presents another check of UV-finiteness which has been performed.

The respective poles of $\sum 2\Re(\mathcal{M}^B \mathcal{M}^{1L*})(uu \rightarrow \tilde{u}_L \tilde{u}_R)$ are shown in figure 7.10. Observe that the single pole is positive for all values of the Mandelstam variable t . This is because infrared integrals are rendered finite when $\epsilon < 0$. This means that the single pole is actually negative and can cancel with the single pole from the real corrections which is forced to be positive as it originates from an absolute square.

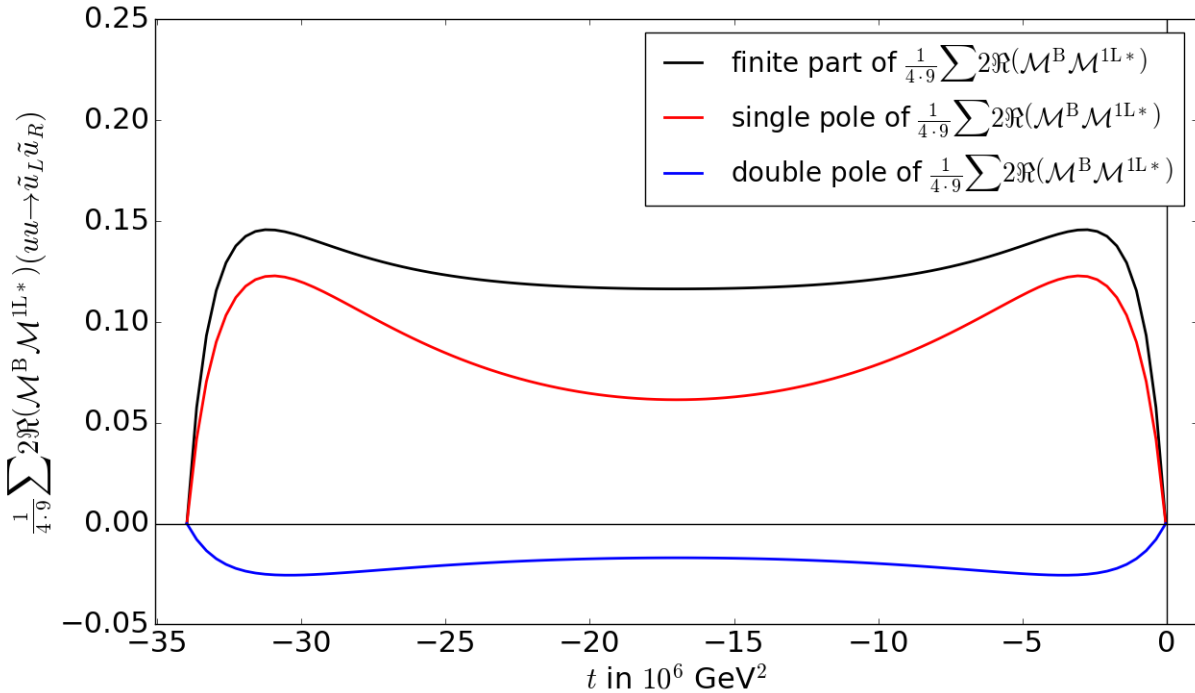


Figure 7.10: Coefficients of $\mathcal{O}(\epsilon^0)$, $\mathcal{O}(\epsilon^{-1})$ and $\mathcal{O}(\epsilon^{-2})$ terms of the dimensionless quantity $\frac{1}{4.9} \sum 2\Re(\mathcal{M}^B \mathcal{M}^{1L*})$ of $uu \rightarrow \tilde{u}_L \tilde{u}_R$ in the MRSSM as a function of the Mandelstam variable t . Final state helicities and colors are averaged. The parameters are fixed to $m_{\tilde{q}} = \mu_R = 1000$ GeV, $m_{\tilde{g}} = 2000$ GeV, $m_{\sigma} = 5000$ GeV and $\sqrt{s} = 6000$ GeV which is the partonic center-of-mass energy.

Note that the extraction of the single pole does not only involve setting the option `SetLamda` $\rightarrow -1$ and `Dminus4` $\rightarrow 0$, but also setting `SetLamda` $\rightarrow -2$ and `Dminus4` $\rightarrow -2$ and subtracting the term obtained by `SetLamda` $\rightarrow -2$ and `Dminus4` $\rightarrow 0$. In doing so, one accounts for the contraction of double poles with terms of ϵ . The same applies to the extraction of finite terms. This is summarized schematically in table 7.2.

ϵ^i	Contribution	Settings in FormCalc
ϵ^{-2}	ϵ^{-2}	(SetLambda $\rightarrow -2$, Dminus4 $\rightarrow 0$)
ϵ^{-1}	ϵ^{-1}	(SetLambda $\rightarrow -1$, Dminus4 $\rightarrow 0$)
	$+\mathcal{O}(\epsilon) \cdot \epsilon^{-2}$	$+(\text{SetLambda} \rightarrow -2, \text{Dminus4} \rightarrow -2)$ $-(\text{SetLambda} \rightarrow -2, \text{Dminus4} \rightarrow 0)$
ϵ^0	ϵ^0	(SetLambda $\rightarrow 0$, Dminus4 $\rightarrow 0$)
	$+\mathcal{O}(\epsilon) \cdot \epsilon^{-1}$	$+(\text{SetLambda} \rightarrow -1, \text{Dminus4} \rightarrow -2)$ $-(\text{SetLambda} \rightarrow -1, \text{Dminus4} \rightarrow 0)$

Table 7.2: The table shows what settings need to be adjusted in `FormCalc` to extract double and single poles as well as finite terms of an expression in `Mathematica` which contains loop-integrals.

Now it becomes clear, why the parameter `FiniteGs` has been introduced. As `SetLambda` only replaces the loop integrals but not every other term in an expression with the corresponding prefactor of ϵ^i , `FiniteGs` needs to be set to zero when `SetLambda` is set to -1 or -2 and `FiniteGs` $\rightarrow 1$ when `SetLambda` $\rightarrow 0$.

The upper plot in figure 7.11 shows the finite contributions from loop diagrams with different topology to $\frac{1}{4 \cdot 9} \sum 2\Re(\mathcal{M}^B \mathcal{M}^{1L})$ as well as their sum as a function of the Mandelstam variable t where $\frac{1}{4 \cdot 9}$ is the averaging over final state spins and colors. The lower plot displays the tree-level absolute squared matrix amplitude with leading order α_s which is compared to its analogue with next-to-leading order α_s and the virtual correction $\frac{1}{4 \cdot 9} \sum 2\Re(\mathcal{M}^B \mathcal{M}^{1L})$. The latter is not given analytically. It can be seen that the virtual corrections are relatively constant. Referring to eq. (10.45), this suggests that in this case virtual corrections do enhance the differential cross section in all directions of the beam axis relatively uniformly.

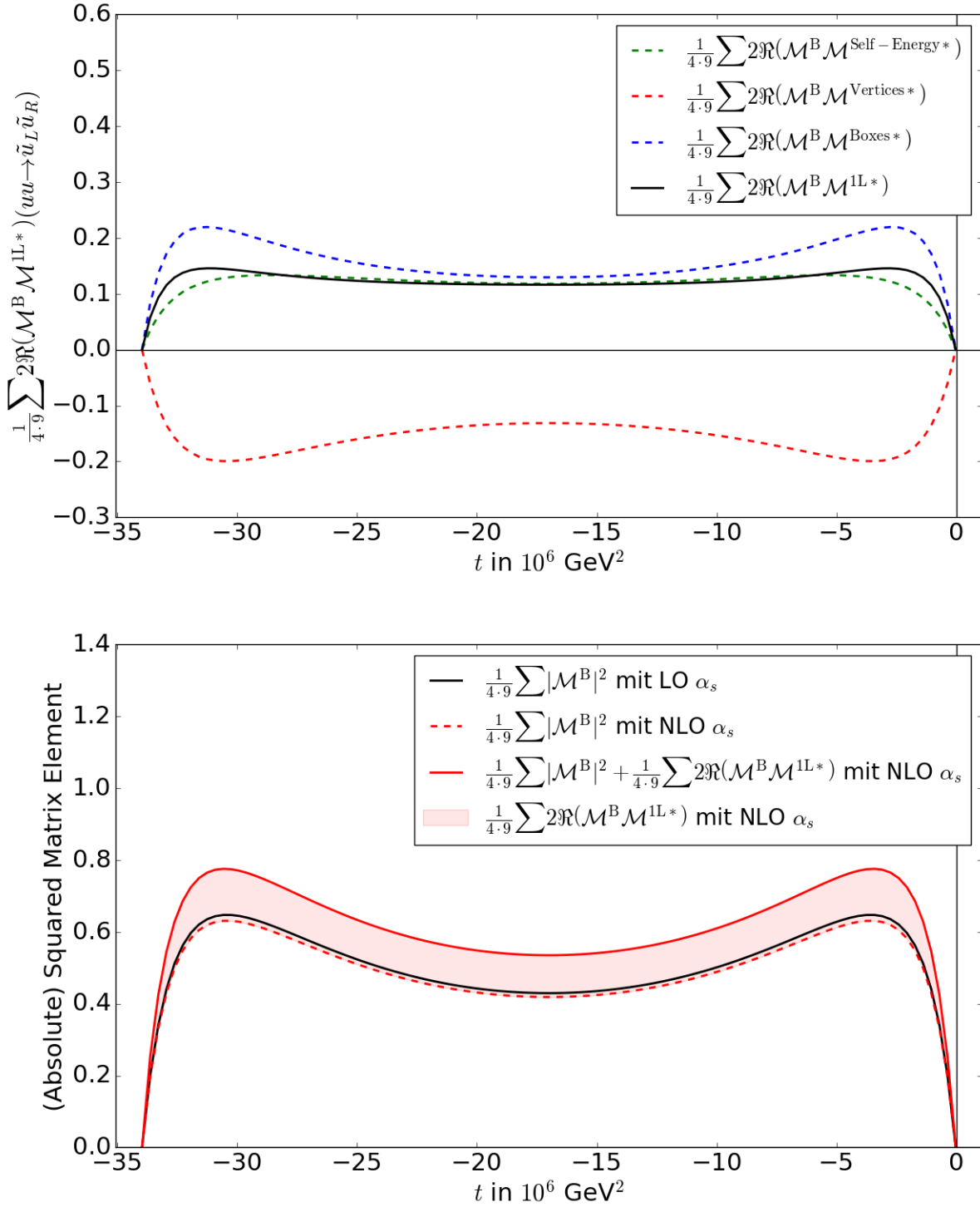


Figure 7.11: The figure at the bottom shows the absolute squared matrix element of $uu \rightarrow \tilde{u}_L \tilde{u}_R$ in the MRSSM at tree-level with $\alpha_s(m_Z) = 0.135$ from the leading order parton density functions **MMHT2014** and $\alpha_s(m_Z) = 0.12$ from the next-to-leading order parton density function as well as the contribution from the virtual corrections to it.

The figure at the top shows the different contributions to the virtual corrections as well as their sum. The used parameters are given under fig. 7.10.

8 Squark Production at One-Loop

This section discusses the cross section for squark production at next-to-leading order σ^{NLO} . To comment on the calculation, the next section gives a justification why on-shell renormalization has been chosen in section 7 and why loop corrections of external particles (see caption of fig:1loopdiagrams) are not taken into account. After that, the setup of the calculation of the different contributions to σ^{NLO} , which has been performed by a C++ program, is explained. This includes a remark on how the calculation was sped up. Finally the results of the computation are presented in the form of K -factors. These are then compared to the ones in the MSSM before the thesis closes with a discussion of the behavior of σ^{NLO} in the limit of large gluon masses.

8.1 The LSZ Theorem

The LSZ theorem [69] or LSZ reduction formula, named after Harry Lehmann, Kurt Symanzik and Wolfhart Zimmermann, prescribes how to obtain the S-matrix element, i.e. a physical observable, from the time ordered correlation function of the respective field operators. The time ordered correlation function of fields in an interacting theory can be calculated perturbatively with the aid of the Gell-Mann and Low theorem and the Wick theorem.

Considering a physical process with kinematics $\vec{k}_1 \dots \vec{k}_n \rightarrow \vec{p}_1 \dots \vec{p}_m$ and taking only one scalar field ϕ for the sake of simplicity, the Fourier transform of the time ordered product of a correlation function is related to the corresponding S-matrix element like²⁵

$$\begin{aligned} & \prod_{i=1}^n \int dx_i e^{ip_i x_i} \prod_{j=1}^m \int dy_j e^{ik_j y_j} \langle \Omega | \mathcal{T} [\phi(x_1) \dots \phi(x_n) \phi(y_1) \dots \phi(y_m)] | \Omega \rangle \\ & \sim \prod_{i=1}^n \frac{i\sqrt{Z}}{p_i^2 - m^2 + i\epsilon} \prod_{j=1}^m \frac{i\sqrt{Z}}{k_j^2 - m^2 + i\epsilon} \left\langle \vec{p}_1 \dots \vec{p}_m \left| S \right| \vec{k}_1 \dots \vec{k}_m \right\rangle. \end{aligned} \quad (8.1)$$

Here \mathcal{T} denotes the time ordering operator, $|\Omega\rangle$ is the ground state of the interacting theory and \sqrt{Z} is the residue of the single particle pole²⁶ in the “full” two-point function

$$\begin{aligned} \int dx e^{ipx} \langle \Omega | \mathcal{T} [\phi(x) \phi(0)] | \Omega \rangle &= \frac{i}{p^2 - m_0^2} + \frac{i}{p^2 - m_0^2} \left(\frac{\Sigma(p^2)}{p^2 - m_0^2} \right) + \frac{i}{p^2 - m_0^2} \left(\frac{\Sigma(p^2)}{p^2 - m_0^2} \right)^2 + \dots \\ &= \frac{i}{p^2 - m_0^2 - \Sigma(p^2)}. \end{aligned} \quad (8.2)$$

which is diagrammatically shown in fig. 8.1. The parameter m_0 is the tree-level mass and the quantity $-i\Sigma(p^2)$ denotes the sum of all one-particle-irreducible contributions to the particle’s

²⁵In this section, \sim indicates that the poles on either side are the same provided that all four-momenta are close to their mass shell, i.e. $p_i^0 \rightarrow E_{\vec{p}_i}$ and $k_j^0 \rightarrow E_{\vec{k}_j}$.

²⁶Note that this does not coincide with the renormalization constant Z in eq. (7.12).

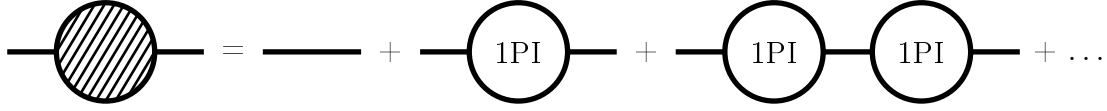


Figure 8.1: Diagrammatic figure of the “full” two-point function of a scalar field: The propagator in an interaction theory can be calculated in a perturbation series in the coupling constant.

self-energy. From eq. (8.2) one can read off the physical mass m^2 of the particle which is associated with the field ϕ . It is determined as the value of p^2 where the propagator has a pole, i.e.

$$[p^2 - m_0^2 - \Sigma(p^2)]_{p^2=m^2} = 0. \quad (8.3)$$

Close to the pole the denominator of eq. (8.2) can be expanded like

$$p^2 - m_0^2 - \Sigma(p^2) = (p^2 - m^2) \left(1 - \frac{\partial \Sigma(p^2)}{\partial p^2} \right) \Big|_{p^2=m^2} + \mathcal{O}((p^2 - m^2)^2). \quad (8.4)$$

The residue of the propagator can therefore be written as

$$Z = \left(1 - \frac{\partial \Sigma(p^2)}{\partial p^2} \right)^{-1} \Big|_{p^2=m^2}. \quad (8.5)$$

Now consider the full $(n + m)$ -point function, depicted in fig. 8.2, in scalar theory. One can decompose it into an amputated $(n + m)$ -point function and “full” propagators like written in eq. (8.2) and depicted in fig. 8.1.

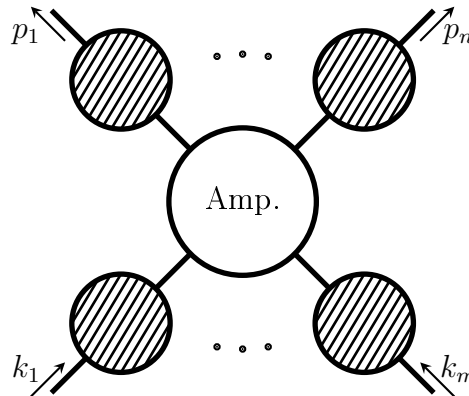
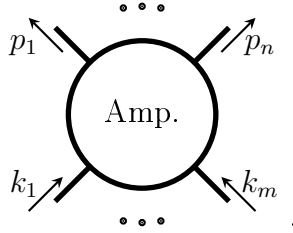


Figure 8.2: Diagrammatic figure of a “full” $(n + m)$ -point function. Apart from the “full” propagators there is the “full” amputated $(n + m)$ -point function.

Inserting the expression

$$\frac{i}{p^2 - m_0^2 - \Sigma(p^2)} \sim \frac{iZ}{p^2 - m^2} \quad (8.6)$$

for the full propagators, one notices the same singularity as in eq. (8.1). Comparing the coefficients of these poles in eq. (8.1), one obtains

$$\langle \vec{p}_1 \dots \vec{p}_n | S | \vec{k}_1 \dots \vec{k}_m \rangle = \sqrt{Z}^{n+m} \cdot \text{Amp.}$$


Now it becomes clear, why the renormalization in the on-shell scheme

$$\left. \frac{\partial \Sigma(p^2)}{\partial p^2} \right|_{p^2=m^2} \stackrel{!}{=} 0 \quad (8.7)$$

introduces no further modification, when turning from the Green function to the S-matrix-element. The residues of the propagator are $Z = 1$ in on-shell renormalization. Furthermore the on-shell condition for the mass renormalization

$$\Sigma(p^2) \Big|_{p^2=m^2} = 0 \quad (8.8)$$

means that the physical mass equals the tree level mass.

Finally one can conclude that loop-corrections of the S-matrix-element correspond only to internal loops, i.e. self-energies of external particles do not contribute.

8.2 The Squark Production Cross Section at Next-to-Leading Order

The squark production cross section at next-to-leading order is composed out of three contributions. These are the Born (tree-level) cross section, the virtual and the real corrections.

$$\sigma^{\text{NLO}} = \sigma^{\text{B}} + \sigma^{\text{V}} + \sigma^{\text{R}} \quad (8.9)$$

All three contributions have to be calculated with next-to-leading order parton density functions and α_s . There are seven mass scales: the squark mass $m_{\tilde{q}}$, the gluino mass $m_{\tilde{g}}$, the center of mass energy of the colliding protons which is set to $\sqrt{S} = 13 \text{ TeV}$, the top-quark mass which is fixed to $m_t = 172 \text{ GeV}$, the mass of the pseudoscalar m_σ and the renormalization and factorization scale. They have been set to $\mu_F = \mu_R = m_{\tilde{q}}$. The next section summarizes how the calculation has been automated within a C++ program.

8.2.1 The Setup of the Calculation

The setup of the calculation is summarized in fig. 8.3. Both the virtual and the Born matrix amplitude have been generated with the `Mathematica` package `FeynArts`. To this end a model file, generated by the `Mathematica` package `SARAH`, has been adjusted appropriately as described in section 7.8.1. The matrix amplitudes have been processed further to $\sum |\mathcal{M}^B|^2$ and $\sum 2\Re(\mathcal{M}^B \mathcal{M}^{1L*})$ by the `Mathematica` package `FormCalc` before this output has then been converted to a `C++` readable code.

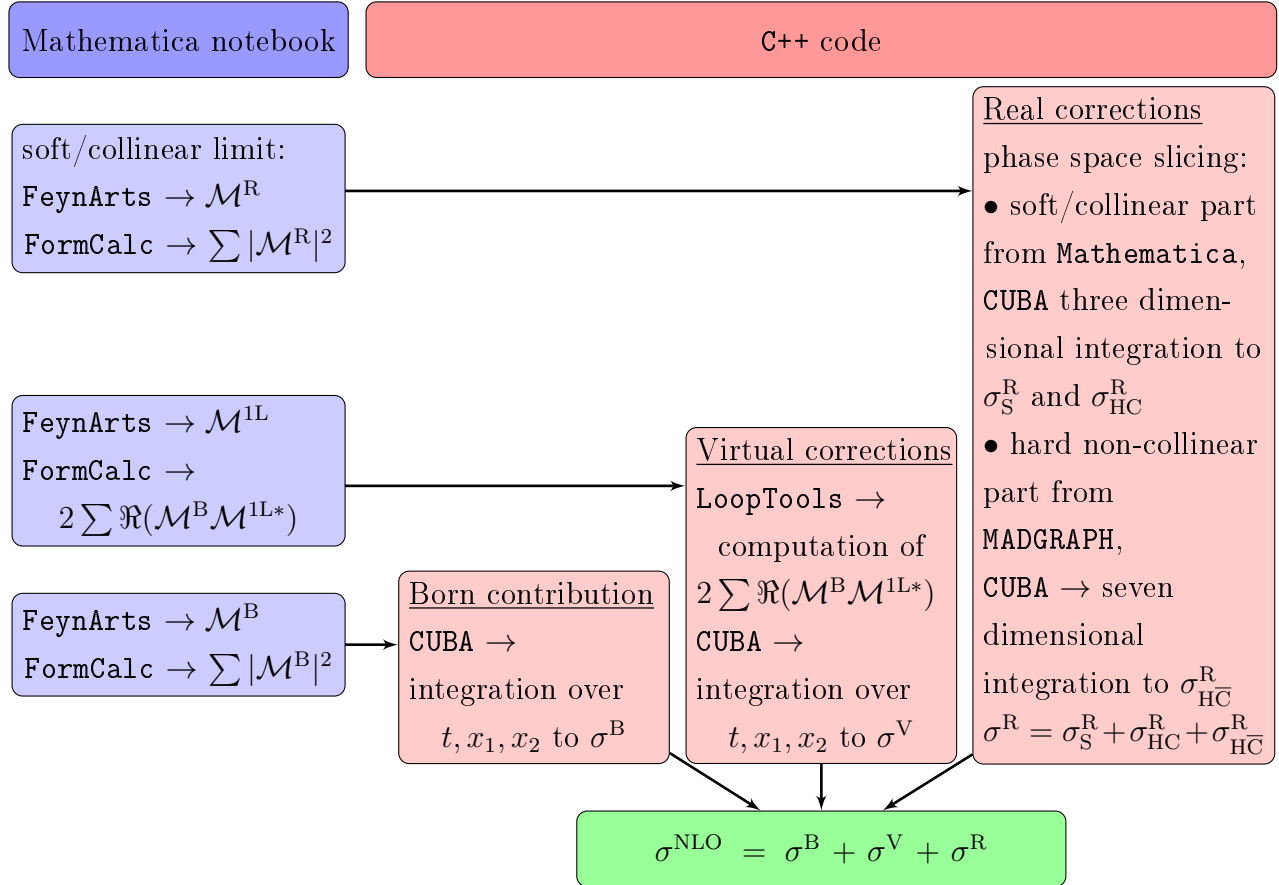


Figure 8.3: This scheme illustrates the setup of the computation of the next-to-leading order cross section. The (absolute) squared matrix amplitudes of the Born contribution the virtual corrections and the real corrections in the soft and/or collinear limit are generated by `Mathematica` packages and imported into a `C++` code. The amplitude from the real corrections is in the soft and collinear limit analytically integrated over the gluon’s four-momentum in D dimensions. Loop integrals are evaluated numerically using `LoopTools`. For the hard non-collinear regime, the matrix amplitude of the real corrections is imported from `MadGraph5`. The `CUBA`-library was used for all three contributions to perform the remaining integration to arrive at the cross sections σ^B , σ^V and σ^R .

This `C++` output is in turn invoked by the main program which evaluates the scalar integrals of $\sum 2\Re(\mathcal{M}^B \mathcal{M}^{1L*})$ numerically by using the package `LoopTools`. Finally the phase space integration and the integration over x_1 and x_2 is performed by the integration routine

“Cuhre” which is part of the CUBA library [50]. The parton density functions are included using LHAPDF6 [70].

The computation of the real corrections has been done by Wojciech Kotlarski, another member of the group. To extract the singularities from the real corrections, the “two cut phase space slicing method”, outlined in section 6.2.1, has been used. For the soft and hard collinear limit, the absolute squared matrix element has been calculated with FormCalc and analytically integrated over the gluon’s four-momentum in D dimensions in Mathematica. This has been exported to the C++ code to perform the rest of the integration numerically with the CUBA library. The matrix element in the hard non-collinear regime has been imported from MadGraph5 [71] and the whole integration has been performed numerically by the CUBA library.

It has been checked for multiple different and quite distinct choices of the parameters $m_{\tilde{q}}$ and $m_{\tilde{g}}$ that the double as well as the single poles of the virtual and real corrections cancel up to machine precision. Regarding the virtual corrections, this has been done by numerically extracting the $\frac{1}{\epsilon}$ and $\frac{1}{\epsilon^2}$ coefficient of loop integrals (see the discussion in section 7.8.2 for more details).

The poles of the real corrections have been calculated analytically. The double pole is actually proportional to the Born cross section:

$$\sigma_{\text{double pole}}^{\text{R}} = -\sigma_{\text{double pole}}^{\text{V}} = C(F) \frac{\alpha_s}{\pi} \sigma^{\text{B}} \frac{1}{\epsilon^2}. \quad (8.10)$$

The single pole does not take such a succinct form and is therefore not quoted here.

8.2.2 Remark on Prefactors in the Calculation

For the discussion of results it will not be distinguished between virtual and real corrections. This is because they have not been separated strictly in the calculation: As already discussed, both σ^{V} and σ^{R} are divergent, i.e. there are poles of the form $\frac{1}{\epsilon}$ and $\frac{1}{\epsilon^2}$. But these pole cancel exactly. On the other hand there are also prefactors from the phase space integral and the loop integral, which can be expanded in a power series in ϵ . In short, the virtual and real correction to the cross section can be expressed with some coefficients A - E , which are functions of the parameters $m_{\tilde{g}}$, $m_{\tilde{q}}$ and m_{σ} , in the following way:

$$\sigma^{\text{V}} = (1 + (A^{\text{V}} + P_1)\epsilon + (B^{\text{V}} + P_2)\epsilon^2 + \mathcal{O}(\epsilon^3)) \left(C^{\text{V}} - \frac{D}{\epsilon} - \frac{E}{\epsilon^2} \right), \quad (8.11)$$

$$\sigma^{\text{R}} = (1 + (A^{\text{R}} + P_1)\epsilon + (B^{\text{R}} + P_2)\epsilon^2 + \mathcal{O}(\epsilon^3)) \left(C^{\text{R}} + \frac{D}{\epsilon} + \frac{E}{\epsilon^2} \right). \quad (8.12)$$

Here, the coefficients A , B and C are in general distinct in the virtual and real part, but D and E are the same as the poles of both contributions cancel.

Some of the prefactors, namely P_1 and P_2 , are the same in both contributions. Keeping them

in eq. (8.12) would slow the computation of the real part down by a factor of about five because this part of the calculation is done analytically. Therefore a speed-up can be achieved by discarding the common prefactors at the cost of loosing track about the origin of the next-to-leading order corrections.

One common prefactor comes from the two-body phase space integral in eq. (6.4):

$$\begin{aligned} \frac{(4\pi)^\epsilon}{\Gamma(1-\epsilon)} \left(\frac{tu - m_{\tilde{q}}^4}{\mu^2 s} \right)^{-\epsilon} &= 1 + \epsilon \left(\ln 4\pi - \gamma_E - \ln \frac{tu - m_{\tilde{q}}^4}{\mu^2 s} \right) + \epsilon^2 \left(\frac{1}{2} \left(\ln 4\pi - \ln \frac{tu - m_{\tilde{q}}^4}{\mu^2 s} \right)^2 \right. \\ &\quad \left. + \frac{\gamma_E^2}{2} - \frac{\pi^2}{12} - \gamma_E \left(\ln 4\pi - \ln \frac{tu - m_{\tilde{q}}^4}{\mu^2 s} \right) \right) + \mathcal{O}(\epsilon^3). \end{aligned} \quad (8.13)$$

In addition, the prefactor of a loop integral defined in `LoopTools` differs from the one usually (and therefore also here) used. The `LoopTools` definition [72] of a loop integral is

$$T_{\mu_1 \dots \mu_P}^N = \frac{\mu^{4-D}}{i\pi^{\frac{D}{2}} r_\Gamma} \int d^D q \frac{q_{\mu_1} \dots q_{\mu_P}}{[q^2 - m_1^2][(q + p_1)^2 - m_2^2] \dots [(q + p_1 + \dots + p_{N-1})^2 - m_N^2]} \quad (8.14)$$

where T^1 is an A -integral, T^2 is a B -integral, etc. and $r_\Gamma = \frac{\Gamma(1-\epsilon)^2 \Gamma(1+\epsilon)}{\Gamma(1-2\epsilon)}$, where $\Gamma(z)$ is the Gamma function. Comparing the prefactors of eq. (8.14) and eq. (10.26) one finds that one has to multiply the `LoopTools` output by

$$r_\Gamma (4\pi)^\epsilon = 1 + \epsilon (\ln 4\pi - \gamma_E) + \epsilon^2 \left(\frac{\gamma_E^2}{2} - \frac{\pi^2}{12} + \frac{\ln^2 4\pi}{2} - \gamma_E \ln 4\pi \right) + \mathcal{O}(\epsilon^3) \quad (8.15)$$

in order to have the same prefactors as in eq. (10.26). Without going into detail why these factors are chosen, the right hand side of eq. (8.13) and eq. (8.15) are the prefactors discarded in the computation. Instead, the prefactor $\left(1 + \frac{\pi^2}{6} \epsilon^2\right)$ has been included in the virtual correction. Therefore P_1 and P_2 are chosen like

$$\begin{aligned} P_1 &= 2 \ln 4\pi - 2\gamma_E - \ln \frac{tu - m_{\tilde{q}}^4}{\mu^2 s}, \\ P_2 &= -\ln 4\pi \cdot \ln \frac{tu - m_{\tilde{q}}^4}{\mu^2 s} + \frac{1}{2} \ln^2 \frac{tu - m_{\tilde{q}}^4}{\mu^2 s} + \gamma_E^2 - \frac{\pi^2}{3} + \ln^2 4\pi - 2\gamma_E \ln 4\pi + \gamma_E \ln \frac{tu - m_{\tilde{q}}^4}{\mu^2 s}. \end{aligned} \quad (8.16)$$

8.2.3 K -factors for Squark Production in the MRSSM

A common way to describe next-to-leading order corrections is stating the K -factor, which is defined to be the ratio of the complete next-to-leading order cross section σ^{NLO} , see eq. (8.9) and the leading order cross section σ^{LO} , obtained using leading order parton density functions and α_s :

$$K(X \rightarrow Y) = \frac{\sigma^{\text{NLO}}(X \rightarrow Y)}{\sigma^{\text{LO}}(X \rightarrow Y)}. \quad (8.17)$$

Here, X denotes the initial state and Y the final state. Figure 8.4 shows the K -factors for the production of up-squarks in the MRSSM for varying masses of both, the squark ($m_{\tilde{q}} = 2000 \text{ GeV}$) and the gluino ($m_{\tilde{g}} = 1000 \text{ GeV}$). The mass of the pseudoscalar has been fixed to $m_{\sigma} = 5000 \text{ GeV}$ in both plots. In addition, the contributions to the K -factor are split into the ones coming from the Born cross section²⁷ and real and virtual corrections.

It can be seen that the K -factor increases with increasing squark mass and decreases with increasing gluino mass. Note that the sum of virtual and real corrections gets negative for very light squarks. But this region of parameter space is already excluded experimentally.

²⁷The contribution of the Born cross section to the K -factor is smaller than one as it has been calculated with next-to-leading order parton density functions.

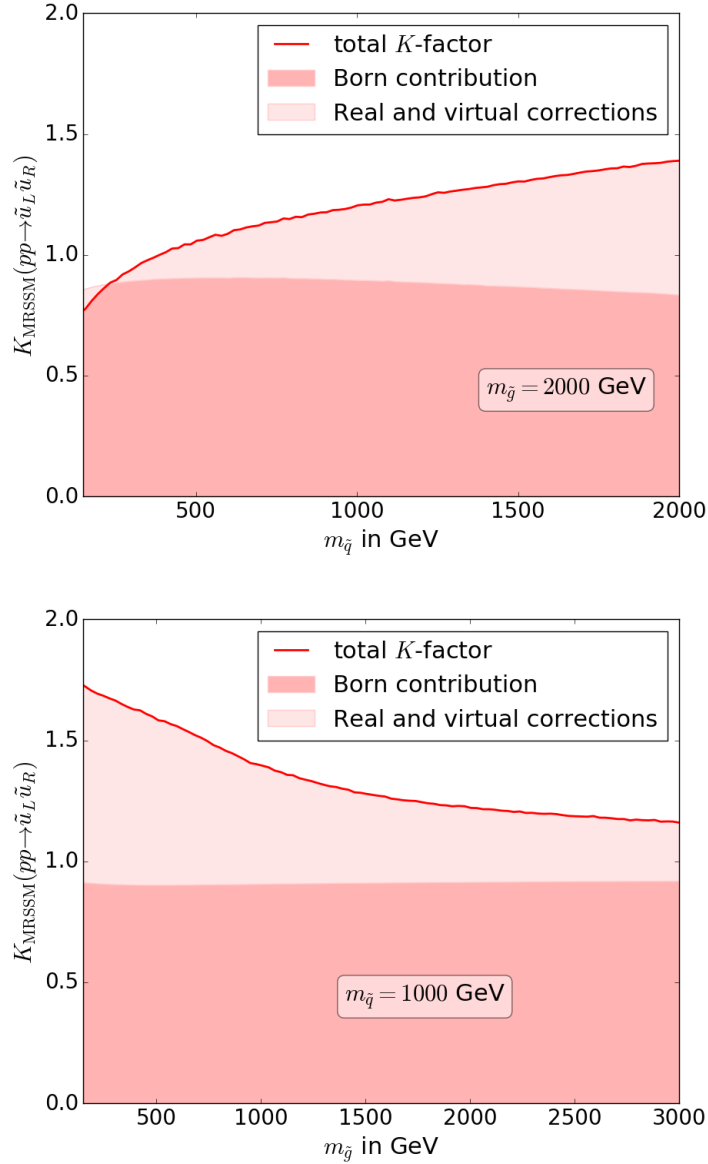


Figure 8.4: Dependence of the K -factor for the process $pp \rightarrow \tilde{u}_L \tilde{u}_R$ in the MRSSM on the squark mass $m_{\tilde{q}}$ for fixed $m_{\tilde{g}} = 2000$ GeV (top) and on the gluino mass $m_{\tilde{g}}$ for fixed $m_{\tilde{q}} = 1000$ GeV (bottom). The mass of the pseudoscalar is $m_{\sigma} = 5000$ GeV. The used parton density function are the one from table 8.1. The missing smoothness of the plot originates from the uncertainty of the integration.

Note further that within the real corrections, only gluon radiation is included. This is because quark radiation, as described in section 6.2.2, involves the treatment of on-shell singularities which have unfortunately not been dealt with, due to a limited time budget. However, [55] suggests that quark radiation gives only a sub percent effect to the next-to-leading order cross section of squark production when $m_{\tilde{g}} < m_{\tilde{q}}$. Of course, this argument applies to the MSSM but as the only difference to the MRSSM comes from diagrams involving gluinos and sgluons, it provides also a strong argument for the suppression of quark radiation in the MRSSM. In

fact, sgluons do not appear at all in diagrams contributing to real corrections. Furthermore, the change from Majorana to Dirac gluinos can never imply an amplification of processes involving gluinos. The reason for this is that if a gluino undergoes a chirality flip, due to its mass, the right handed part of it, namely the octino, does neither couple to quarks nor to squarks. However, the effect of quark radiation is thought to increase when $m_{\tilde{g}} > m_{\tilde{q}}$. This is quantified within the next section, when squark production in the MSSM is discussed. Nonetheless, quark radiation is by no means to be thought of a dominant contribution to squark production at next-to-leading order.

Table 8.1 shows σ^{LO} and σ^{NLO} as they have been calculated by the devised C++ program.

$m_{\tilde{q}}$ in GeV	$m_{\tilde{g}}$ in GeV	σ^{LO} in fb	σ^{NLO} in fb	K
500	500	966.4	1440	1.49
500	1000	303.4	383	1.26
1000	1000	42.63	61.8	1.45
1000	2000	11.56	14.3	1.24
1500	3000	0.9166	1.13	1.23

Table 8.1: K -factors of the process $pp \rightarrow \tilde{u}_L \tilde{u}_R$ in the MRSSM for a selected set of masses. The pseudoscalar mass is fixed to $m_\sigma = 5000$ GeV. For the calculation of σ^{LO} MMHT2014LO (LHAPDF ID: 25000) are used as parton density functions, whereas for σ^{NLO} MMHT2014NLO (LHAPDF ID: 25100) are used.

It can be seen that the K -factors depend strongly on the ratio $\frac{m_{\tilde{q}}}{m_{\tilde{g}}}$ but not that strongly on the masses themselves. This is also depicted in fig. 8.5 which shows the K -factors in the $m_{\tilde{q}}$ - $m_{\tilde{g}}$ plane. The contour lines follow approximately rays from the origin. By performing the calculation without the shuffling of prefactors as explained in section 8.2.2, the raising of the K -factors for increasing values of $\frac{m_{\tilde{q}}}{m_{\tilde{g}}}$ has been traced down to the real corrections. As quark radiation is not included, this effect can further be pinned down to originate from the diagrams in fig. 6.2. However, at least for small $m_{\tilde{g}}$, fig. 8.5 suggests that the K -factors drop again for increasing $m_{\tilde{q}}$.

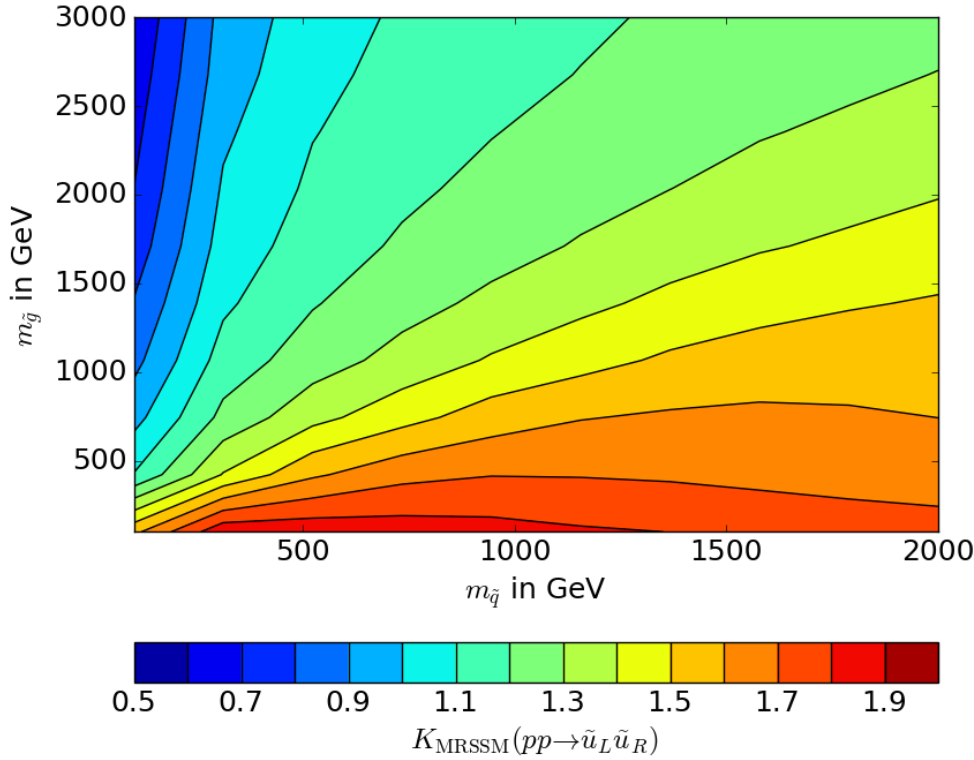


Figure 8.5: Contour plot of the K -factor of up-squark production in the MRSSM. The pseudoscalar mass is set to $m_\sigma = 5000 \text{ GeV}$. The used parton density functions are the same as in table 8.1.

For three different choices of $m_{\tilde{q}}$ and $m_{\tilde{g}}$, Philip Dießner checked the results up to permille accuracy by doing the calculation using `GoSam` [73, 74] and `MadGraph5_aMC@NLO` [71].

The next-to-leading order cross sections of this chapter bear a relative uncertainty of one percent due to the numerical integration. The uncertainty which corresponds to the variation of the scales μ_R and μ_F , see section 5.3, evaluate to $\approx 15\%$.

8.2.4 K -factors for Squark Production in the MSSM

To compare the results of K -factors in the MRSSM to those in the MSSM, the cross sections in question have been calculated using the program `MadGraph5_aMC@NLO` with the same parton density functions as before, i.e. `MMHT2014`. When generating the code for the pertaining processes, e.g. two protons to $\tilde{u}_L + \tilde{u}_R$, with

```
generate p p > ul ur [QCD] $$go
```

the s -channel gluinos were omitted, with the addendum \$\$\$go as `MadGraph5` does not deal with divergences coming from the gluino in the on-shell limit. As already discussed, these contributions are only of sub percent order when $m_{\tilde{q}} > m_{\tilde{g}}$ [55] but increase for $m_{\tilde{g}} > m_{\tilde{q}}$ as indicated in table 8.2, which compares σ^{NLO} obtained using `MadGraph5` and the program `Prospino2` [75] for both scenarios.

$m_{\tilde{q}}$ in GeV	$m_{\tilde{g}}$ in GeV	$\sigma_{\text{MadGraph}}^{\text{NLO}}$ in fb	$\sigma_{\text{Prospino2}}^{\text{NLO}}$ in fb
1500	1000	9.49 ± 0.03	9.48 ± 0.09
1000	2000	13.32 ± 0.05	13.89 ± 0.11

Table 8.2: $\sigma^{\text{NLO}}(pp \rightarrow \tilde{u}_L \tilde{u}_R)$ in the MSSM obtained from `MadGraph5` and `Prospino2` for a selected set of masses. `MadGraph5` uses parton density function given in 8.1 whereas `Prospino2` uses CTEQ6L1 parton density functions [76] for leading order calculations and CTEQ66 [77] for next-to-leading order calculations. The stated uncertainties originate from the phase space integration. Within the `MadGraph5` calculation, the s -channel gluino diagrams have been discarded. This becomes relevant only when $m_{\tilde{g}} > m_{\tilde{q}}$.

In fact, comparing $\sigma^{\text{NLO}}(pp \rightarrow \tilde{u}_L \tilde{u}_R)$ from `MadGraph5` with the one obtained by using `Prospino2`, which does include quark radiation, shows good agreement for the case $m_{\tilde{g}} < m_{\tilde{q}}$ but a small deviation for $m_{\tilde{g}} > m_{\tilde{q}}$. The given uncertainties are the uncertainties of the integration over the phase space and the chosen parameters are: $\mu_F = \mu_R = m_{\tilde{q}}$ and $\sqrt{S} = 13 \text{ TeV}$.

Figure 8.6 shows the K -factors for squark production in the MSSM, broken down to K -factors for “chirality” like $(\tilde{u}_L \tilde{u}_L)$ and unlike squarks $(\tilde{u}_L \tilde{u}_R)$. It can be seen, that the mass dependence of $K(pp \rightarrow \tilde{u}_L \tilde{u}_R)$ in the MSSM is quite similar to the one in the MRSSM and that the K -factors are slightly smaller than in the MSSM. However, the K -factors for “chirality” like squarks are distinctly larger. The mass dependence of them is quite the same as for the $pp \rightarrow \tilde{u}_L \tilde{u}_R$ channel. The only difference is a local maximum of the K -factor as a function of the gluino mass at $m_{\tilde{g}} \approx 500 \text{ GeV}$, where $m_{\tilde{q}} = 1000 \text{ GeV}$. Adding the cross sections for the three possible channels $\tilde{u}_L \tilde{u}_R$, $\tilde{u}_L \tilde{u}_L$ and $\tilde{u}_R \tilde{u}_R$ together one ends up with K -factors which have the very similar mass dependence as in the MRSSM but which can, depending on the chosen parameters, be significantly smaller.

Table 8.3 displays the leading order and next-to-leading order cross section of up-squark production in the MSSM. The total cross section for the production of all possible channels $\{\tilde{u}_L \tilde{u}_R, \tilde{u}_L \tilde{u}_L, \tilde{u}_R \tilde{u}_R\}$ is broken down to the contribution, coming from the channel $\tilde{u}_L \tilde{u}_R$ whose tree-level cross section is the same as in the MRSSM.

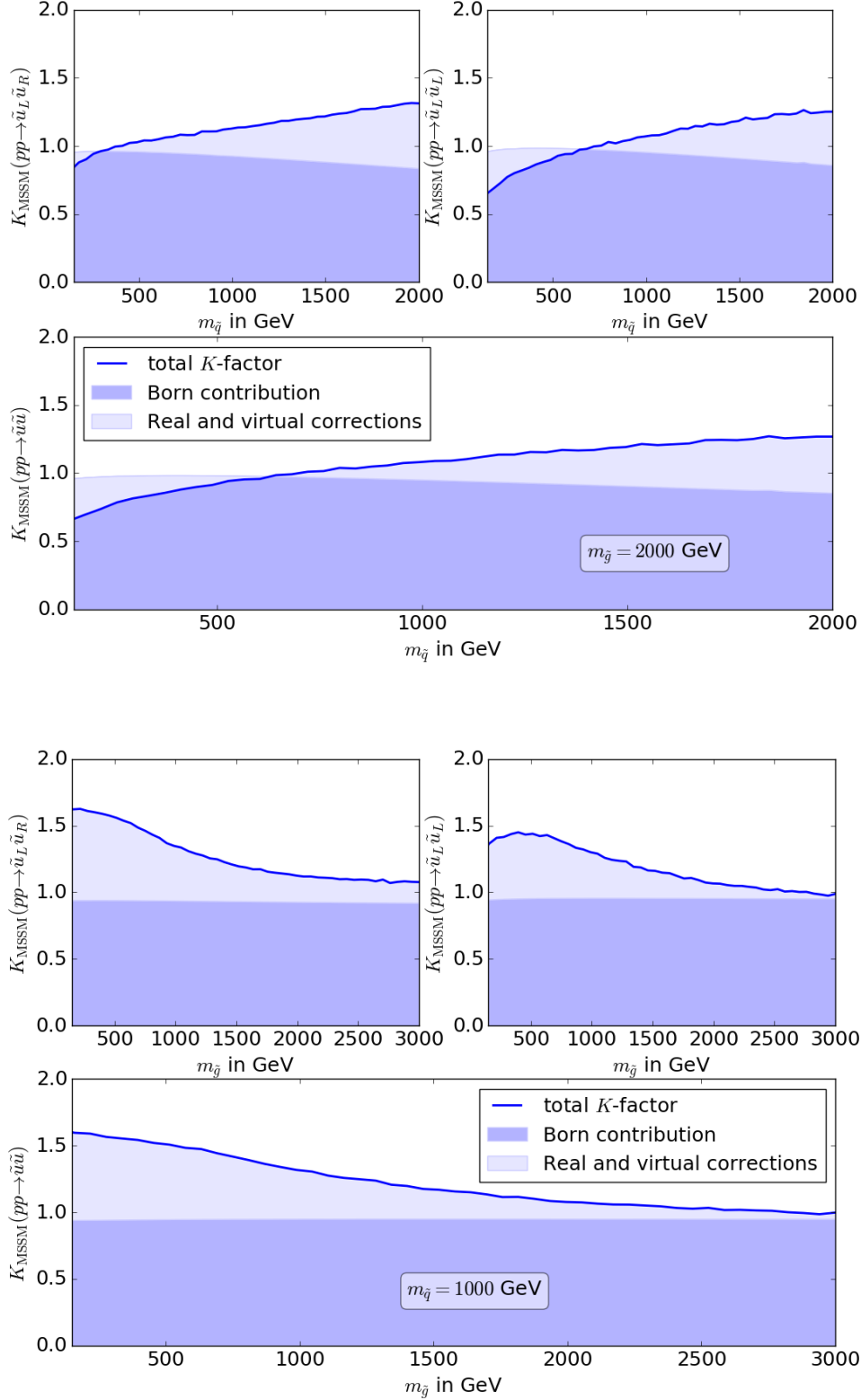


Figure 8.6: Dependence of the K -factor for the process $pp \rightarrow \tilde{u}\tilde{u}$, where $\tilde{u}\tilde{u} \in \{\tilde{u}_L \tilde{u}_R, \tilde{u}_L \tilde{u}_L, \tilde{u}_R \tilde{u}_R\}$, in the MSSM on the squark mass $m_{\tilde{q}}$ for fixed $m_{\tilde{g}} = 2000$ GeV (top) and on the gluino mass $m_{\tilde{g}}$ for fixed $m_{\tilde{q}} = 1000$ GeV (bottom). The used parton density functions are the same as in table 8.1. The K -factors have been broken down to contributions coming from $pp \rightarrow \tilde{u}_L \tilde{u}_R$ and from $pp \rightarrow \tilde{u}_L \tilde{u}_L$. The latter equals the contributions coming from $pp \rightarrow \tilde{u}_R \tilde{u}_R$. The missing smoothness of the plot originates from the uncertainty of the integration.

		$p + p \rightarrow \tilde{u}_L + \tilde{u}_R$			$p + p \rightarrow \tilde{u} + \tilde{u}$		
$m_{\tilde{q}}$ in GeV	$m_{\tilde{g}}$ in GeV	σ^{LO} in fb	σ^{NLO} in fb	K	σ^{LO} in fb	σ^{NLO} in fb	K
500	500	966.4	1328	1.37	2333	3102	1.33
500	1000	303.4	352	1.16	1271	1393	1.10
1000	1000	42.63	58.5	1.37	122.2	161.3	1.32
1000	2000	11.56	13.3	1.15	66.36	72.1	1.09
1500	3000	0.9166	1.05	1.14	7.045	7.57	1.07

Table 8.3: K -factors of the process $pp \rightarrow \tilde{u}_L \tilde{u}_R$ and $pp \rightarrow \tilde{u} \tilde{u}$, where $\tilde{u} \tilde{u} \in \{\tilde{u}_L \tilde{u}_R, \tilde{u}_L \tilde{u}_L, \tilde{u}_R \tilde{u}_R\}$, in the MSSM for a selected set of masses. The used parton density functions are the same as in table 8.1.

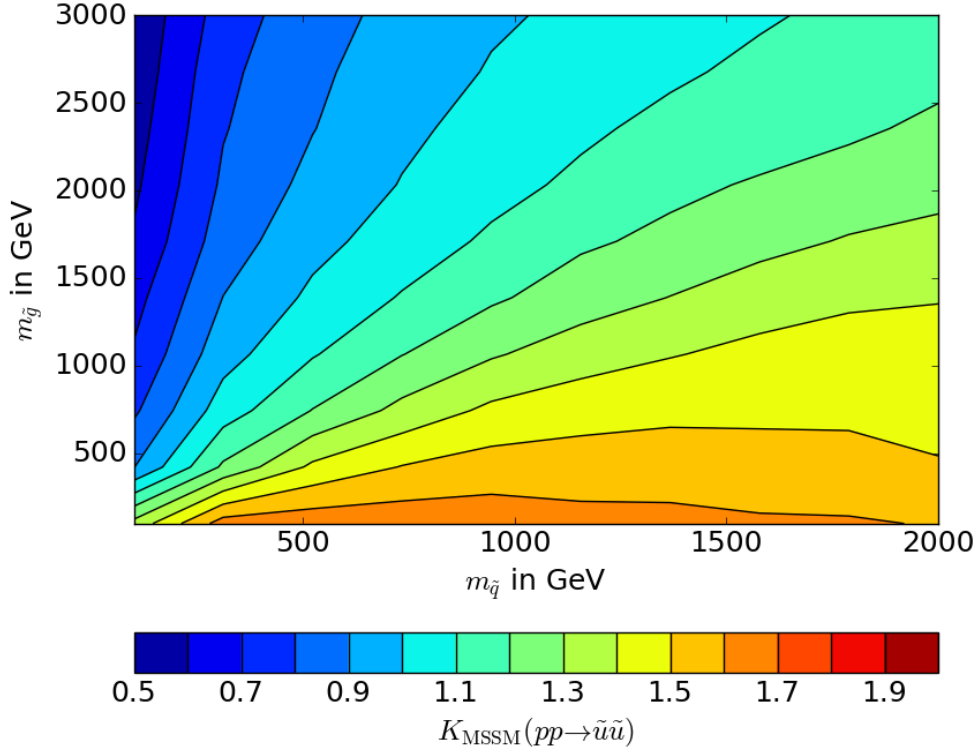


Figure 8.7: Contour plot of the K -factor of the process $pp \rightarrow \tilde{u}_L \tilde{u}_R$ and $pp \rightarrow \tilde{u} \tilde{u}$, where $\tilde{u} \tilde{u} \in \{\tilde{u}_L \tilde{u}_R, \tilde{u}_L \tilde{u}_L, \tilde{u}_R \tilde{u}_R\}$, in the MSSM. The used parton density functions are the same as in table 8.1.

Again, it is clearly visible that the K -factors depend rather strongly on the ratio $\frac{m_{\tilde{g}}}{m_{\tilde{q}}}$ but not that strongly on the masses themselves (see also fig. 8.7). As the real corrections are identical to those in the MRSSM, it is again these very real corrections which are responsible

for an enhancement of the K -factor for large values of $\frac{m_{\tilde{g}}}{m_{\tilde{q}}}$. This has also been found in [42]. Comparing with the results from the MRSSM in table 8.1, one can state that the K -factors of the MRSSM are slightly larger. This might be the case, as there are additional degrees of freedom in the R -symmetric model, namely the octino which enters the gluino self-energy contributions (see second diagram from the right in fig. 7.3) and sgluons which enter box diagrams (see lower right diagram in fig. 6.1). The dependence on the sgluon mass is discussed within the next section.

The uncertainties of next-to-leading order cross sections, due to the phase space integration, within this section are of percent order. The uncertainty which corresponds to the scale variation does not exceed 15%.

8.3 The Cross Section in the Limit of Large Sgluon Masses

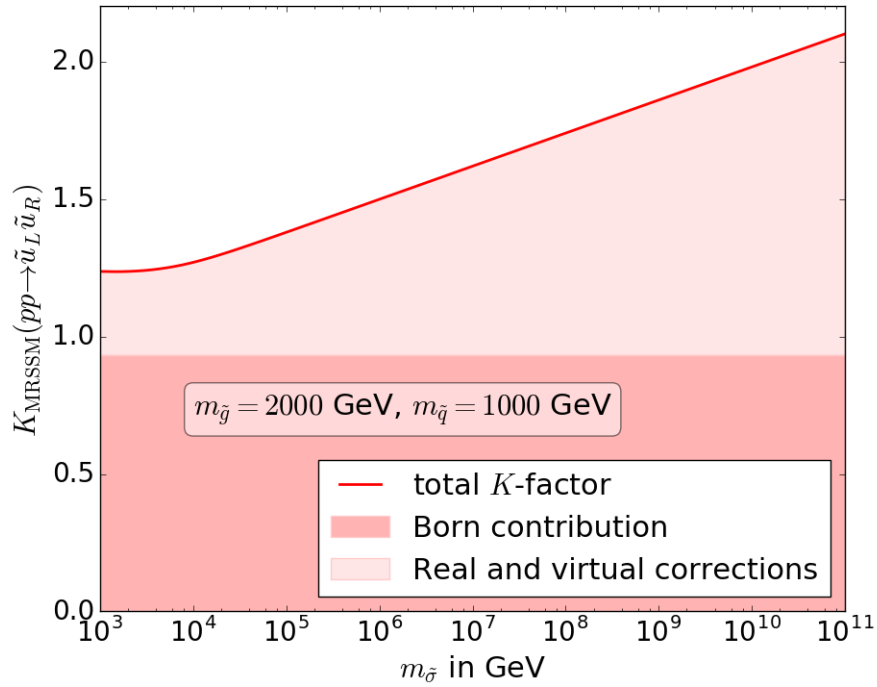


Figure 8.8: Dependence of the K -factor for the process $pp \rightarrow \tilde{u}\tilde{u}$ on the mass of the pseudoscalar sgluon. Squark and gluino mass have been fixed to $m_{\tilde{q}} = 1000 \text{ GeV}$ and $m_{\tilde{g}} = 2000 \text{ GeV}$. The used parton density functions are the same as in table 8.1. For $m_{\sigma} \approx 10^5 \text{ GeV}$ onwards, one finds a logarithmic scaling as predicted by [78].

The cross section for squark production does not exist in the limit of an infinitely large sgluon mass, instead it was found that it diverges logarithmically:

$$\lim_{m_{\sigma} \rightarrow \infty} \sigma(qq \rightarrow \tilde{q}\tilde{q}) \sim \ln \frac{m_{\sigma}^2}{\mu^2}. \quad (8.18)$$

This is actually expected as an effective field theory of the MRSSM where the sgluon is integrated out is no longer supersymmetric. This is because the sgluon is together with the octino part of a supermultiplet. Integrating out only the sgluon means that the octino misses its superpartner in the effective field theory. In this case the decoupling theorem [79] does no longer hold²⁸. The logarithmic scaling of the cross section as a function of the mass of the pseudoscalar is shown in fig. 8.8.

²⁸It is even possible to predict the logarithmic scaling of $\sigma(qq \rightarrow \tilde{q}\tilde{q})$ quantitatively. The coefficient of the logarithm is proportional to the difference of the one-loop β function coefficients of g_s and \hat{g}_s in the effective theory with the heavy particle integrated out, see eq. (4) in [78].

9 Summary

The Standard Model of particle physics describes all known fundamental particles and the non-gravitational interactions among them. It belongs to the best tested theories within physics but is on the other hand known to be incomplete.

Supersymmetry provides an attractive extension of the Standard Model. Within this thesis, a specific supersymmetric extension of the Standard Model – the Minimal R -Symmetric Supersymmetric Standard Model (MRSSM) – is studied. This is particularly appealing from the point of view of symmetries because it comprises the maximal possible symmetry group a reasonable quantum field theory can have. The theorem stating this is the Haag-Łopuszański-Sohnius theorem. In contrast to the common notion, supersymmetry alone does not extend the Poincaré symmetry to the largest possible symmetry group. There is a further non-trivial extension by a global continuous symmetry, referred to as R -symmetry.

This thesis introduces an R -symmetric model in its minimal form. R -symmetry forbids some of the terms which are allowed in the Minimal Supersymmetric Standard Model (MSSM). These include the A -terms and the μ -term which are responsible for squark mixing and flavor changing processes. Furthermore, R -symmetry also prohibits Majorana mass terms for the gauginos. To be phenomenologically viable, the MRSSM needs to accommodate Dirac gauginos. This requires the gauge sector of this model to be an $N = 2$ supersymmetric theory which in turn implies further degrees of freedom.

Focusing on the strongly coupling sector, there is, apart from the “usual” gluino, another fermionic degree of freedom which is referred to as octino. The superpartner of this right handed part of the strongly coupling gaugino is a spin-0 particle: the scalar gluon (sgluon). As a matter of fact, there are two distinct real sgluons with distinct masses.

Within the framework of this thesis, the production cross section of squarks and gluinos in the MRSSM has been calculated at tree-level. To this end, Feynman rules for the strongly coupling sector of the MRSSM have been derived. The cross sections and intermediate results are given explicitly for each process. In comparison to the corresponding processes in the MSSM, it has been found that gluino production is enhanced by a factor of about two because of gluino and antigluino being distinguishable particles, unlike in the MSSM. In order to meet the absence of signals alluding to supersymmetry at the Large Hadron Collider (LHC), this suggests that gluinos might be heavier than squarks if they should be realized as Dirac fermions in nature. Focusing on this regime of parameter space, it has been found that the production of squarks and gluinos in the MRSSM is significantly suppressed compared to the MSSM. The most striking difference has been found in the production channel of squarks. Motivated by this fact, the next-to-leading order cross section for squark production has been calculated.

As this had not been done so far, it was not possible to use a tool like **MadGraph** or **Prospino** to perform the calculation. Instead, a new program needed to be devised to calculate the next-to-leading order cross section of squark production in the MRSSM in an automated way.

To this end, a model file generated by **Sarah**, which serves only for leading order processes, has been adjusted manually to incorporate counterterm Feynman rules. At this point, Philip Dießner contributed significantly by changing model file. After this, the model file has been provided with appropriate renormalization constants which are explicitly given in the thesis. This also includes a supersymmetry restoring counterterm. By means of this model file, renormalized one-loop corrections to the matrix element of squark production have been calculated in **Mathematica**, using the packages **FeynArts** and **FormCalc**. After this, the virtual contributions, which had been checked for ultraviolet-finiteness, have been passed to a **C++** code and evaluated using the **Looptools** package. Finally, the phase space integration has been performed numerically using the **CUBA** library for parallelized numerical integration. However, the virtual corrections to the cross section are not infrared finite. To render the next-to-leading order cross section σ^{NLO} finite, real corrections needed to be included. This has been done by Wojciech Kotlarski. After including them, σ^{NLO} has been found to contain no further divergences.

Equipped with this program, the K -factors for up-squark production have been calculated as a function of the squark and of the gluino mass. Table 9.1 summarizes leading and next-to-leading order cross sections as well as the K -factors for up-squark production in the MRSSM and MSSM at the LHC for a selected set of masses.

		MRSSM: $p + p \rightarrow \tilde{u}_L + \tilde{u}_R$			MSSM: $p + p \rightarrow \tilde{u} + \tilde{u}$		
$m_{\tilde{q}}$ in GeV	$m_{\tilde{g}}$ in GeV	σ^{LO} in fb	σ^{NLO} in fb	K	σ^{LO} in fb	σ^{NLO} in fb	K
500	500	966.4	1441	1.49	2333	3102	1.33
500	1000	303.4	383	1.26	1271	1393	1.10
1000	1000	42.63	61.8	1.45	122.2	161.3	1.32
1000	2000	11.56	14.3	1.24	66.36	72.1	1.09
1500	3000	0.9166	1.13	1.23	7.045	7.57	1.07

Table 9.1: Total hadronic cross sections for the production of up-squarks through protons in the MRSSM and the MSSM at leading and next-to-leading order. Also given are the K -factors. As a consequence of R -charge conservation, the only allowed channel in the MRSSM is $\tilde{u}_L + \tilde{u}_R$ production, whereas in the MSSM also $\tilde{u}_L + \tilde{u}_L$ and $\tilde{u}_R + \tilde{u}_R$ production are allowed.

The results are shown for a selected set of masses. The center-of-mass energy is $\sqrt{S} = 13$ TeV and within the MRSSM the pseudoscalar mass is fixed to $m_\sigma = 5000$ GeV.

As a result, the comparison of K -factors for squark production in the MRSSM and the MSSM showed that they are slightly larger in the MRSSM. But since the tree-level cross section of squark production in the MRSSM is, depending on the choice of squark and gluino mass, up to a factor of about eight smaller than in the MSSM, this renders the MRSSM, in this respect, to a perfectly viable extension of the Standard Model.

Among other advantages compared to the MSSM, it explains a suppressed cross section for the production of supersymmetric particles at the LHC.

10 Appendix

10.1 System of Units and Metric

In this thesis the natural units are used, i.e. $c = \hbar (= k_B) = 1$. Furthermore the Minkowski metric is chosen to be

$$g^{\mu\nu} = \text{diag}(1, -1, -1, -1). \quad (10.1)$$

10.2 Constants of the Color Algebra $SU(N)$

The Casimir operator $C(R)1$ of a semi-simple Lie algebra in the irreducible representation R is given by [80]

$$g^{ab}T^a(R)T^b(R) = C(R)1, \quad (10.2)$$

where $T^a(R)$ is the a -th generator of the matrix valued representation R , g^{ab} is the metric of the group, $C(R)$ is the quadratic Casimir invariant of the representation R and 1 is the identity in representation space.

Apart from $C(R)$ it is common to define the Dynkin-Index $T(R)$:

$$\text{Tr} [T^a(R)T^b(R)] = T(R)\delta^{ab}. \quad (10.3)$$

The two constants are connected by

$$C(R) \cdot \dim(R) = T(R) \cdot \dim(G), \quad (10.4)$$

where $\dim(G)$ is the dimension of the group and $\dim(R)$ is the dimension of the irreducible representation R .

In the case of $SU(N)$ one has a diagonal metric $g^{ab} = \delta^{ab}$ and therefore eq. 10.2 turns to

$$\sum_a (T^a(R))^2 = C(R)1_{\dim(R) \times \dim(R)} \quad (10.5)$$

and one can write down the following useful formulae for the fundamental representation $R = F$: $T_{ij}^a = \frac{\lambda_{ij}^a}{2}$ and the adjoint representation $R = A$: $(T_{ij}^a)^{adj} = -if_{aij}$:

$$\begin{aligned} T_{ik}^a T_{kj}^a &= C(F)1_{ij} & \text{with } C(F) &= \frac{N^2 - 1}{2N} = \frac{4}{3}, \\ f^{abc} f^{dbc} &= C(A)\delta^{ab} & \text{with } C(A) &= N = 3, \\ \text{Tr} [T^a T^b] &= T(F)\delta^{ab} & \text{with } T(F) &= \frac{1}{2}, \end{aligned} \quad (10.6)$$

where λ_{ij}^a are for $N_c = 3$ the Gell-Mann matrices and f_{abc} are the structure constants of $SU(N_c)$, defined in eq. (2.4).

10.3 Weyl Basis and Two-Spinor Notation

As representation of the γ -matrices the Weyl or chiral representation is chosen:

$$\gamma^\mu = \begin{pmatrix} 0 & \sigma^\mu \\ \bar{\sigma}^\mu & 0 \end{pmatrix}, \quad \gamma_5 = \begin{pmatrix} -1_2 & 0 \\ 0 & 1_2 \end{pmatrix}. \quad (10.7)$$

with

$$\sigma^\mu = \begin{pmatrix} 1_2 & \sigma^i \\ 0 & 0 \end{pmatrix}, \quad \bar{\sigma}^\mu = \begin{pmatrix} 1_2 & -\sigma^i \\ 0 & 0 \end{pmatrix}, \quad (10.8)$$

where σ^i are the Pauli matrices and 1_n is the $n \times n$ unit matrix. The left and right handed projectors are then given by

$$P_L = \frac{1}{2}(1_4 - \gamma_5) = \begin{pmatrix} 1_2 & 0 \\ 0 & 0 \end{pmatrix}, \quad P_R = \frac{1}{2}(1_4 + \gamma_5) = \begin{pmatrix} 0 & 0 \\ 0 & 1_2 \end{pmatrix}. \quad (10.9)$$

The representation of generators of the Lorentz group on four-spinor space is composed of the matrices above. Because of the block form of those it, is not surprising that the representation on four-spinor space is reducible to two representations on two-spinor (Weyl spinor) spaces. It is therefore sensible to decompose a four-spinor into a left and a right handed Weyl spinor²⁹

$$\Psi = \begin{pmatrix} \psi_\alpha \\ \bar{\chi}^{\dot{\alpha}} \end{pmatrix} \quad (10.10)$$

where $\alpha, \dot{\alpha} \in \{1, 2\}$. Left handed Weyl spinors are labeled with undotted and right handed Weyl spinors with dotted indices. One distinguishes four different Weyl spinors:

$$\psi^\alpha, \quad \bar{\psi}^{\dot{\alpha}} = (\psi^\alpha)^*, \quad \psi_\alpha = \epsilon_{\alpha\beta} \psi^\beta \quad \text{and} \quad \psi_{\dot{\alpha}} = \epsilon_{\dot{\alpha}\dot{\beta}} \psi^{\dot{\beta}} = (\psi_\alpha)^*, \quad (10.11)$$

where $*$ denotes complex conjugation and indices are lowered with the antisymmetric $\epsilon_{\alpha\beta}$ ($\epsilon_{\dot{\alpha}\dot{\beta}}$), which obeys

$$\epsilon^{\alpha\beta} = \epsilon_{\beta\alpha}, \quad \epsilon^{\dot{\alpha}\dot{\beta}} = \epsilon_{\dot{\beta}\dot{\alpha}} \quad \text{and} \quad \epsilon_{12} = \epsilon_{\dot{1}\dot{2}} = 1. \quad (10.12)$$

²⁹The projectors in the chiral basis (eq. (10.9)) explain the names left and right handed Weyl spinors.

By virtue of the antisymmetry of $\epsilon^{\alpha\beta}$ one finds the Lorentz invariant products:

$$\begin{aligned}\psi\chi &:= \psi^\alpha\chi_\alpha = -\chi_\alpha\psi^\alpha = \chi^\alpha\psi_\alpha = \chi\psi, \\ \bar{\psi}\bar{\chi} &:= \bar{\psi}_{\dot{\alpha}}\bar{\chi}^{\dot{\alpha}} = -\bar{\chi}^{\dot{\alpha}}\bar{\psi}_{\dot{\alpha}} = \bar{\chi}_{\dot{\alpha}}\bar{\psi}^{\dot{\alpha}} = \bar{\chi}\bar{\psi}.\end{aligned}\tag{10.13}$$

To make the index structure of the Pauli matrices explicit, one writes $\sigma_{\alpha\dot{\alpha}}^\mu$ and $\bar{\sigma}^{\mu\dot{\alpha}\alpha}$ for the formulae in eq. (10.8). For the definition of the supersymmetry algebra in section 3.1 the representation of the generators of the Lorentz group on the left and right handed Weyl spinor space is introduced:

$$\begin{aligned}\frac{1}{2}(\sigma^{\mu\nu})_\alpha{}^\beta &:= \frac{i}{4}(\sigma^\mu\bar{\sigma}^\nu - \sigma^\nu\bar{\sigma}^\mu)_\alpha{}^\beta, \\ \frac{1}{2}(\bar{\sigma}^{\mu\nu})^{\dot{\alpha}}{}_{\dot{\beta}} &:= \frac{i}{4}(\bar{\sigma}^\mu\sigma^\nu - \bar{\sigma}^\nu\sigma^\mu)^{\dot{\alpha}}{}_{\dot{\beta}}.\end{aligned}\tag{10.14}$$

With the definition of overlined and charge conjugated four-spinors³⁰

$$\bar{\Psi} := \Psi^\dagger\gamma^0, \quad \Psi^C := i\gamma^2\gamma^0\bar{\Psi}^T, \tag{10.15}$$

one obtains:

$$\begin{aligned}\Psi &= \begin{pmatrix} \psi_\alpha \\ \bar{\chi}^{\dot{\alpha}} \end{pmatrix}, & \bar{\Psi} &= \begin{pmatrix} \chi^\alpha & \bar{\psi}_{\dot{\alpha}} \end{pmatrix}, \\ \Psi^C &= \begin{pmatrix} \chi_\alpha \\ \bar{\psi}^{\dot{\alpha}} \end{pmatrix}, & \bar{\Psi}^C &= \begin{pmatrix} \psi^\alpha & \bar{\chi}_{\dot{\alpha}} \end{pmatrix}.\end{aligned}\tag{10.16}$$

The four-spinor of an arbitrary quark q is given in terms of Weyl spinors q_L and \bar{q}_R by

$$q = \begin{pmatrix} q_L \\ \bar{q}_R \end{pmatrix}, \tag{10.17}$$

whereas the four-spinor of the Dirac gauginos is given in terms of the Weyl spinors λ and $\bar{\chi}$:³¹

$$\tilde{g}^a = \begin{pmatrix} -i\lambda^a \\ i\bar{\chi}^a \end{pmatrix}. \tag{10.18}$$

10.4 Anticommuting Numbers

Anticommuting numbers θ^α are also referred to as Grassmann numbers. These are defined by $\theta^\alpha\theta^\beta = -\theta^\beta\theta^\alpha$ and commute with ordinary c-numbers.

³⁰ Ψ^T denotes the transpose of the spinor Ψ and Ψ^\dagger is the Hermitian adjoint of Ψ .

³¹ λ is the superpartner of the gluon, called the gluino and $\bar{\chi}$ is the Weyl spinor of the chiral superfield which is associated with the gluon, referred to as the octino.

They occur in superspace formalism in the form of two-tuples, i.e. θ^α with $\alpha \in \{1, 2\}$. The complex conjugate of this tuple is denoted with $\bar{\theta}^{\dot{\alpha}}$. Derivatives are defined by

$$\begin{aligned} \partial^\alpha \theta_\beta &:= \frac{\partial}{\partial \theta_\alpha} \theta_\beta := \delta_\beta^\alpha, & \partial_\alpha \theta^\beta &:= \frac{\partial}{\partial \theta_\alpha} \theta^\beta := \delta_\alpha^\beta, \\ \bar{\partial}^{\dot{\alpha}} \bar{\theta}_{\dot{\beta}} &:= \frac{\partial}{\partial \bar{\theta}_{\dot{\alpha}}} \bar{\theta}_{\dot{\beta}} := \delta_{\dot{\beta}}^{\dot{\alpha}}, & \bar{\partial}_{\dot{\alpha}} \bar{\theta}^{\dot{\beta}} &:= \frac{\partial}{\partial \bar{\theta}_{\dot{\alpha}}} \bar{\theta}^{\dot{\beta}} := \delta_{\dot{\alpha}}^{\dot{\beta}}, \end{aligned} \quad (10.19)$$

whereby one needs to be cautious as these definitions imply

$$\partial_\alpha = -\epsilon_{\alpha\beta} \partial^\beta, \quad \bar{\partial}_{\dot{\alpha}} = -\epsilon_{\dot{\alpha}\dot{\beta}} \bar{\partial}^{\dot{\beta}}. \quad (10.20)$$

Integrals are defined by:

$$\begin{aligned} \int d\theta_\alpha (a + b\theta^\beta + c\theta^\beta \theta^\gamma) &:= b\delta_\alpha^\beta + c(\delta_\alpha^\beta \theta^\gamma - \delta_\alpha^\gamma \theta^\beta) \quad \text{and} \\ \int d\theta_\alpha (a\bar{\theta}^{\dot{\beta}}) &:= (a\bar{\theta}^{\dot{\beta}}) \int d\theta_\alpha \end{aligned} \quad (10.21)$$

where the first line mirrors the claim of translation invariance. One furthermore introduces the shortcuts

$$\begin{aligned} \int d\theta^2 &:= \int \frac{1}{4} \epsilon_{\alpha\beta} d\theta^\alpha d\theta^\beta, & \int d\bar{\theta}^2 &:= \int \frac{1}{4} \epsilon_{\dot{\alpha}\dot{\beta}} d\bar{\theta}^{\dot{\alpha}} d\bar{\theta}^{\dot{\beta}} \quad \text{and} \\ \int d^4\theta &:= \int d\theta^2 d\bar{\theta}^2. \end{aligned} \quad (10.22)$$

For the definition of (anti-)chiral superfields and the field strength chiral superfields, it proves useful to introduce supersymmetry (or chiral) covariant derivatives :

$$\begin{aligned} \mathcal{D}_\alpha &:= \frac{\partial}{\partial \theta^\alpha} - i(\sigma^\mu \bar{\theta})_\alpha \partial_\mu, & \mathcal{D}^{\dot{\alpha}} &:= \frac{\partial}{\partial \bar{\theta}_{\dot{\alpha}}} - i(\bar{\sigma}^\mu \theta)^{\dot{\alpha}} \partial_\mu, \\ D^\alpha &:= \epsilon^{\alpha\beta} D_\beta = -\frac{\partial}{\partial \theta_\alpha} + i(\bar{\theta} \bar{\sigma}^\mu)^\alpha \partial_\mu, & \mathcal{D}_{\dot{\alpha}} &:= \epsilon_{\dot{\alpha}\dot{\beta}} \mathcal{D}^{\dot{\beta}} = -\frac{\partial}{\partial \bar{\theta}^{\dot{\alpha}}} + i(\sigma^\mu \theta)_{\dot{\alpha}} \partial_\mu. \end{aligned} \quad (10.23)$$

By construction they are supersymmetry invariant, i.e. they fulfill the following anticommutation relations with the supersymmetry generators from eq. (3.2):

$$\{Q_\alpha, \mathcal{D}_\beta\} = \{\bar{Q}_{\dot{\alpha}}, \mathcal{D}_{\dot{\beta}}\} = \{Q_\alpha, \mathcal{D}_{\dot{\beta}}\} = \{\bar{Q}_{\dot{\alpha}}, \mathcal{D}_\beta\} = 0. \quad (10.24)$$

10.5 Feynman Rules for the RSQCD

The following Feynman rules (fig. 10.1 - 10.3) are derived from the Lagrangian of the R -symmetric supersymmetric quantum chromodynamics (RSQCD) eq. (4.17). When compared with the Feynman rules of the supersymmetric QCD the diagrams involving scalar gluons

are new. In addition the gluon-quark-squark vertex is different in RSQCD for the gauginos are Dirac fermions. Note that for calculations involving fermions one needs to multiply the Feynman rules in the opposite direction of the fermion flow which is given by a curved arrow next to the diagrams in fig. 10.2 and does not always agree with the flow of fermion number given by the direction of the Dirac propagator. This renders the evaluation of fermion number violating processes like $qq \rightarrow \tilde{q}\tilde{q}$ unambiguous, cf. [42].

① $(\sigma^0)^a \cdots (\sigma^0)^b \hat{=} \frac{i}{p^2 - m_{\sigma^0}^2 + i\varepsilon} \delta_{ab}$

③ $\tilde{q}_{Ai} \cdots \tilde{q}_{Bj}^\dagger \hat{=} \frac{i\delta_{AB}}{p^2 - m_{\tilde{q}}^2 + i\varepsilon} \delta_{ij}$

⑤ $G_\mu^a \cdots G_\nu^b \hat{=} -i \frac{g^{\mu\nu}}{p^2 + i\varepsilon} \delta_{ab}$

⑦ $c^a \cdots \bar{c}^b \hat{=} \frac{i}{p^2 + i\varepsilon} \delta_{ab}$

⑧ $G_\mu^a \cdots \begin{array}{l} \nearrow \bar{q}_i \\ \searrow q_j \end{array} \hat{=} -ig_s T_{ij}^a \gamma^\mu$

⑩ $G_\mu^a \cdots \begin{array}{l} \nearrow \tilde{q}_{Ai}^\dagger \\ \searrow \tilde{q}_{Bj} \end{array} \hat{=} ig_s^2 g^{\mu\nu} \{T^a, T^b\}_{ij} \delta_{AB}$

⑪ $G_\rho^c(p_c) \cdots \begin{array}{l} \nearrow G_\mu^a(p_a) \\ \searrow G_\nu^b(p_b) \end{array} \hat{=} -g_s f_{abc} [g_{\mu\nu}(p_a - p_b)^\rho + g_{\nu\rho}(p_b - p_c)^\mu + g_{\rho\mu}(p_c - p_a)^\nu]$

② $(\phi^0)^a \cdots (\phi^0)^b \hat{=} \frac{i}{p^2 - m_{\phi^0}^2 + i\varepsilon} \delta_{ab}$

④ $q_i \cdots \bar{q}_j \hat{=} i \frac{\not{p} + m_q}{p^2 - m_q^2 + i\varepsilon} \delta_{ij}$

⑥ $\tilde{g}^a \cdots \bar{\tilde{g}}^b \hat{=} i \frac{\not{p} + m_{\tilde{g}}}{p^2 - m_{\tilde{g}}^2 + i\varepsilon} \delta_{ab}$

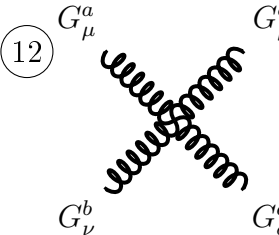
⑨ $G_\mu^a \cdots \begin{array}{l} \nearrow \tilde{q}_{Ai}^\dagger(-p_1) \\ \searrow \tilde{q}_{Bj}(p_2) \end{array} \hat{=} -ig_s (p_2 + p_1)^\mu T_{ij}^a \delta_{AB}$

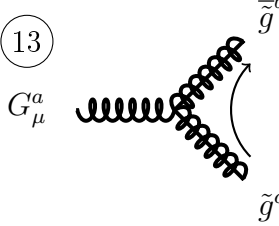
10a $G_\mu^b \cdots \begin{array}{l} \nearrow \bar{c}^a(-p_1) \\ \searrow c^c \end{array} \hat{=} -g_s f^{abc} p_1^\mu$

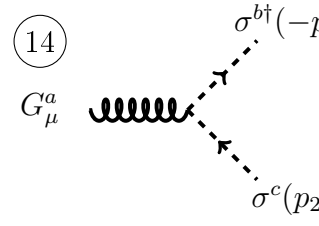
Figure 10.1: In the Feynman diagrams of the propagators the momentum is flowing from the right to the left hand side. The gluon propagator is given in Feynman gauge.

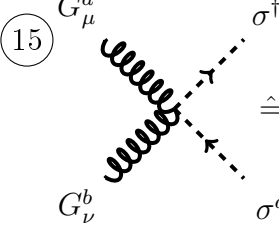
In the Feynman diagrams of the vertices all momenta flow towards the vertex, i.e. in diagram 9 and 10a: $-p_1$ flows towards the vertex.

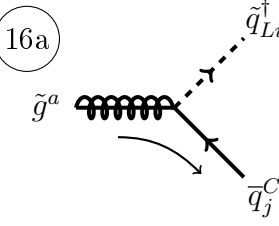
The indices $A, B \in \{L, R\}$ label the left/right “handedness” of the squarks. The indices $i, j = 1, 2, 3$ are the color indices in the (anti)fundamental representation where $a, b, c, \dots = 1, \dots, 8$ are the color indices of the adjoint representation.

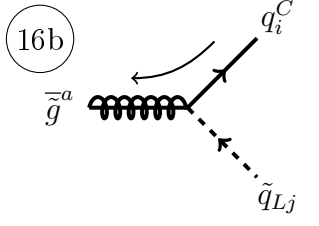
(12)  $\hat{=} -ig_s^2[f^{abe}f^{cde}(g^{\mu\rho}g^{\nu\sigma} - g^{\mu\sigma}g^{\nu\rho}) + f^{ace}f^{bde}(g^{\mu\nu}g^{\rho\sigma} - g^{\mu\sigma}g^{\nu\rho}) + f^{ade}f^{bce}(g^{\mu\nu}g^{\rho\sigma} - g^{\mu\rho}g^{\nu\sigma})]$

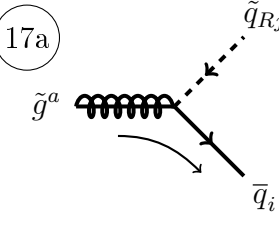
(13)  $\hat{=} -g_sf_{abc}\gamma^\mu$

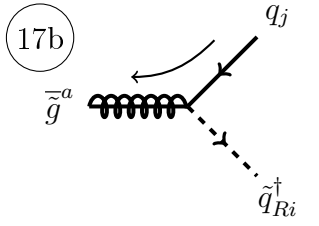
(14)  $\hat{=} -g_s(p_1 + p_2)^\mu f_{abc}$

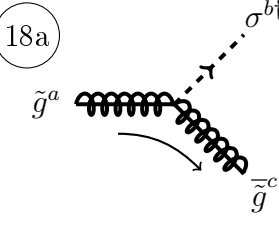
(15)  $\hat{=} +ig_s^2g^{\mu\nu}[f^{aec}f^{bed} + f^{bec}f^{aed}]$

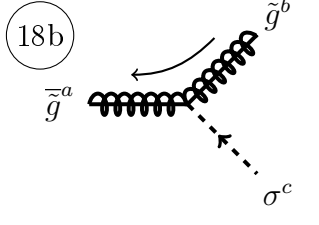
(16a)  $\hat{=} -i\sqrt{2}g_sT_{ij}^aP_L$

(16b)  $\hat{=} -i\sqrt{2}g_sT_{ij}^aP_R$

(17a)  $\hat{=} +i\sqrt{2}g_sT_{ij}^aP_L$

(17b)  $\hat{=} +i\sqrt{2}g_sT_{ij}^aP_R$

(18a)  $\hat{=} -\sqrt{2}g_sf^{abc}P_L$

(18b)  $\hat{=} +\sqrt{2}g_sf^{abc}P_R$

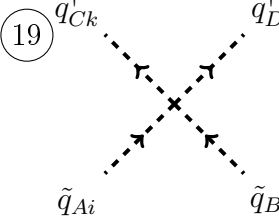
(19)  $\hat{=} -ig_s^2[T_{ki}^aT_{lj}^a(\delta_{AL}\delta_{CL} - \delta_{AR}\delta_{CR})(\delta_{BL}\delta_{DL} - \delta_{BR}\delta_{DR}) + T_{kj}^aT_{li}^a(\delta_{BL}\delta_{CL} - \delta_{BR}\delta_{CR})(\delta_{AL}\delta_{DL} - \delta_{AR}\delta_{DR})]$

Figure 10.2: The curved arrows indicate the fermion flow. The Feynman rules 16b, 17b and 18b are the complex conjugates of 16a, 17a and 18a respectively. Applying a flipping rule to a vertex one has to reverse the curved arrow, i.e. the fermion flow and replace Ψ with $\bar{\Psi}^C$. In addition one has to add a minus sign for Feynman rule 13.

(20) $\hat{=} -g_s^2 T_{ij}^a f^{abc} (\delta_{AL} \delta_{CL} - \delta_{AR} \delta_{BR})$

(21) $\hat{=} -i\sqrt{2} g_s m_{\tilde{g}} T_{ij}^a (\delta_{AL} \delta_{BL} - \delta_{AR} \delta_{BR})$

(22) $\hat{=} i g_s^2 (f^{abc} f^{ade} + f^{abe} f^{adc})$

Figure 10.3: Feynman rules involving only sgluons and other scalar fields.

10.6 Passarino-Veltman Integrals

The definition of the momenta within the Passarino-Veltman integrals in this thesis agrees with the one from `LoopTools` [68]. The original paper [81] uses slightly different conventions. A pedagogical introduction to the evaluation of one-loop integrals can be found in [82]. A , B and C integrals are defined by:

$$\begin{aligned}
 \frac{i}{16\pi^2} A_0(m^2) &:= \int_l \frac{1}{l^2 - m^2}, \\
 \frac{i}{16\pi^2} B_{0,\mu,\mu\nu}(p^2, m_1^2, m_2^2) &:= \int_l \frac{\{1, l_\mu, l_\mu l_\nu\}}{[l^2 - m_1^2][(l+p)^2 - m_2^2]}, \\
 \frac{i}{16\pi^2} C_{0,\mu,\mu\nu}(p_1^2, p_2^2, (p_1+p_2)^2, m_1^2, m_2^2, m_3^2) &:= \int_l \frac{\{1, l_\mu, l_\mu l_\nu\}}{[l^2 - m_1^2][(l+p_1)^2 - m_2^2][(l+p_1+p_2)^2 - m_3^2]},
 \end{aligned} \tag{10.25}$$

with the shortcut $\int_l = \mu^{2\epsilon} \int \frac{d^D l}{(2\pi)^D}$. Furthermore there are suppressed ε 's which prescribe how the poles in the complex plane are avoided. They are hidden in the infinitesimal shift of the masses: $m_i^2 \rightarrow m_i^2 - i\varepsilon$.

The tensor integrals can be decomposed as

$$\begin{aligned}
B_\mu &:= p_\mu B_1, \\
B_{\mu\nu} &:= g_{\mu\nu} B_{00} + p_\mu p_\nu B_{11}, \\
C_\mu &:= p_{1\mu} C_1 + p_{2\mu} C_2, \\
C_{\mu\nu} &:= g_{\mu\nu} C_{00} + p_{1\mu} p_{1\nu} C_{11} + p_{2\mu} p_{2\nu} C_{22} + (p_{1\mu} p_{2\nu} + p_{2\mu} p_{1\nu}) C_{12}.
\end{aligned} \tag{10.26}$$

The A -integral reads

$$A_0(m^2) = m^2 \left(\Delta_\epsilon - \ln \frac{m^2}{\mu^2} + 1 \right) + \mathcal{O}(\epsilon). \tag{10.27}$$

where the typical UV-divergent constant $\Delta_\epsilon = \frac{1}{\epsilon} - \gamma_E + \ln 4\pi$ is defined. It comprises the Euler-Mascheroni constant γ_E . The relation between ϵ and the dimension D is given by $D = 4 - 2\epsilon$. In the special case of vanishing momenta, the further integrals take a succinct form. Some formulae which are needed for the calculation of renormalization constants are

$$B_0(0, m_1^2, m_2^2) = \frac{A_0(m_1^2) - A_0(m_2^2)}{m_1^2 - m_2^2} = \Delta_\epsilon + 1 - \frac{m_1^2 \ln \frac{m_1^2}{\mu^2} - m_2^2 \ln \frac{m_2^2}{\mu^2}}{m_1^2 - m_2^2} + \mathcal{O}(\epsilon), \tag{10.28}$$

$$B_0(0, m^2, m^2) = \frac{\partial}{\partial m^2} A_0(m^2) = \Delta_\epsilon - \ln \frac{m^2}{\mu^2} + \mathcal{O}(\epsilon), \tag{10.29}$$

$$B_0(0, 0, 0) = 0, \tag{10.30}$$

$$B_1(0, m_1^2, m_2^2) = -\frac{\Delta_\epsilon}{2} + \frac{1}{2} \ln \frac{m_1^2}{\mu^2} + \frac{-3 + 4t - t^2 - 4t \ln t + 2t^2 \ln t}{4(t-1)^2} + \mathcal{O}(\epsilon), \tag{10.31}$$

$$B_1(0, 0, 0) = 0. \tag{10.32}$$

The scaleless integrals equal to zero due to their definition on how they scale in D dimensions [57]. The parameter t is given by $\frac{m_2^2}{m_1^2}$. As can be seen from eq. (10.31), B_1 is, in contrast to B_0 , not symmetric in its masses but it can be shown [83] that

$$B_1(p^2, m_1^2, m_2^2) = -(B_0(p^2, m_2^2, m_1^2) + B_1(p^2, m_2^2, m_1^2)). \tag{10.33}$$

It can further be shown that

$$C_{00}(0, 0, 0, m_1^2, m_1^2, m_2^2) = -\frac{1}{2} B_1(0, m_1^2, m_2^2) \tag{10.34}$$

and that $C_{00}(0, 0, 0, m_1^2, m_1^2, m_2^2)$ is a symmetric function of its masses.

From the generic ϵ -expansion of the B_0 integral [84]

$$B_0(p^2, m_1^2, m_2^2) = \Delta_\epsilon - \int_0^1 dx \ln \frac{-x(1-x)p^2 + xm_2^2 + (1-x)m_1^2}{\mu^2} \tag{10.35}$$

and Passarino-Veltman decomposition, [81] one can determine the UV-divergent part of all B and C integrals. In chapter 7.7 this is necessary in order to obtain the renormalization constants in the $\overline{\text{MS}}$ -scheme. Infrared and collinear singularities arise from the special case where one or multiple masses and momenta tend to zero. These poles can be regularized with a small mass cutoff Λ leading to singularities of the form $\ln \Lambda$ or dimensionally which leads to ϵ -poles as in the treatment of UV-divergences. In the latter case the integral first needs to undergo the limit to zero masses and evaluated afterwards.

The following list shows all necessary integrals needed to determine the renormalization constants in 7.7:

$$A_0(m^2)|_{\text{UV-div}} = m^2 \Delta_\epsilon, \quad (10.36)$$

$$B_0(p^2, m_1^2, m_2^2)|_{\text{UV-div}} = \Delta_\epsilon, \quad (10.37)$$

$$B_1(p^2, m_1^2, m_2^2)|_{\text{UV-div}} = -\frac{1}{2} \Delta_\epsilon, \quad (10.38)$$

$$C_{00}(p_1^2, p_2^2, (p_1 + p_2)^2, m_1^2, m_2^2, m_3^2)|_{\text{UV-div}} = \frac{1}{4} \Delta_\epsilon. \quad (10.39)$$

The UV-divergent part of C_{11} , C_{22} , C_{12} equals zero. As can be seen already from the superficial degree of divergence also $C_i|_{\text{UV-div}} = 0$ for $i \in \{0, 1, 2\}$.

10.7 Cross Section and Phase Space Integration

Once the Feynman amplitude \mathcal{M} for a $2 \rightarrow N$ body scattering³² is computed one can calculate physical observables with it. The differential cross section for $2 \rightarrow N$ scattering is given by

$$d\sigma = \frac{1}{F} d\Phi_N |\mathcal{M}|^2. \quad (10.40)$$

The flux factor is defined by $F = 4\sqrt{(k_a \cdot k_b)^2 - (m_a m_b)^2}$ which equals $F = 2s$ for massless initial state particles. The differential for the N body phase space in D dimensions is given by

$$d\Phi_N = (\mu^{2\epsilon})^{N-1} \left(\prod_{f=1}^N \frac{d^{D-1} p_f}{(2\pi)^{D-1}} \frac{1}{2E_f} \right) (2\pi)^D \delta^{(D)}(k_a + k_b - \sum_{f=1}^N p_f). \quad (10.41)$$

The factor $\mu^{2\epsilon}$ is included to maintain the mass dimension of the cross section. As in this thesis the sum of $|\mathcal{M}|^2$ over helicities and colors $\sum |\mathcal{M}|^2$ has been calculated one can write

$$d\sigma = \frac{1}{2s} d\Phi_2 K_{ab} \sum |\mathcal{M}|^2 \quad (10.42)$$

where K_{ab} encodes the averaging over initial state helicities and colors. Specifying to the center-of-mass frame and using that $\sum |\mathcal{M}|^2$ is only a function of the modulus of one of the

³²with kinematics $k_a + k_b \rightarrow p_1 + \dots p_N$

final state particle's three-momentum $|\vec{p}_i|$ and the angle θ between \vec{k}_a and \vec{p}_1 one can write

$$\begin{aligned} \int d\Phi_2 &= \mu^{2\epsilon} \int \frac{d|\vec{p}_1| d\Omega_1^{D-1}}{(2\pi)^{D-2} 4E_1 E_2} |\vec{p}_1|^{D-2} \delta \left(k_a^0 + k_b^0 - \sqrt{m_1^2 + |\vec{p}_1|^2} - \sqrt{m_2^2 + |\vec{p}_1|^2} \right) \\ &= \frac{1}{(2\pi)^{D-2}} \frac{2\pi^{\frac{D}{2}-1}}{\Gamma(\frac{D}{2}-1)} \mu^{2\epsilon} \int_0^\infty d|\vec{p}_1| \int_0^\pi d\cos\theta \frac{1}{4E_1 E_2} p_1^{D-2} \sin^{D-4}\theta \\ &\quad \delta \left(k_a^0 + k_b^0 - \sqrt{m_1^2 + |\vec{p}_1|^2} - \sqrt{m_2^2 + |\vec{p}_1|^2} \right). \end{aligned} \quad (10.43)$$

In the second line the integral over the D -dimensional hypersphere

$$\int d\Omega^D = \int_0^{2\pi} d\phi \prod_{i=1}^{D-2} \int_0^\pi \sin^i \theta_i d\theta_i = \frac{2\pi^{\frac{D}{2}}}{\Gamma(\frac{D}{2})} \quad (10.44)$$

has been used. Because $\sum |\mathcal{M}|^2$ is calculated in terms of Mandelstam variables

$$\begin{aligned} t &= (k_a - p_1)^2 \\ t &= -2 \left(|\vec{k}_a| \sqrt{m_1^2 + |\vec{p}_1|^2} - |\vec{k}_a| |\vec{p}_1| \cos\theta \right) + m_1^2 \end{aligned} \quad (10.45)$$

$$\begin{aligned} u &= (k_a - p_2)^2 \\ u &= -2 \left(|\vec{k}_a| \sqrt{m_2^2 + |\vec{p}_1|^2} + |\vec{k}_a| |\vec{p}_1| \cos\theta \right) + m_2^2 \end{aligned} \quad (10.46)$$

it is useful to perform a change of coordinates yielding

$$d|\vec{p}_1| d\cos\theta = -\frac{E_1 E_2}{4|\vec{k}_a|^2 |\vec{p}_1|^2 (E_1 + E_2)} du dt. \quad (10.47)$$

Inserting eq. (10.47) into eq. (10.43) and using $2|\vec{k}_a| = \sqrt{s} = E_1 + E_2$ gives

$$\begin{aligned} \int d\Phi_2 &= \frac{1}{s} \frac{\pi^{-\frac{D}{2}+1}}{2^{D-3} \Gamma(\frac{D}{2}-1)} \int du dt \left(\frac{tu - m_1^2 m_2^2}{\mu^{2\epsilon} s} \right)^{\frac{D-4}{2}} \\ &\quad \frac{1}{4} \Theta(tu - m_1^2 m_2^2) \delta(s + t + u - m_1^2 - m_2^2) \end{aligned} \quad (10.48)$$

where the Θ -function comes from the bounds of $|\vec{p}_1|$ and θ , visible in eq. (10.43) and the combination of eq. (10.45) and eq. (10.46). Working in $D = 4 - 2\epsilon$ dimensions and inserting $\Theta(s - 4m^2)$ with $m = \frac{m_1 + m_2}{2}$ to account for the production threshold one finds

$$\begin{aligned} \frac{d^2\sigma}{dt du} &= \frac{K_{ab}}{s^2} \frac{\pi S_\epsilon}{\Gamma(1-\epsilon)} \left[\frac{tu - m_1^2 m_2^2}{\mu^2 s} \right]^{-\epsilon} \Theta(tu - m_1^2 m_2^2) \\ &\quad \Theta(s - 4m^2) \delta(s + t + u - m_1^2 - m_2^2) \sum |\mathcal{M}|^2 \end{aligned} \quad (10.49)$$

where $S_\epsilon = (4\pi)^{-2+\epsilon}$ as defined in [42]. The averaging factors K_{ab} are given by

$$K_{qq} = \frac{1}{4N_c^2} \quad K_{GG} = \frac{1}{4(1-\epsilon)^2(N_c^2-1)^2} \quad K_{qG} = \frac{1}{4(1-\epsilon)N_c(N_c^2-1)}. \quad (10.50)$$

11 References

- [1] M. Maggiore, *A modern introduction to quantum field theory*. Oxford master series in physics 12, Oxford University Press, 2005.
- [2] M. E. Peskin and D. V. Schroeder, *An introduction to quantum field theory*. Advanced book program, Boulder (Colo.): Westview Press Reading (Mass.), 1995. Autre tirage : 1997.
- [3] C. N. Yang and R. L. Mills, “Conservation of isotopic spin and isotopic gauge invariance,” *Phys. Rev.*, vol. 96, pp. 191–195, Oct 1954.
- [4] P. Dießner, “Vergleich nicht-minimaler supersymmetrischer Modelle mit LHC-Ergebnissen,” Master’s thesis, TU Dresden, 2012.
- [5] M. Bach, “Das anomale magnetische Moment des Myons im minimalen supersymmetrischen Standardmodell für $\tan \beta = \infty$,” Master’s thesis, TU Dresden, 2013.
- [6] P. W. Higgs, “Broken symmetries, massless particles and gauge fields,” *Phys. Lett.*, vol. 12, pp. 132–133, 1964.
- [7] P. W. Higgs, “Broken Symmetries and the Masses of Gauge Bosons,” *Phys. Rev. Lett.*, vol. 13, pp. 508–509, 1964.
- [8] P. W. Higgs, “Spontaneous Symmetry Breakdown without Massless Bosons,” *Phys. Rev.*, vol. 145, pp. 1156–1163, 1966.
- [9] F. Englert and R. Brout, “Broken Symmetry and the Mass of Gauge Vector Mesons,” *Phys. Rev. Lett.*, vol. 13, pp. 321–323, 1964.
- [10] G. S. Guralnik, C. R. Hagen, and T. W. B. Kibble, “Global Conservation Laws and Massless Particles,” *Phys. Rev. Lett.*, vol. 13, pp. 585–587, 1964.
- [11] T. W. B. Kibble, “Symmetry breaking in nonAbelian gauge theories,” *Phys. Rev.*, vol. 155, pp. 1554–1561, 1967.
- [12] J. Bernstein, “Spontaneous symmetry breaking, gauge theories, the higgs mechanism and all that,” *Rev. Mod. Phys.*, vol. 46, pp. 7–48, 1974. [Erratum: *Rev. Mod. Phys.* 46, 855 (1974)].
- [13] A. D. H. J. Manfred Böhm, Manfred Böhm (Dr. rer. nat.), *Gauge Theories of the Strong and Electroweak Interaction*. Vieweg + Teubner, 3rd rev. ed. 2001 ed., 2001.
- [14] N. Cabbibo, “Leptonic Decays in the Unitary Symmetry Scheme,” in *Proceedings, International Conference on Fundamental Aspects of Weak Interactions*, pp. 299–302, 1964.

-
- [15] M. Kobayashi and T. Maskawa, “CP Violation in the Renormalizable Theory of Weak Interaction,” *Prog. Theor. Phys.*, vol. 49, pp. 652–657, 1973.
 - [16] C. Becchi, A. Rouet, and R. Stora, “The Abelian Higgs-Kibble Model. Unitarity of the S Operator,” *Phys. Lett.*, vol. B52, pp. 344–346, 1974.
 - [17] C. Becchi, A. Rouet, and R. Stora, “Renormalization of the Abelian Higgs-Kibble Model,” *Commun. Math. Phys.*, vol. 42, pp. 127–162, 1975.
 - [18] C. Becchi, A. Rouet, and R. Stora, “Renormalization of Gauge Theories,” *Annals Phys.*, vol. 98, pp. 287–321, 1976.
 - [19] R. Adam *et al.*, “Planck 2015 results. I. Overview of products and scientific results,” 2015.
 - [20] S. P. Martin, “A Supersymmetry primer,” 1997. [Adv. Ser. Direct. High Energy Phys.18,1(1998)].
 - [21] S. R. Coleman and J. Mandula, “All Possible Symmetries of the S Matrix,” *Phys. Rev.*, vol. 159, pp. 1251–1256, 1967.
 - [22] O. Pelc and L. P. Horwitz, “Generalization of the Coleman-Mandula theorem to higher dimension,” *J. Math. Phys.*, vol. 38, pp. 139–172, 1997.
 - [23] R. Haag, J. T. Łopuszański, and M. Sohnius, “All Possible Generators of Supersymmetries of the s Matrix,” *Nucl. Phys.*, vol. B88, p. 257, 1975.
 - [24] G. 't Hooft, “Symmetry Breaking Through Bell-Jackiw Anomalies,” *Phys. Rev. Lett.*, vol. 37, pp. 8–11, 1976.
 - [25] G. D. Kribs, E. Poppitz, and N. Weiner, “Flavor in supersymmetry with an extended R-symmetry,” *Phys. Rev.*, vol. D78, p. 055010, 2008.
 - [26] P. Dießner, J. Kalinowski, W. Kotlarski, and D. Stöckinger, “Higgs boson mass and electroweak observables in the MRSSM,” *JHEP*, vol. 12, p. 124, 2014.
 - [27] P. J. Fox, A. E. Nelson, and N. Weiner, “Dirac gaugino masses and supersoft supersymmetry breaking,” *JHEP*, vol. 08, p. 035, 2002.
 - [28] A. E. Nelson, N. Rius, V. Sanz, and M. Unsal, “The Minimal supersymmetric model without a mu term,” *JHEP*, vol. 08, p. 039, 2002.
 - [29] G. D. Kribs and A. Martin, “Supersoft Supersymmetry is Super-Safe,” *Phys. Rev.*, vol. D85, p. 115014, 2012.
 - [30] E. Hardy, “Is Natural SUSY Natural?,” *JHEP*, vol. 10, p. 133, 2013.

-
- [31] G. D. Kribs and A. Martin, “Dirac Gauginos in Supersymmetry – Suppressed Jets + MET Signals: A Snowmass Whitepaper,” 2013.
- [32] S. Y. Choi, M. Drees, J. Kalinowski, J. M. Kim, E. Popenda, and P. M. Zerwas, “Color-Octet Scalars of N=2 Supersymmetry at the LHC,” *Phys. Lett.*, vol. B672, pp. 246–252, 2009.
- [33] D. Goncalves-Netto, D. Lopez-Val, K. Mawatari, T. Plehn, and I. Wigmore, “Sgluon Pair Production to Next-to-Leading Order,” *Phys. Rev.*, vol. D85, p. 114024, 2012.
- [34] W. Kotlarski, *Analysis of the R-symmetric supersymmetric models including quantum corrections*. PhD thesis, University of Warsaw, 10 2016.
- [35] T. Hahn, “Generating Feynman diagrams and amplitudes with FeynArts 3,” *Comput. Phys. Commun.*, vol. 140, pp. 418–431, 2001.
- [36] B. Chokoufe Nejad, J. N. Lang, T. Hahn, and E. Mirabella, “FormCalc 8: Better Algebra and Vectorization,” *Acta Phys. Polon.*, vol. B44, no. 11, pp. 2231–2239, 2013.
- [37] T. Hahn and M. Perez-Victoria, “Automatized one loop calculations in four-dimensions and D-dimensions,” *Comput. Phys. Commun.*, vol. 118, pp. 153–165, 1999.
- [38] F. Staub, “SARAH 4 : A tool for (not only SUSY) model builders,” *Comput. Phys. Commun.*, vol. 185, pp. 1773–1790, 2014.
- [39] F. Staub, “SARAH 3.2: Dirac Gauginos, UFO output, and more,” *Comput. Phys. Commun.*, vol. 184, pp. 1792–1809, 2013.
- [40] F. Staub, “Automatic Calculation of supersymmetric Renormalization Group Equations and Self Energies,” *Comput. Phys. Commun.*, vol. 182, pp. 808–833, 2011.
- [41] F. Staub, “From Superpotential to Model Files for FeynArts and CalcHep/CompHep,” *Comput. Phys. Commun.*, vol. 181, pp. 1077–1086, 2010.
- [42] W. Beenakker, R. Hopker, M. Spira, and P. M. Zerwas, “Squark and gluino production at hadron colliders,” *Nucl. Phys.*, vol. B492, pp. 51–103, 1997.
- [43] L. A. Harland-Lang, A. D. Martin, P. Motylinski, and R. S. Thorne, “Parton distributions in the LHC era: MMHT 2014 PDFs,” *Eur. Phys. J.*, vol. C75, no. 5, p. 204, 2015.
- [44] V. N. Gribov and L. N. Lipatov, “Deep inelastic e p scattering in perturbation theory,” *Sov. J. Nucl. Phys.*, vol. 15, pp. 438–450, 1972. [*Yad. Fiz.*15,781(1972)].
- [45] Y. L. Dokshitzer, “Calculation of the Structure Functions for Deep Inelastic Scattering and e+ e- Annihilation by Perturbation Theory in Quantum Chromodynamics,” *Sov. Phys. JETP*, vol. 46, pp. 641–653, 1977. [*Zh. Eksp. Teor. Fiz.*73,1216(1977)].

-
- [46] G. Altarelli and G. Parisi, “Asymptotic Freedom in Parton Language,” *Nucl. Phys.*, vol. B126, pp. 298–318, 1977.
 - [47] G. Dissertori, I. Knowles, and M. Schmelling, *Quantum Chromodynamics: High Energy Experiments and Theory*. International series of monographs on physics, Clarendon Press, 2003.
 - [48] J. C. Collins, D. E. Soper, and G. F. Sterman, “Factorization of Hard Processes in QCD,” *Adv. Ser. Direct. High Energy Phys.*, vol. 5, pp. 1–91, 1989.
 - [49] R. Brock *et al.*, “Handbook of perturbative QCD: Version 1.0,” *Rev. Mod. Phys.*, vol. 67, pp. 157–248, 1995.
 - [50] T. Hahn, “CUBA: A Library for multidimensional numerical integration,” *Comput. Phys. Commun.*, vol. 168, pp. 78–95, 2005.
 - [51] A. Lahiri and P. Pal, *A First Book of Quantum Field Theory*. Alpha Science International, 2005.
 - [52] B. W. Harris and J. F. Owens, “The Two cutoff phase space slicing method,” *Phys. Rev.*, vol. D65, p. 094032, 2002.
 - [53] T. Kinoshita, “Mass Singularities of Feynman Amplitudes,” *Journal of Mathematical Physics*, vol. 3, pp. 650–677, July 1962.
 - [54] T. D. Lee and M. Nauenberg, “Degenerate systems and mass singularities,” *Phys. Rev.*, vol. 133, pp. B1549–B1562, Mar 1964.
 - [55] R. Gavin, C. Hangst, M. Krämer, M. Mühlleitner, M. Pellen, E. Popena, and M. Spira, “Matching Squark Pair Production at NLO with Parton Showers,” *JHEP*, vol. 10, p. 187, 2013.
 - [56] G. ’t Hooft and M. J. G. Veltman, “Regularization and Renormalization of Gauge Fields,” *Nucl. Phys.*, vol. B44, pp. 189–213, 1972.
 - [57] J. C. Collins, *Renormalization: an introduction to renormalization, the renormalization group, and the operator-product expansion*. Cambridge monographs on mathematical physics, Cambridge: Cambridge Univ. Press, 1984.
 - [58] I. Jack and D. R. T. Jones, “Regularization of supersymmetric theories,” 1997. [Adv. Ser. Direct. High Energy Phys.21,494(2010)].
 - [59] W. Hollik and D. Stockinger, “Regularization and supersymmetry restoring counterterms in supersymmetric QCD,” *Eur. Phys. J.*, vol. C20, pp. 105–119, 2001.

-
- [60] D. Stockinger, “Regularization by dimensional reduction: consistency, quantum action principle, and supersymmetry,” *JHEP*, vol. 03, p. 076, 2005.
- [61] P. Varso, “Supersymmetrie restaurierende Counterterme in Einschleifenordnung,” Master’s thesis, TU Dresden, 2010.
- [62] D. Stockinger and P. Varso, “FeynArts model file for MSSM transition counterterms from DREG to DRED,” *Comput. Phys. Commun.*, vol. 183, pp. 422–430, 2012.
- [63] S. P. Martin and M. T. Vaughn, “Regularization dependence of running couplings in softly broken supersymmetry,” *Phys. Lett.*, vol. B318, pp. 331–337, 1993.
- [64] T. Hahn, *FormCalc 8 User’s Guide*, 2015.
- [65] H. D. Politzer, “Reliable Perturbative Results for Strong Interactions?,” *Phys. Rev. Lett.*, vol. 30, pp. 1346–1349, 1973.
- [66] D. J. Gross and F. Wilczek, “Asymptotically Free Gauge Theories. 1,” *Phys. Rev.*, vol. D8, pp. 3633–3652, 1973.
- [67] T. Hahn, *FeynArts 3.9 User’s Guide*, 2015.
- [68] T. Hahn and M. Perez-Victoria, “Automatized one loop calculations in four-dimensions and D-dimensions,” *Comput. Phys. Commun.*, vol. 118, pp. 153–165, 1999.
- [69] H. Lehmann, K. Symanzik, and W. Zimmermann, “On the formulation of quantized field theories,” *Nuovo Cim.*, vol. 1, pp. 205–225, 1955.
- [70] A. Buckley, J. Ferrando, S. Lloyd, K. Nordström, B. Page, M. Rüfenacht, M. Schönherr, and G. Watt, “LHAPDF6: parton density access in the LHC precision era,” *Eur. Phys. J.*, vol. C75, p. 132, 2015.
- [71] J. Alwall, R. Frederix, S. Frixione, V. Hirschi, F. Maltoni, O. Mattelaer, H. S. Shao, T. Stelzer, P. Torrielli, and M. Zaro, “The automated computation of tree-level and next-to-leading order differential cross sections, and their matching to parton shower simulations,” *JHEP*, vol. 07, p. 079, 2014.
- [72] T. Hahn, *LoopTools 2.8 User’s Guide*, 2012.
- [73] G. Cullen *et al.*, “GOSAM-2.0: a tool for automated one-loop calculations within the Standard Model and beyond,” *Eur. Phys. J.*, vol. C74, no. 8, p. 3001, 2014.
- [74] G. Cullen, N. Greiner, G. Heinrich, G. Luisoni, P. Mastrolia, G. Ossola, T. Reiter, and F. Tramontano, “Automated One-Loop Calculations with GoSam,” *Eur. Phys. J.*, vol. C72, p. 1889, 2012.

-
- [75] W. Beenakker, R. Hopker, and M. Spira, “PROSPINO: A Program for the production of supersymmetric particles in next-to-leading order QCD,” 1996.
 - [76] J. Pumplin, D. R. Stump, J. Huston, H. L. Lai, P. M. Nadolsky, and W. K. Tung, “New generation of parton distributions with uncertainties from global QCD analysis,” *JHEP*, vol. 07, p. 012, 2002.
 - [77] P. M. Nadolsky, H.-L. Lai, Q.-H. Cao, J. Huston, J. Pumplin, D. Stump, W.-K. Tung, and C. P. Yuan, “Implications of CTEQ global analysis for collider observables,” *Phys. Rev.*, vol. D78, p. 013004, 2008.
 - [78] H.-C. Cheng, J. L. Feng, and N. Polonsky, “Superoblique corrections and nondecoupling of supersymmetry breaking,” *Phys. Rev.*, vol. D56, pp. 6875–6884, 1997.
 - [79] T. Appelquist and J. Carazzone, “Infrared Singularities and Massive Fields,” *Phys. Rev.*, vol. D11, p. 2856, 1975.
 - [80] M. von Steinkirch, *Introduction to Group Theory for Physicists*. 2010.
 - [81] G. Passarino and M. J. G. Veltman, “One Loop Corrections for $e^+ e^-$ Annihilation Into $\mu^+ \mu^-$ in the Weinberg Model,” *Nucl. Phys.*, vol. B160, pp. 151–207, 1979.
 - [82] R. K. Ellis, Z. Kunszt, K. Melnikov, and G. Zanderighi, “One-loop calculations in quantum field theory: from Feynman diagrams to unitarity cuts,” *Phys. Rept.*, vol. 518, pp. 141–250, 2012.
 - [83] J. C. Romao, *Modern Techniques for One-Loop Calculations*. 2006.
 - [84] A. Denner, “Techniques for the Calculation of Electroweak Radiative Corrections at the One-Loop Level and Results for W-physics at LEP 200,” *Fortschritte der Physik*, vol. 41, pp. 307–420, 1993.

Acknowledgements

First of all, I like to thank Dominik Stöckinger who enthused me with theoretical particle physics and provided me with this interesting topic. In addition, he was always available for helping discussions whenever I was in need of them.

Special thanks go to Philip Dießner and Wojciech Kotlarski, who contributed significantly to results within this thesis. In addition, I like to thank them, Markus Bach, Thomas Kwasnitza, Josua Unger and Tom Steudtner for many valuable discussions and support regarding physical questions as well as programming issues and a pleasant atmosphere in the office. Furthermore, I like to give them thanks for proofreading this thesis.

I am particularly grateful for Rebecca Schmidt's support within the last month which enabled me to focus on my thesis. In addition, I like to thank her for proofreading.

Last but not least, I would like to thank my family. Without them my physics studies would by no means have been possible in the way they were.

Erklärung

Hiermit erkläre ich, dass ich diese Arbeit im Rahmen der Betreuung am Institut für Kern- und Teilchenphysik ohne unzulässige Hilfe Dritter verfasst und alle Quellen als solche gekennzeichnet habe.

Sebastian Liebschner
Dresden, Juli 2016